OVERPRESSURE IN THE EASTERN BENGAL BASIN, BANGLADESH, AND ITS RELATION TO COMPRESSIONAL TECTONICS

Except where reference is made to the work of others, the described in this thesis is my own work or was done in collaboration with my advisory committee. This thesis does not include proprietary or classified information.

_____
Muhammad Shahadat Hossain

Certificate of Approval:

_____	_____
Ming–Kuo Lee Professor Geology and Geography	Ashraf Uddin, Chair Associate Professor Geology and Geography
_____	_____
Charles E. Savrda Professor Geology and Geography	Willis E. Hames Professor Geology and Geography

_____
George T. Flowers
Dean
Graduate School

OVERPRESSURE IN THE EASTERN BENGAL BASIN, BANGLADESH, AND ITS RELATION TO COMPRESSIONAL TECTONICS

Muhammad Shahadat Hossain

A Thesis

Submitted to

the Graduate Faculty of

Auburn University

in Partial Fulfillment of the

Requirements for the

Degree of

Master of Science

Auburn, Alabama

December 18, 2009

OVERPRESSURE IN THE EASTERN BENGAL BASIN, BANGLADESH, AND ITS RELATION TO COMPRESSIONAL TECTONICS

Muhammad Shahadat Hossain

_____
Muhammad Shahadat Hossain

_____
Date of Graduation

VITA

Muhammad Shahadat Hossain, son of Muhammad Delwar Hossain and Mansura Akter, was born July 03, 1978, in Nangalkot, Comilla, Bangladesh. He passed his Higher Secondary Certificate Examination in 1996 from Government Science College, Dhaka with distinctions. He received his Bachelor of Science and Master of Science degrees in Geology in 2003 and 2006, respectively, from the University of Dhaka, Bangladesh. He entered the graduate school at Auburn University to pursue his second Master of Science degree from the department of Geology and Geography in Fall 2007.

THESIS ABSTRACT

OVERPRESSURE IN THE EASTERN BENGAL BASIN, BANGLADESH, AND ITS RELATION TO COMPRESSIONAL TECTONICS

Muhammad Shahadat Hossain

Master of Science, December 18, 2009
(Master of Science, University of Dhaka, Bangladesh, 2006)
(Bachelor of Science, University of Dhaka, Bangladesh, 2003

119 Typed Pages

Directed by Ashraf Uddin

Proximity to the Indian craton, the Himalayas, and the Indo–Burman ranges and rapid orogenic sedimentation have resulted in the generation of overpressure in the Bengal basin. In eastern Bengal basin, overpressure zones frequently have been reported from the Miocene sequences in exploratory wells. The majority of the wells drilled so far in the eastern Bengal Basin encountered overpressure zones at depths ranging from less than 1 km (Patharia–5) to 4.5 km (Muladi–1).

The average geothermal gradient in the eastern Bengal basin area ranges from 15.8 to 30° C/km. In the western stable shelf area, the average geothermal gradients range from 21.1 to 31.6° C/km. The depth–pressure profile indicates that formation pressure gradient increases from 0.12 atm/m in the west and north to 0.18 atm/m in the east and southeast. The depth to the top of the overpressure zone is shallower where the amplitude

of structures is lower and depth to the top of Miocene Bhuban Formation is shallower. Therefore, the depth to the top of overpressure becomes shallower toward the east.

Miocene Bhuban sediments exhibit transformation of smectite into illite through intermediate illite/smectite mixed layer clay. The most important change is the loss/gradual decrease of the illite/smectite mixed layer clay, which indicates gradual diagenetic changes with increasing burial depth.

Compaction–induced hydrofracturing and clay injection have been identified in the Fenchuganj–2 well below the overpressure zone. Feldspar dissolution has played an important role in secondary porosity development in the Bengal basin.

$^{40}Ar/^{39}Ar$ analysis of detrital muscovite from the Kamta–1 well provides muscovite cooling ages between ca 15 Ma and 554 Ma. However, the youngest age cluster in all three samples shows average cooling ages ranging from #15 Ma to 16 Ma. Considering the average cooling age and depth of the samples, rate of deposition is estimated to be 0.96 mm/year to 1.88 mm/year.

Incomplete dewatering of fine–grained sediments, smectite dehydration, increase in pressure gradients toward the east, and high rates of sedimentation contributed the development of overpressure in the eastern Bengal basin.

ACKNOWLEDGEMENTS

First of all, I would like to convey my heartfelt gratitude to my advisor Dr. Ashraf Uddin for bringing me here to Auburn University, where I have been able to further my studies and do my Masters in Geology. Over the last two years, he has been a loyal and faithful mentor who extended his hand to whatever need I had.

Secondly, I would like to thank the members of my advisory committee, Dr. Ming–Kuo Lee, Dr. Charles E. Savrda, and Dr. Willis E. Hames. They have shown me great patience and have helped me in any queries I had. I am most grateful to them for spending their valuable time and reviewing my thesis and for providing helpful feedback, without which this end result would not have been possible.

Thirdly, I would like to thank Bangladesh Petroleum Exploration & Production Company Limited (BAPEX) for providing me with the data upon which I have been able to build my research. I would also like to thank Albrecht Schmidt laboratory in chemistry department of Auburn University for allowing me to use their X–ray diffractometer and also the helpful students of the chemistry department for their generosity.

Fourthly, I would like to convey a special thanks to Zohir Uddin from Dhaka University, Bangladesh for helping me in collection of data or anything else that I had needed over the last two years to build this project. He had given his valuable time and energy without asking for anything in return. He had also given me immense encouragement for which I am forever grateful to him.

Fifthly, I would like to thank my colleagues, friends and my family, and Mrs. Uddin for their unconditional support, love and encouragement. I honestly have no words to express the gratitude I feel towards my wife who has stayed by my side and patiently supported me in all the ups and downs I had to go through over the last two years in building this thesis.

Last but not least, I would like to convey my gratitude to the National Science Foundation (EAR–0310306), the Geological Society of America, and Auburn University who funded my research and studies, without which this chapter of my life would have never happened.

Style manual or journal used

Geological Society of America Bulletin

Computer software used

Adobe Photoshop CS2

Adobe Illustrator CS

ArcGIS Desktop 9. 2

Golden Software Grapher 5®

Golden Software Surfer 8®

Microsoft Office Excel 2007

Microsoft Office PowerPoint 2007

Microsoft Office Word 2007

Thomson EndNote X

TABLE OF CONTENTS

LIST OF FIGURES

LIST OF TABLES

CHAPTER 1: INTRODUCTION

1.1 INTRODUCTION

Many sedimentary basins throughout the world exhibit some degree of non–hydrostatic fluid pressure, particularly overpressure (Hunt, 1990; Fertl et al., 1994; Neuzil, 1995; McPherson and Garven, 1999; Xie et al., 2001; Zahid and Uddin, 2005). Proximity to the Indian craton, the Himalayas, and the Indo–Burman ranges and rapid orogenic sedimentation have resulted in the common occurrence of overpressure zones in the Bengal basin. In eastern Bangladesh, overpressure zones frequently have been reported in Miocene formations in exploratory wells (Khan and Husain, 1980; Zahid and Uddin, 2005). Incomplete dewatering of fine–grained sediments, clay diagenesis, and tectonic compression associated with the Indo–Burman ranges are possible causes for overpressure development in the Bengal basin (Zahid and Uddin, 2005).

Although overpressure zones are known to host prolific hydrocarbon reserves in many parts of the world (Law and Spencer, 1998), their status in Bangladesh is not satisfactorily known. Nevertheless, considering the wide distribution of overpressure zones in the basin and the occurrence of hydrocarbons in similar deltaic sequences elsewhere, the prospect of finding hydrocarbons in the overpressure zones in Bangladesh cannot be ruled out (Imam and Hussain, 2002). The primary objective of this research is to study the distribution of overpressure zones in the Bengal basin and their relation to compressional tectonics and rapid sedimentation.

1.2 GEOGRAPHIC CONTEXT OF THE BENGAL BASIN

The Bengal basin lies roughly between 20°34′ to 26°38′ N and 88°01′ to 92°41′ E (Fig. 1.1). It is located in the northeastern part of the Indian subcontinent between the Indian shield to the west and the Indo–Burman ranges to the east. The basin is located primarily in Bangladesh with a smaller part in the West Bengal State of India. The Himalayas and the Shillong Plateau bound the basin to the north. The Bengal basin is open towards the south and extends into the Bay of Bengal. It has one of the world's largest deltaic plains, associated with the flow of three big rivers – the Ganges, the Brahmaputra, and the Meghna.

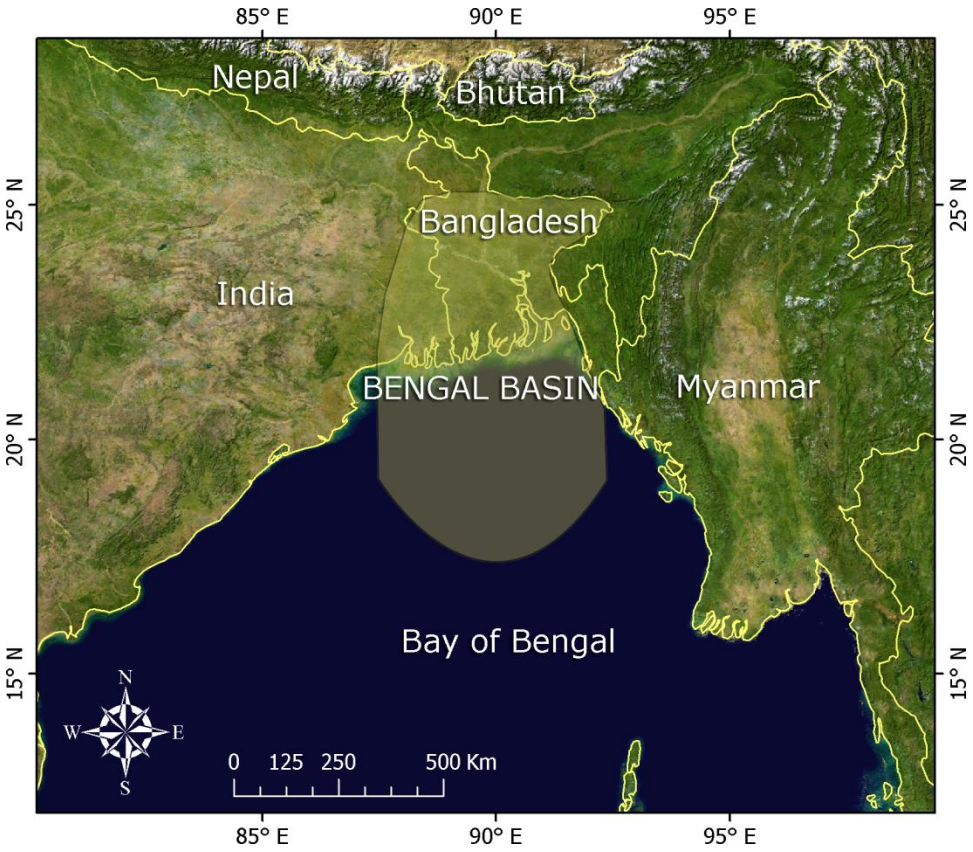

Figure 1.1 Location of the Bengal basin and surrounding areas [data source: Geography network services hosted by Environmental Systems Research Institute (ESRI)].

1.3 PREVIOUS STUDIES OF OVERPRESSURE

1.3.1 General

Many mechanisms for the generation of overpressure in sedimentary basins have been proposed (Osborne and Swarbrick, 1997). The most commonly cited mechanisms of overpressure generation are disequilibrium compaction and hydrocarbon generation (Law and Spencer, 1998; Ruth et al., 2003; Hansom and Lee, 2005). An increase in horizontal stress (tectonic loading) is recognized as a potential overpressure–generating mechanism (Berry, 1973; Yassir and Bell, 1996). There is a strong relationship between the occurrence of overpressure and contemporary compressional tectonics worldwide (Ruth et al., 2003). Tectonic loading can generate overpressure by increasing mean stress and thereby causing disequilibrium compaction–related overpressure (Yassir and Bell, 1996; Goulty, 1998).

Overpressure detection is based on the premise that pore pressure affects compaction–dependent geophysical properties such as density, resistivity, and sonic velocity (Bowers, 2002; Fig. 1.2). Costly misinterpretations are best avoided by studying a combination of several formation–pressure indicators, including surface and borehole seismic, drilling, and well–log data (Fertl and Chilingarian, 1987). Clay is the preferred lithology for pore–pressure interpretation as excess pore pressure can be preserved in low–permeability media over time (Bowers, 2002).

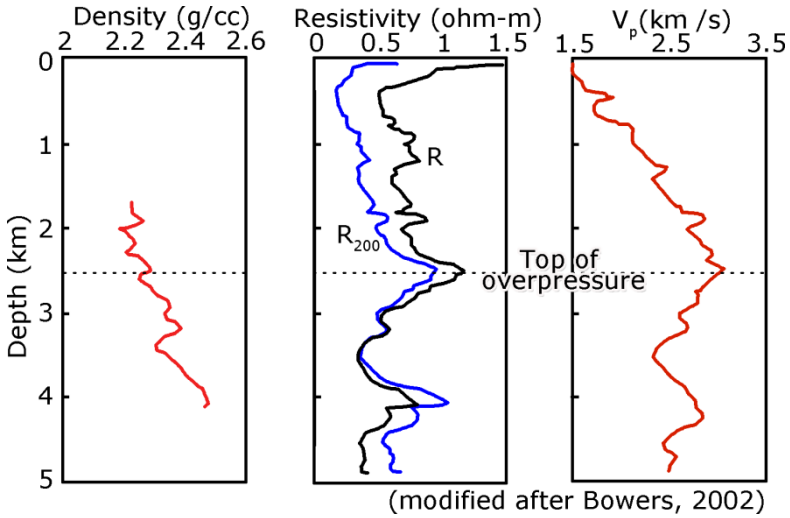

Figure 1.2 High pressure well examples. Sonic and resistivity logs undergo reversals not seen by the density logs. Curve R are raw resistivity data, and curve R_{200} are resistivity data corrected to a common temperature of 200°F (modified after Bowers, 2002).

During burial under normal pressure conditions, effective stress increases continually with depth. Density, resistivity, and sonic velocity increase with effective stress. Overpressure prevents effective stress from increasing as rapidly as it would during burial under normal pressure conditions. Consequently, the top of overpressure zones can be identified where compaction–dependent geophysical properties first depart from their normal trends.

Overpressure can be generated within the pore space by fluid expansion mechanisms such as heating, hydrocarbon maturation, and the expulsion/expansion of intergranular water during clay diagenesis (Bowers, 1995). Here, overpressure results from the rock matrix constraining the pore fluid as the fluid tries to increase in volume. Load transfer from smectite grains to pore water during illitization is another potential way that clay diagenesis can cause overpressure (Lahann, 1980; Bowers, 2002).

Fluid expansion–like overpressure also can result from a sealed interval having pore fluid pumped into it from another, higher-pressure zone. Sometimes this can be caused by charging along faults. It also can occur along dipping sands enclosed in shale. This process is known as lateral transfer (Yardley and Swarbrick, 2000). Lateral transfer can generate pore pressures high enough to fracture overlying shale seals (Bowers, 2002).

Trapped pore fluid squeezed by tectonically driven lateral stresses induces overpressure in the same way that undercompaction does. However, unlike undercompaction, tectonic loading is capable of generating high overpressure (Yassir and Addis, 2002). This also means that tectonic loading can cause vertical effective stresses to decrease. However, in tectonic environments, compaction is no longer controlled by vertical effective stress alone (Bowers, 2002).

Wolf et al. (2005) used mathematical and numerical modeling techniques to evaluate overpressure resulting from topographic–driven flow in the Mississippi Embayment. They showed that gravity–driven flow generates overpressure at the end of the flow domain, i.e., in the discharge zone. This model can be applied to the Bengal basin with large formation slope maintained by the Himalayas.

1.3.2 Overpressure in the Bengal basin

The history of hydrocarbon exploration in Bangladesh began in 1910 when the Indian Petroleum Prospecting Company and Burma Oil Company (BOC) drilled four exploratory wells in Sitakund Anticline of southeastern Bangladesh. Subsequently, fifty–two onshore and twelve offshore exploration wells were drilled through 2002, twenty–two of which have been reported as lucrative (Imam and Hussain, 2002).

The majority of the wells drilled so far in eastern fold belts and foreland basin areas of the Bengal basin encountered overpressure zones in the Lower Miocene Bhuban Formation (Surma Group) at depths ranging from between less than 1 km (Patharia-5) to 4.5 km (Muladi-1; Imam and Hussain, 2002). Based on similar studies of Tertiary deltaic sequences elsewhere (Law and Spencer, 1998; Swarbrick and Osborne, 1998), it seems probable that the overpressure zones are caused by compactional disequilibria of thick shale sequences in the Bhuban Formation (Imam and Hussain, 2002). Clay dehydration also may have contributed to increasing overpressure; illitization and clay dehydration in the Neogene Surma Group shale sequences in a number of wells in the area have been reported (Imam and Shaw, 1985; Imam, 1994; Imam and Hussain, 2002). Similar phenomena have been observed in the California coast range, where tectonics played a major role in overpressure development (Berry, 1973). Rapid subsidence and sedimentation played a dominant role in overpressure development in the U.S. Gulf coast (Dickinson, 1953 ; Bethke, 1986). Zeng and Xiao (2003) studied overpressure generation in the Kuche foreland thrust structural belt of China. After a careful inquiry of geological characteristics of overpressure, study of tectonic stress field and physical simulation experiments, these authors concluded that level tectonic compression in the late of Himalayan Movement is most likely the mechanism for overpressure development in the Kuche foreland thrust belt. Consequently, occurrence of overpressure in the eastern Bangladesh similarly could be due to late movements in the Himalayas.

Very little work has been done to study the overpressure zones in eastern Bangladesh. Zahid (2005) attempted to compare seismic velocity data with temperature,

depth, and lithologic information to understand the overpressure phenomenon in only four exploratory wells of eastern Bangladesh. Zahid and Uddin (2005) showed that acoustic velocity decreases due to the presence of overpressured mudrocks in the lower Miocene Bhuban Formation. Tectonic compression, associated with plate convergence may have contributed the most to the formation of subsurface overpressure.

Uddin and Lundberg (2004) described Miocene sedimentation and subsidence patterns in the Bengal basin. According to their investigation, deltaic progradation in Miocene followed earlier deltaic accumulation closer to the Himalayas in the Eocene–Oligocene. Since the Miocene, the deltaic depocenter has continued to prograde southward toward the Bengal deep–sea fan. Zahid (2005) canvassed Oligocene and lower Miocene sequences of the Bengal basin and suggested a mixed provenance from the Indian craton and the Himalayan orogenic belts. This research helps better understand overpressure and tectonics in the Bengal basin and, hence, will be of importance in future petroleum exploration.

CHAPTER 2: BENGAL BASIN

2.1 INTRODUCTION

The Bengal Basin, a major geotectonic element of the Assam–Himalayan region, is considered to be the largest depositional feature in the world today (Graham et al., 1975; Salt et al., 1986; Kuehl et al., 1989). It is located in the northeastern part of the Indian subcontinent between the Indian shield to the west and Indo–Burman ranges to the east. The Himalayas and Shillong Plateau bound the basin to the north. The Bengal basin is open toward the south and extends into the Bay of Bengal (Fig. 2.1).

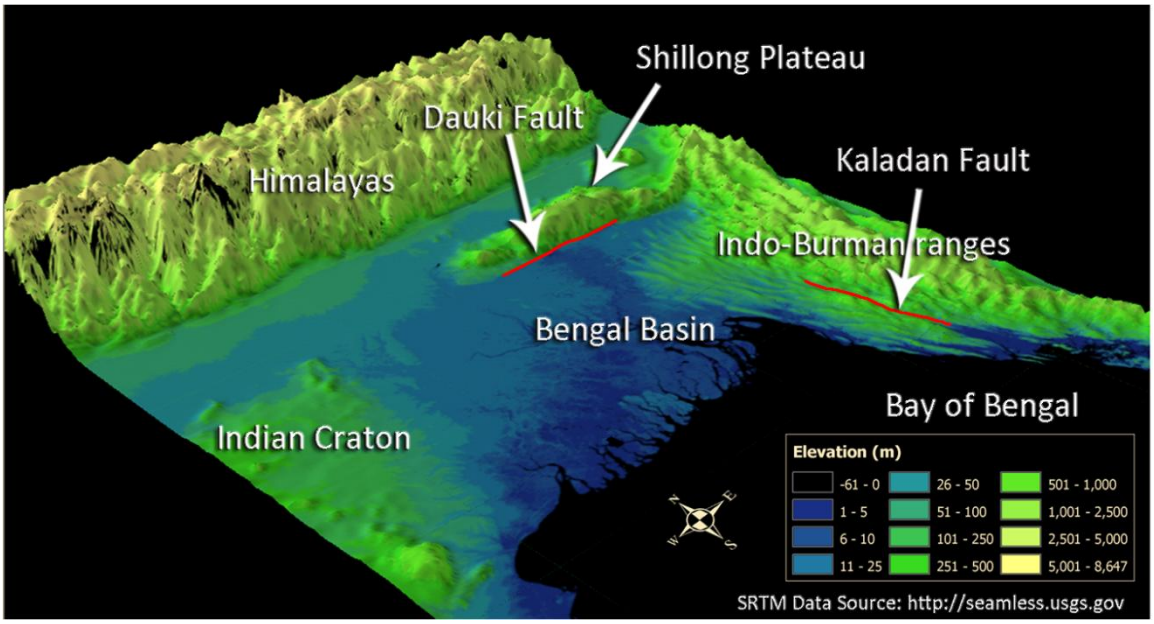

Figure 2.1 Major tectonic elements in and around the Bengal basin. The Dauki fault separates the Sylhet trough from the uplifted Shillong Plateau to the north. The Kaladan fault demarcates the eastern edge of the Bengal basin (data source: http://seamless.usgs.gov).

The dynamic nature of the Bengal basin can be attributed to the interaction of the Indian, Tibetan (Eurasian), and Burmese plates. Temporal variations in plate–to–plate interaction affected basin architecture and sedimentation patterns.

Bengal basin began to develop in the Early Cretaceous (~127Ma) when the Indian plate drifted apart from Antarctica along an inferred northeast-southwest-trending ridge system (Sclater and Fisher, 1974). After plate reorganization about 90 Ma, the Indian plate migrated rapidly northward and collided with Asia between 55 and 40 Ma (Curray et al., 1982; Molnar, 1984; Rowley, 1996). After collision, the Indian block started to rotate in a counter–clockwise direction (Lee and Lawver, 1995) and the basin in the east began to close from north to south (oblique subduction). However, the rise of Himalayas may not have begun until the Miocene (Gansser, 1964).

Sedimentation in the Bengal basin has been controlled by Indian–Tibetan–Burmese plate interaction and by upheaval and erosion in the Himalayas (Alam, 1989). The sedimentation in the Basin has been continuous since the Cretaceous except for some localized hiatuses.

2.2 STRUCTURE AND TECTONICS

Bengal basin is gradually closing due to oblique subduction and orogeny along the eastern and northern margins (Rowley, 1996). The Bengal basin is asymmetric; sediment thickness increases toward the south and the east (Bakhtine, 1966; Curray and Moore, 1971; Murphy, 1988; Khandoker, 1989; Uddin and Lundberg, 2004). The basin contains approximately twenty kilometers of Cenozoic siliciclastic sediments. The basement of the Indian platform slopes to the northwest and southeast from a central

ridge, which is underlain by the shallowest occurrence (~140 m) of Precambrian rocks in Bangladesh. These basement rocks are the eastward subsurface continuation of the Indian shield.

The Bengal basin has two broad tectonic provinces: (1) the stable shelf, where thin sedimentary successions overlie the rocks of the Indian craton in the northwestern part of Bangladesh and (2) thick basin fill that overlies the basement of undetermined origin in the south and east (Bakhtine, 1966; Khandoker, 1989). These two provinces are separated by a northeast–southwest trending hinge zone (Fig. 2.2; Sengupta, 1966).

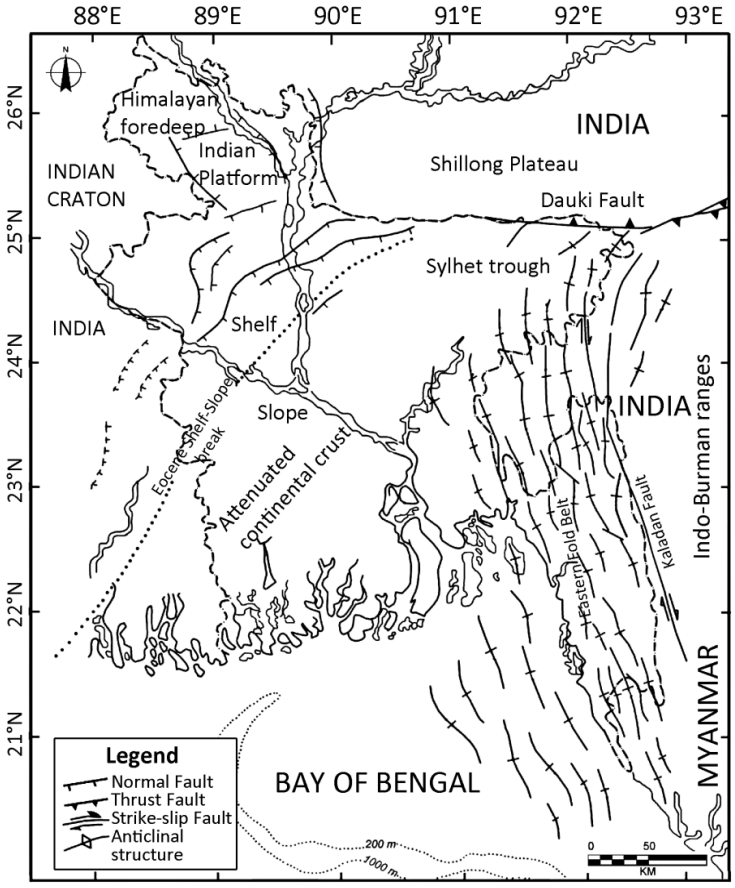

Figure 2.2 Structural elements of the Bengal basin showing Eocene hinge zone (shelf–slope break), Dauki fault, which separates Shillong Plateau from Sylhet trough, and anticlinal trends in the eastern Bengal basin (modified after Hoque, 1982).

Desikachar (1974) proposed a plate tectonic model to explain the origin of the Bengal basin. He considered the Bengal basin as a peri–cratonic basin of the Indian plate, where the central portion of the Bengal basin forms part of the Indian plate and the eastern margin is actually part of the Burmese plate. The Burmese plate moved toward the Indian plate beginning in the Miocene and overrode the Indian plate as the two plates converged (Uddin and Lundberg, 2004). This convergent margin has been complicated by right–lateral strike–slip motion (e.g., along the Kaladan and Sagaing faults), possibly throughout the history of the collision (Ni et al., 1989; Uddin and Lundberg, 2004).

The Bengal basin is essentially an Oligocene to Recent sedimentary depocenter (Salt et al., 1986). The evolution of the Bengal basin started in early Cretaceous with rifting of the Indian plate away from Antarctica. However, the basin did not become a major depocenter until the northward–drifting Indian plate collided with the Eurasian plate, resulting in the initial uplift of the Himalayas (Curray and Moore, 1971; Molnar and Tapponnier, 1975; Lindsay et al., 1991; Imam and Hussain, 2002). The motion of the Indian continent slowed markedly from the early Eocene to early Oligocene and then resumed in a north–northwesterly direction (Sclater and Fisher, 1974; Uddin and Lundberg, 2004). Deposition in the Bengal basin accelerated with the arrival of clearly orogenic sediments from the Himalayas and Indo-Burman ranges during the earliest Miocene (Brunschweiler, 1980; Imam and Hussain, 2002). From at least the Miocene to the present, the Ganges–Brahmaputra and associated or ancestral rivers have been transporting clastic sediments to the Bengal basin (Uddin and Lundberg, 1999).

The deeper part of the Bengal basin is bounded by the hinge zone to the west and the fold belt to the east (Fig. 2.2). The Bengal basin covers approximately 11,000 square kilometers, roughly half of which records deposition within offshore settings (Reimann, 1993). The width of the basin ranges from 200 km in the north to more than 500 km in the south where it extends into the Bay of Bengal.

Compared to those in the fold belt area, strata in the deeper basin have experienced limited tectonic deformation. A few deep basement faults and very gentle, low angle folds with narrow closure have been recognized from seismic data (Salt et al., 1986; Murphy, 1988; Imam and Hussain, 2002).

The Sylhet trough in northeastern Bangladesh is characterized by a large, closed, negative gravity anomaly (–84 mGal) (Fig. 2.3; Ali and Raghava, 1985; Zahid, 2005). The sedimentary succession in the Sylhet trough has been estimated to be 12 to 16 km thick (Hiller and Elahi, 1984). It has been studied extensively as result of successful petroleum exploration (Holtrop and Keizer, 1971; Woodside, 1983; Uddin and Lundberg, 2004). The Sylhet trough is a depositional–low located just south of the crystalline Shillong Plateau. Structural relief between the trough and Plateau is about 20 km (Murphy, 1988; Johnson and Nur Alam, 1991; Uddin and Lundberg, 2004). The eastern portion of the deep basin is characterized by north–northwest to south–southeast trending folds (Khan, 1991a). Subsidence may have increased slightly during the Oligocene in response to crustal loading from the developing Indo-Burman ranges (Mitchell, 1993).

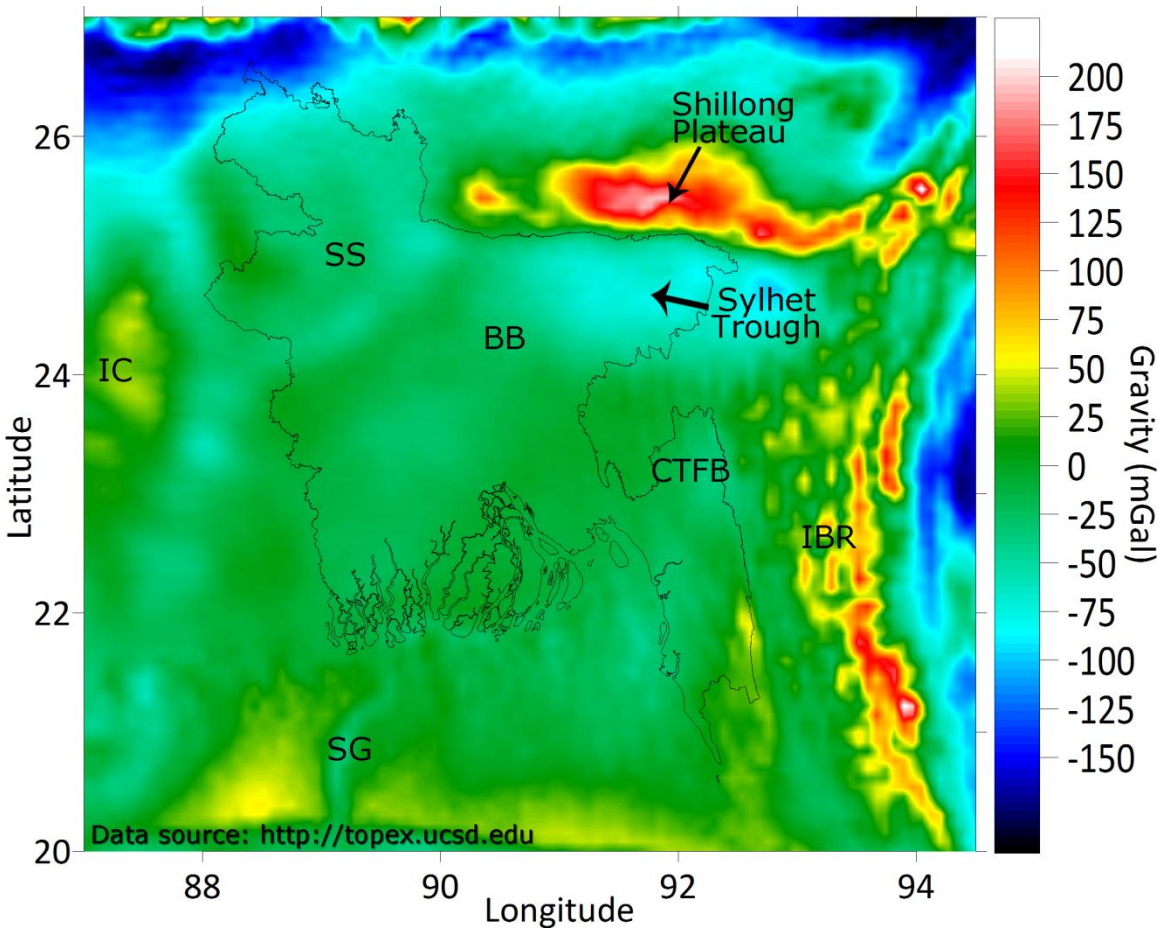

Figure 2.3 Gravity anomaly map of Bangladesh (SS=Stable Shelf, BB=Bengal Basin, CTFB=Chittagong–Tripura Fold Belt, IC= Indian Craton, IBR=Indo–Burman Ranges, SG=Swatch of no Ground; gravity data source: http://topex.ucsd.edu).

2.3 STRATIGRAPHY AND SEDIMENTARY HISTORY

An understanding of the Bengal basin is limited by thick sequences of alluvial cover and relative paucity of fossils. Comparative lithologic studies have been the principle means to establish and to interpret the Stratigraphy (Uddin and Lundberg, 2004). Stratigraphic nomenclature of the Bengal basin has been established based on type sections in the Assam basin (northeast India; Khan and Muminullah, 1980; Uddin and Lundberg, 2004).

Pre–Tertiary stratigraphic units of the Bengal basin are known only from the northwestern part of the basin. A Precambrian basement complex composed of diorite, gneiss, schist, amphibolite, diabase, migmatite, granite, granodiorite, and quartz-diorite makes up part of the Indian craton (Rahman and Sen Gupta, 1980; Zaher and Rahman, 1980; Khan, 1991a; Uddin and Lundberg, 1999; Ameen et al., 2007; Hossain et al., 2007; Hossain and Tsunogae, 2008; Hossain et al., 2009). Basement rocks are overlain by an ~1–km–thick bituminous coal–bearing sequence formed during the Permo–Carboniferous in intracratonic, fault–bounded basins (Zaher, 1970; Zaher and Rahman, 1980). This coal–bearing sequence is overlain by ~500 m of Cretaceous volcanic rocks, the Rajmahal/Sylhet Traps, which are older than the Late Cretaceous Deccan Traps of western India. These are composed of hornblende basalt, olivine basalt, and andesite (Khan and Muminullah, 1980; Uddin and Lundberg, 1999).

The generalized post–Mesozoic stratigraphy of the Bengal basin is shown in Table 2.1. The Paleocene–Eocene units of Tura/Cherra Sandstone have been recovered in drill holes in the northwest platform region (Khan and Muminullah, 1980) and are exposed at a single locality, in a south–dipping block near the Shillong Plateau in the northwestern part of the Sylhet trough (Uddin and Lundberg, 1999). This unit is overlain by middle Eocene open–marine Sylhet Limestone and late Eocene marine Kopili Shale (Reimann, 1993; Shamsuddin et al., 2001; Chowdhury et al., 2003).

The Kopili Shale is overlain by the Oligocene Barail Group. This group, deposited in tide–dominated shelf environments (Alam, 1991) is exposed along the northern fringe of the Sylhet trough near the Dauki fault and its thickness ranges from

Table 2.1 Generalized Cenozoic stratigraphic succession of the Bengal basin (based on Johnson and Nur Alam, 1991; Uddin and Lundberg, 1998a, 1999).

Age	Group	Formation	Thickness (m)	Lithology
Holocene	Alluvium			
Pleistocene	Dihing	Dihing	129	Yellow and gray, medium–grained, occasionally pebbly sandstone
Pliocene	Dupi Tila	Dupi Tila Sandstone	2393	Medium–to coarse–grained, gray to yellow sandstone with clay balls
	Tipam	Girujan Clay	3500	Red, brown, and purple mottled clay with sand lenses
		Tipam Sandstone		Gray to brown, coarse–grained, cross-bedded, massive sandstone
Miocene	Surma	Boka Bil	3100	Alternating shale, siltstone and sandstone
		Bhuban		Sandstone, siltstone, clayey sandstone, clays and lenticular conglomerate
Oligocene	Barail	Renji	800-1600	Coarse–grained sandstone, carbonaceous shale and lenses of coal
		Jenam		Dark gray silty and sandy shale
Eocene to Paleocene	Jaintia	Kopili Shale	15-150	Alternating dark–gray calcareous shale, with thin limestones
		Sylhet Limestone	148	Gray to dark gray, highly fossiliferous limestone
		Tura/Cherra Sandstone	240	White, pink to brown, coarse–grained, cross–bedded, carbonaceous sandstone
Pre–Paleocene	Undifferentiated sedimentary rock			

800 meters (Johnson and Nur Alam, 1991) to 1600 meters (Ahmed, 1983). In platform areas, Barail equivalent rock units are less than 200 meters thick and are known as Bogra Formation (Khan and Muminullah, 1980).

In Assam basin, the upward transition of the Barail Group to the Surma Group reflects transgressive onlap (Banerji, 1981; Salt et al., 1986) , which has been linked to a major upthrust along the Dauki fault during early Miocene or subsidence associated with the subduction zone (Murthy et al., 1976).

The Miocene Surma Group is subdivided into two units: 1) The Bhuban and 2) Boka Bil formations (Holtrop and Keizer, 1970; Hiller and Elahi, 1984; Khan et al., 1988), both of which extend throughout the Bengal basin. The Surma Group was deposited in transitional delta–front settings and comprises progradational sequences (Alam, 1989). The Surma Group is unconformably overlain by the upper Miocene to Pliocene Tipam Group. The Tipam Group consists of the Tipam Sandstone and Girujan Clay units which were deposited in a bed–load dominated, braided–fluvial, and lacustrine environments (Johnson and Nur Alam, 1991; Reimann, 1993). The overlying Dupi Tila Formation was deposited in meandering river environments (Johnson and Nur Alam, 1991).

CHAPTER 3: OVERPRESSURE MECHANICS

3.1 INTRODUCTION

Overpressure, which is fluid pressure higher than hydrostatic pressure (Fig. 3.1), occurs in almost every sedimentary basin. Swarbrick and Osborne (1998) identified four principal aspects of abnormal pressures. These are fluid type, timing and rate of pressure generation/depletion, permeability, and mechanisms that generate abnormal pressure.

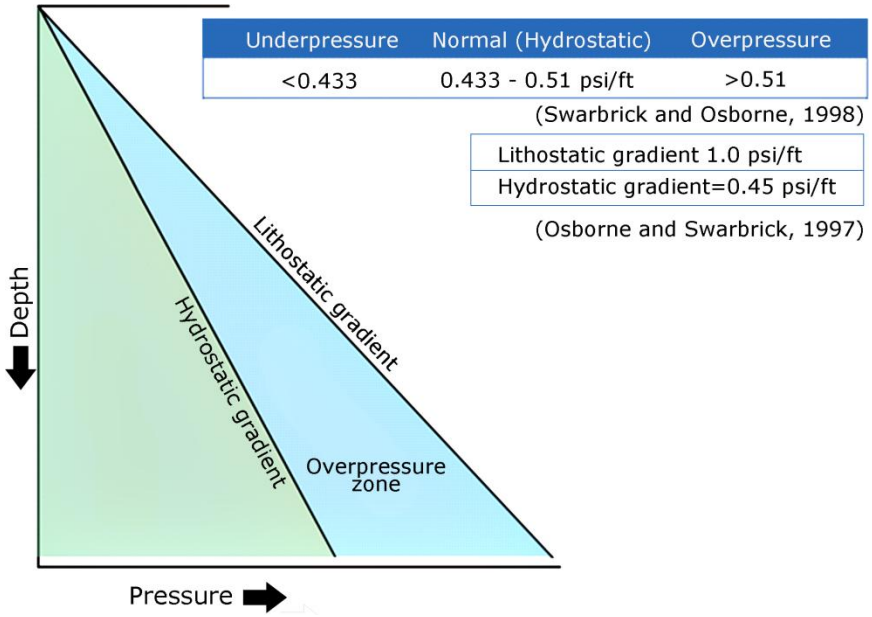

Figure 3.1 A graphical representation of abnormal pressure in the subsurface.

The most common type of fluid in any basin is water, either fresh or brine. Total dissolved solids within the fluid, which affects density and viscosity and influences flow properties, determines the pressure gradient (Swarbrick and Osborne, 1998). Fluid and flow properties, where oil and gas are present, are dependent on the composition of the

hydrocarbons, temperature, hydrocarbon saturation, and rock properties. Hydrocarbons seem to have a significant influence on overpressures, where their buoyancy and capillary effects can control relative permeability and entry pressure (Swarbrick and Osborne, 1998). However, buoyancy is inversely related to fluid density. Areas with elevated pressures often contain less dense fluids, which are more buoyant. An example is the Central North Sea graben where the deeper reservoirs with higher pressures have higher API liquids (American Petroleum Institute gravity, or API gravity is a measure of how heavy or light a petroleum is compared to water) than the shallow, lower pressured reservoirs (Isaksen, 2004).

Abnormal pressures tend to be in disequilibrium and will change over geologic time depending on the rate of generation or dissipation. This change depends on the evolution and dynamics of the system, including effective permeability, which may stay the same or approach zero, the phase of the pressures (over- or under hydrostatic), and temporal (generation or dissipation of pressure). In most cases it is unlikely, and very difficult, to maintain static pressures over geologic time (Swarbrick and Osborne, 1998). Two contrasting models for the development of abnormal pressures can be differentiated on the basis of timing and rate of pressure generation/depletion: the static model (not time dependent) of Hunt (1990); and the dynamic model (time dependant) of Bredehoeft et al. (1994). Fluid pressures are transient; i.e., they will change given enough time.

Permeability is an intrinsic property of a rock that is controlled by size, shape, and torsion of grains and interstitial fluids (Swarbrick and Osborne, 1998). In a petroleum system, permeability differences distinguish reservoir and non–reservoir rocks. Non–

reservoir rocks, or seals, are the primary requirement for the maintenance of abnormal formation pressures; without a seal, pressures would quickly equalize and become normal (Bradley, 1975). There are two distinct types of sealing mechanisms for reservoirs; (1) a seal that forms an impermeable boundary on one or more sides of a reservoir that is still in hydraulic continuity with the surface, and (2) seals that completely isolate a compartment from its surroundings.

The mineral transformation from smectite to illite is the sealing effect produced by the release of Si, Ca, Fe, and Mg ions. Boles and Franks (1979) suggested that the ions released from the shales can migrate into adjacent sandstones and precipitate quartz, chlorite, ankerite, and calcite cements. This could potentially cause cementation at the shale–sand contact and help retain pore waters within the shales. Freed and Peacor (1989), however, argued that the coincidence of overpressure near the depth of the smectite-to-illite transformation results from a reduction in the permeability of the shales not because of cementation promoted by the reaction, but because of cementation promoted by the formation of illite packets within the smectite, which would decrease the number of dislocations available for transport of water and ions, and may produce an effective hydraulic seal.

3.2 MECHANISMS THAT GENERATE OVERPRESSURE

The amount and rate at which abnormal pressures are generated relate directly to the mechanisms that generate them. A wide variety of mechanisms have been proposed for the generation of abnormal subsurface pressures (Fig. 3.2). These mechanisms can be grouped into three main categories: stress-related, fluid volume, and fluid movement and

buoyancy (Swarbrick and Osborne, 1998). Both overpressures and underpressures are generated by mechanisms that fit into each of these categories. Some of the more important mechanisms are those that evolve by mechanical means (Swarbrick and Osborne, 1998).

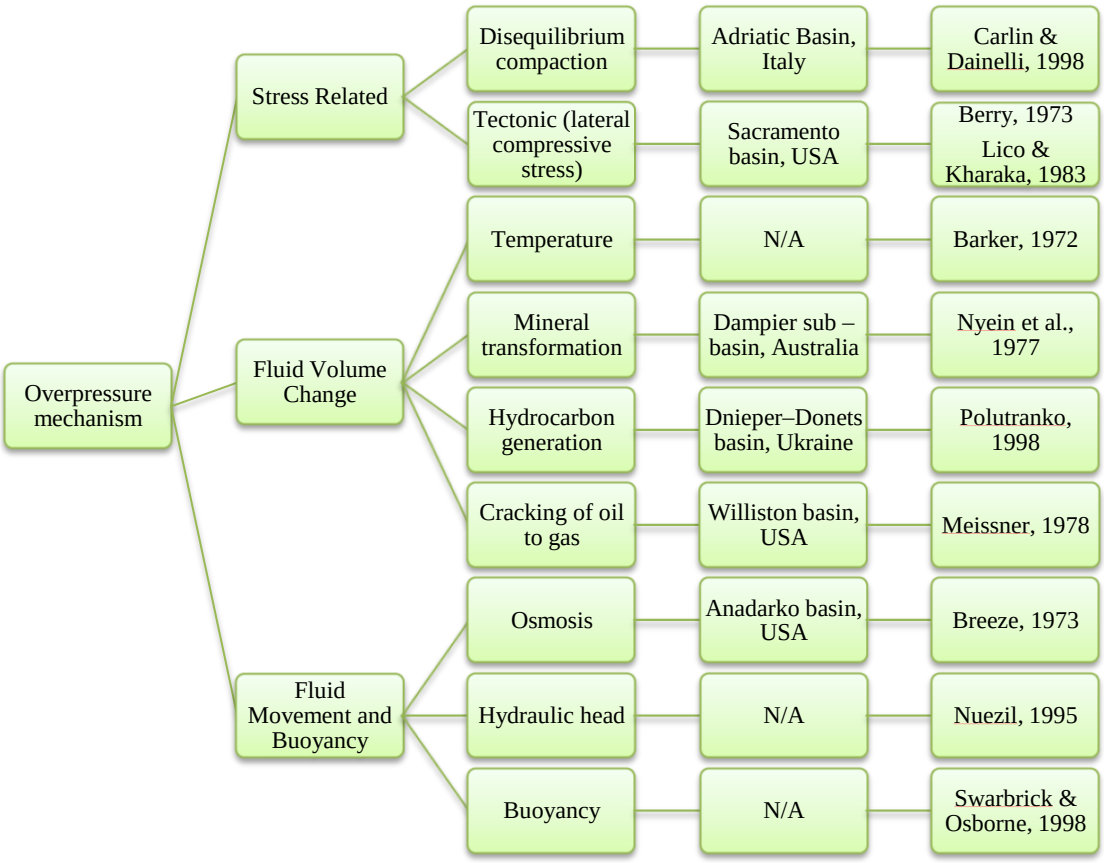

Figure 3.2 Overpressure mechanisms and localities where these mechanisms are believed to function.

3.3 STRESS–RELATED MECHANISMS

Disequilibrium compaction (vertical loading stress): This mechanism is related to the vertical stresses on rocks during burial. Under normal conditions, in either rapid or slow sedimentation, the equilibrium between overburden stress and reduction of pore fluid volume is easily maintained by the expulsion of fluids with simultaneous

compaction. However, in those cases where the fluids cannot be expelled fast enough in low–permeability sediments, the pressure of pore fluids increases, causing disequilibrium compaction (Swarbrick and Osborne, 1998).

Tectonic (lateral compressive stress): The same outcome as the disequilibrium compaction is generated from tectonic stresses. Compaction and incomplete dewatering occurs, but in this case the stresses are applied by horizontal tectonic compression. This is often the overpressure mechanism that operates along major fault zones, both within the fault and adjacent strata (Swarbrick and Osborne, 1998).

3.4 MECHANISMS RELATED TO FLUID VOLUME CHANGE

Temperature increase (aquathermal expansion): This principle is based on the expansion of water when heated above 4°C. For this mechanism to increase pressure, the reservoir must be completely contained and isolated from surrounding pressure environments with no change in pore volume (Swarbrick and Osborne, 1998). While several studies (Lee and Williams, 2000; Tanikawa et al., 2008) have shown that the conditions for this mechanism are rarely met , Hunt (1990) suggests that there are deep (~ 3.0 km) diagenetic seals that are laterally extensive enough to satisfy the conditions for aquathermal expansion. However, modeling study showed that this mechanism generates less significant overpressure as compared to disequilibrium compaction (Bethke, 1985).

Mineral transformation: This mechanism generates overpressures as bound water is released during mineral transformations. The most common of these transformations is smectite dehydration. Smectite dehydration can increase the volume of pore fluids by 4.0%, but only if the reservoir is compartmentalized (Swarbrick and

Osborne, 1998). Thus this mechanism is not as important as pore collapse from compaction, which may produce >50% pore volume changes. The transformation of gypsum to anhydrite can potentially generate pressures close to lithostatic stresses (Swarbrick and Osborne, 1998). This transformation is important in evaporate–dominated sections. The transformation of a potentially water–saturated smectite to illite also can generate overpressures, but the overall volume change from reaction is not well constrained (Swarbrick and Osborne, 1998). Most mineral transformations are thought to be secondary mechanisms for overpressure generation; they often occur in conjunction with some degree of disequilibrium compaction (Swarbrick and Osborne, 1998).

Hydrocarbon generation: The generation of liquid and gaseous hydrocarbons from solid kerogen has been linked to the generation of overpressures in the subsurface (Swarbrick and Osborne, 1998). Generation of hydrocarbons from mature source rocks releases fluids (oil and gas) into pore spaces. If the pores are already saturated and the fluid cannot migrate, either due to seals or compartmentalization, the formation pressures should increase. Hansom and Lee (2005) showed that oil generation can cause excess pore pressure up to 40% of that generated by compaction only. Oil and CH_4 generation together yield the maximum excess pressure up to about 150% of that generated by compaction only. In any sedimentary basin, overpressures generated by this mechanism are dependent upon availability of maturing source rocks and TOC (Total Organic Carbon) contents within hydraulic connectivity of the reservoir.

Cracking of oil to gas: Thermal cracking of oil and bitumen to gas is initiated at temperatures of 120°-140°C and completed at temperatures in excess of 180°C. Through

this process one volume of standard crude oil cracks into 534.3 volumes of gas and residue (Swarbrick and Osborne, 1998). If the reservoir is compartmentalized or well sealed, there would be an immediate and dramatic increase in pressure as the oil cracks to gas (Swarbrick and Osborne, 1998).

3.5 FLUID MOVEMENT AND BUOYANCY RELATED MECHANISM

Osmosis: Osmotic pressure arises when two solutions of different salinities are separated by a semi–permeable seal (Fertl et al., 1976). Diffusion will result in the solute transfer from the less dilute to the more dilute solution. If the reservoir on the more concentrated side of the seal is already saturated, then theoretically it should become overpressured. However, there is some doubt concerning the effectiveness of this mechanism. It has been observed that brines in overpressured zones tend to be of lower salinity than adjacent normally pressured brines, which would act to reduce the pressure in overpressured zones (Swarbrick and Osborne, 1998).

Hydraulic head: The hydraulic head or potentiometric head resulting from elevation of the water table in recharge areas will produce an artesian affect if the reservoir is overlain by a seal. This artesian affect, which produces water flow at the surface due to excess pressure, will create overpressured reservoirs in the discharge zone if the reservoir maintains lateral continuity (Swarbrick and Osborne, 1998; Wolf et al., 2005).

Hydrocarbon buoyancy: All gases and most oils have a lower density than the associated formation waters and therefore will always create overpressures where there is a column of oil or gas lying on top of water (Swarbrick and Osborne, 1998). This

mechanism is restricted to structural and stratigraphic traps of hydrocarbons, and does not create regional overpressures (Swarbrick and Osborne, 1998). The amount of overpressures generated by this mechanism is a function of the pressure gradients of oil, gas, and water and the height of the hydrocarbon column. Buoyancy–driven pressures are often not regarded as important by themselves but may add to the effects of other mechanisms (Swarbrick and Osborne, 1998).

CHAPTER 4: GEOPHYSICAL LOG ANALYSIS

4.1 INTRODUCTION

Geophysical well–log data have been widely used to detect overpressure zones in many places, including the Gulf coast of the United States (Fertl et al., 1976), offshore Nova Scotia (Mudford and best, 1989), and eastern Delaware Basin, Western Texas (Luo et al., 1994). Fertl et al. (1976) provided a complete discussion of well–logging techniques to evaluate abnormal formation pressure. Overpressure detection is based on the premise that pore–pressure affects compaction–dependent geophysical properties such as density, resistivity, and sonic velocity (Bowers, 2002). Mudrocks are the preferred lithology for pore–pressure interpretation because they tend to preserve overpressure then most rock types (Bowers, 2002). Consequently, overpressure detection centers around shale deformation behavior (Bowers, 2002). In this study, well–logging data from the eastern Bengal basin were examined to look for evidence of overpressure in the Bengal basin.

4.2 DETECTING OVERPRESSURE

During burial under normal pressure conditions, effective stress (the difference between total applied stress and pore fluid pressure, $\sigma_T = \sigma_e + p$, or $\Delta p = -\sigma_e$, where σ_T=Total applied stress, Δp, σ_e=effective stress, and p=pore–fluid stress) continually increases with depth. Density, resistivity, and sonic velocity also increase with depth. Overpressure prevents the effective stress from increasing as rapidly as it would during

burial under normal pressure conditions (Fig. 4.1). Consequently, the top of overpressure zones is reflected by the departure of compaction–dependent geophysical properties from normal trends.

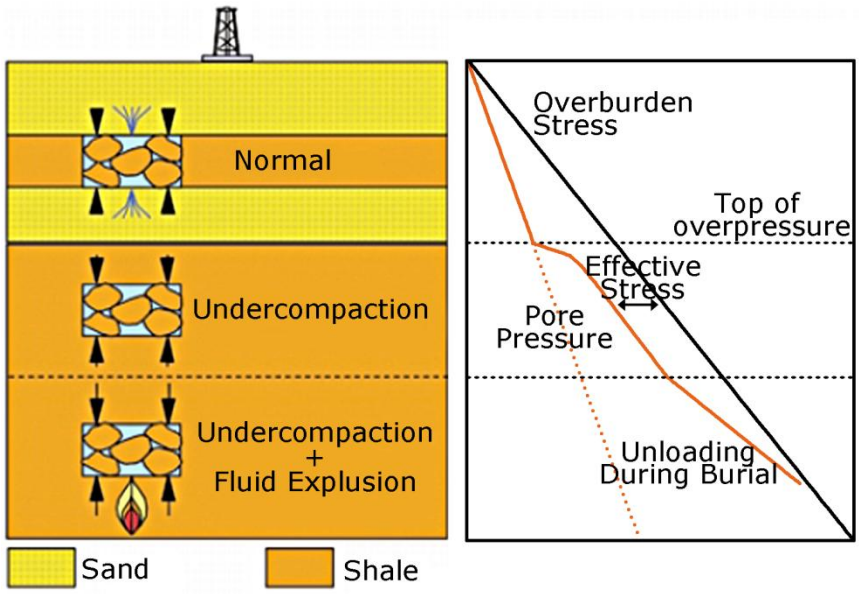

Figure 4.1 Response of vertical effective stress to different overpressure mechanisms (Bowers, 2002).

Overpressure occurs when low permeability prevents pore fluid from escaping as rapidly as pore spaces tries to compact (Bowers, 2002). Excess pressure is generated as newly deposited sediments squeeze the trapped fluid. This process of overpressure generation is known as undercompaction or compaction disequilibrium. It generally occurs where there is a transition between sand–prone and clay–prone deposits. Overpressure generated through undercompaction can be identified by reversals in density, resistivity, and sonic velocity logs, meaning they all drop below normal values at some shallower depth (Bowers, 2002; Fig. 1.2).

Overpressure generated through fluid expansion causes unloading, and will show elastic rebound. Therefore, sonic velocity and resistivity data in highly overpressured intervals should show large reversals than bulk–density measurements.

The factors governing the conductivity of a porous media include fluid content and mineralogy. Generally, conductivity decreases with depth in sedimentary basins buried under normal pressure conditions and dewatering.

Resistivity of a porous media is controlled by porosity, temperature, fluid content, salinity, and mineral composition (Luo et al., 1994). In a sedimentary basin buried under normal pressure conditions, resistivity is expected to increase with depth as the sediments become more compacted and therefore less porous and dry.

The best geophysical tool for overpressure detection is sonic velocity because these logs are relatively unaffected by hole size, temperature, and fluid salinity (Luo et al., 1994). In normal pressure conditions, the interval transit time follows a predictable trend with depth. Transit time decreases with increasing density due to compaction. However, in an overpressured sequence, sonic velocity departs from its usual increasing trend with depth (Fig. 1.2).

Gamma–ray logs are helpful in assessing overpressured zones because they measure the amount of gamma radiation emitted from geological materials and are good indicators of clay content. Overpressure tends to develop within low permeability zones composed of clay materials. Therefore, gamma–ray logs are used to identify changes in clay content.

4.3 METHODOLOGY

Geophysical well logs were used to study the distribution of overpressure in the Bengal basin. The logs were collected from Bangladesh Petroleum Exploration & Production Company Limited (BAPEX). These well logs include sonic, resistivity, gamma, and temperature logs. Resistivity, sonic velocity decreases near the top of overpressure zones. Figure 4.2 shows an example of decrease in sonic velocity near the top of overpressure in the Sitakund–1 well located in the southeastern part of the Bengal basin.

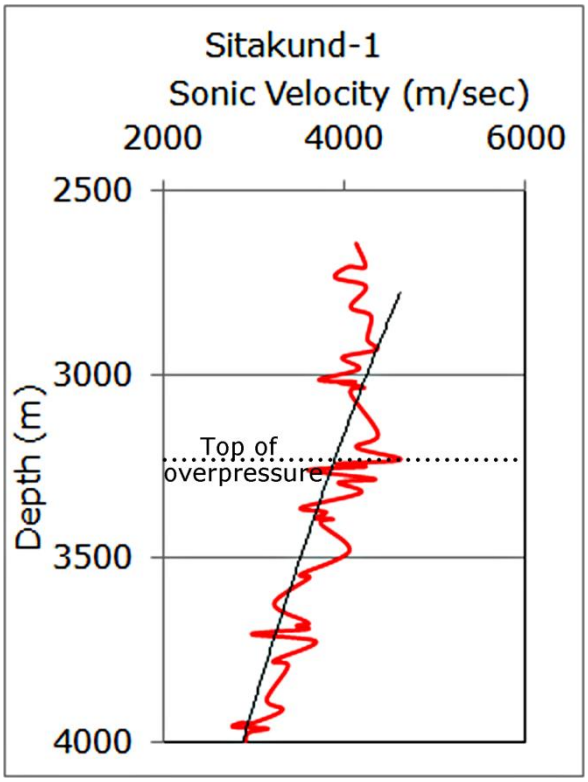

Figure 4.2 Sonic velocity log data shows decrease in sonic velocity with depth in the Sitakund–1 well (modified after Zahid and Uddin, 2005).

Geophysical well logs were first scanned into image format. Golden Software Surfer 8® was used to digitize the logs. Microsoft Excel was used to smooth the digitized

data. Temperature data up to a depth of 4 km were collected from twenty–nine deep exploratory wells (Fig. 4.3). Linear regression method was applied to estimate subsurface temperature at 1 km, 2 km, 3 km, and 4 km depth. Geothermal gradient was calculated for each well. Gamma ray logs also were collected and analyzed to identify changes in clay content. Golden Software Surfer 8® and ArcGIS Desktop 9.2 softwares were used to prepare contour maps. A temperature–depth profile was constructed using temperature data collected from BAPEX and Matin et al. (1982).

Formation pressure data were also collected from BAPEX and a depth–pressure profile was constructed modifying Matin et al. (1982).

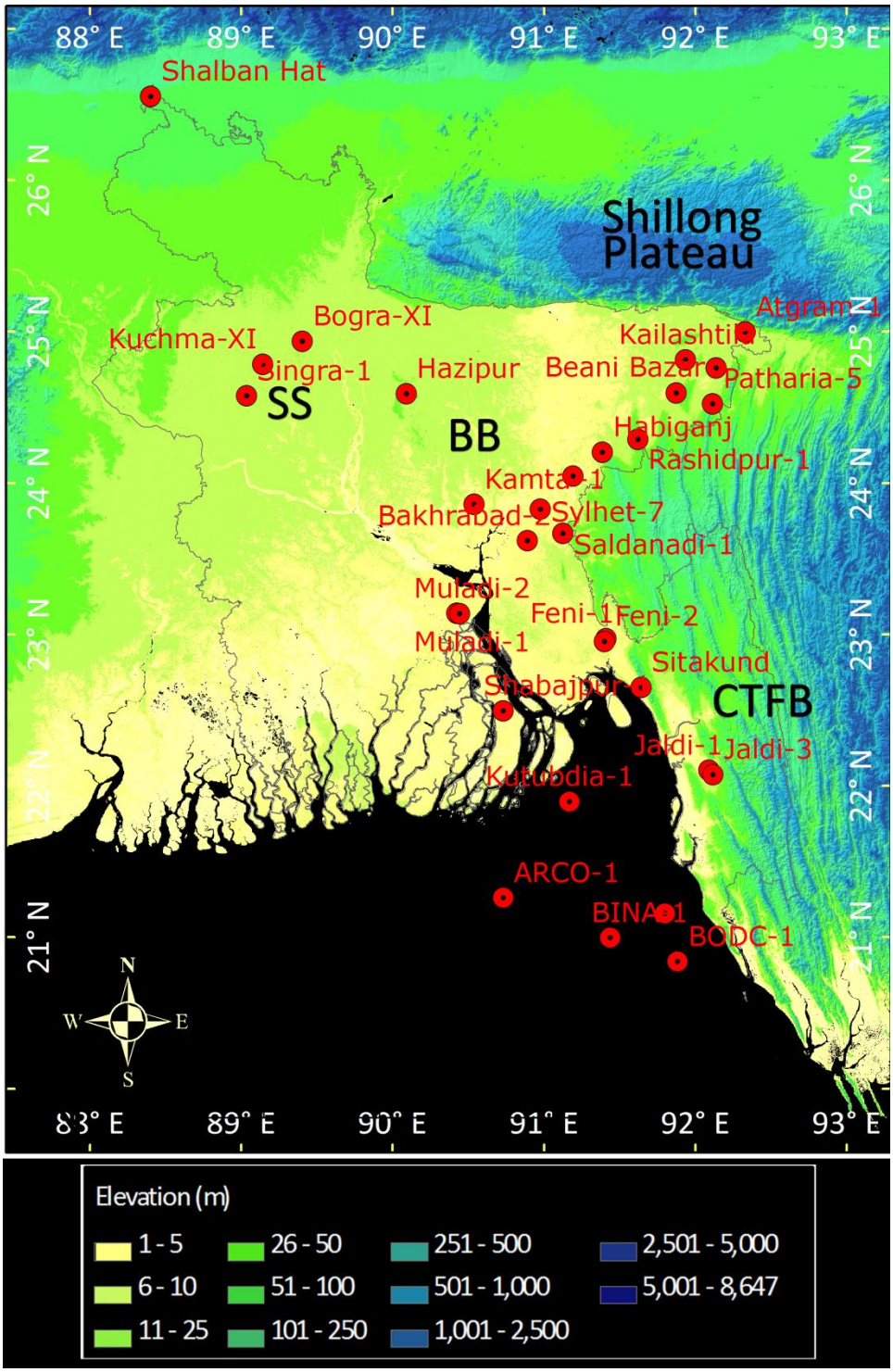

Figure 4.3 Location of geophysical logs used in this study (SS= Stable shelf, BB=Bengal basin, CTFB=Chittagong–Tripura fold belt; data source: Geography network services hosted by ESRI, and BAPEX).

4.4 RESULTS

Subsurface temperature log data used in this study is shown in Table 4.1. Contour maps show subsurface temperature distributions up to 4 km depth (Fig. 4.4).

The deeper parts of the Bengal basin covering central, eastern, and southern Bangladesh have an average geothermal gradient of about 21.3° C/km (Fig. 4.5). However, data from a total of 62 wells drilled in the deeper part of the Bengal basin (22 of which resulted in the discovery of gas) indicate significant variations in geothermal gradient across the basin. In the deeper part of the basin, depths of the petroleum exploratory wells range from 2100 m to 4977 m. The geothermal gradient of these wells ranges from 15.8° C/km to 30° C/km.

In the stable shelf area, temperature data from deep exploratory wells show higher geothermal gradients than the deep basin area to the southeast. Sedimentary thickness in the stable shelf varies from 130 m (Rangpur saddle) to 7 km (Bogra shelf) above a granitic Precambrian basement (Bakhtine, 1966). The geothermal gradient calculated for stable shelf area varies from 21.1° C/km to 31.6° C/km (Fig. 4.5). In Maddhyapara hard rock mine (near Barapukuria coal mine), the 130–meter–thick sedimentary section above the Precambrian basement has a geothermal gradient of 13.3° C/km, whereas the geothermal gradient increases to 32° C/km in the basement rocks.

A temperature–depth profile was constructed for the Bengal basin by adding new data to Matin et al. (1982) diagram (Fig. 4.6). A linear trend line suggests that the average temperature gradient for the selected wells is 30.35° C/km (Fig. 4.6).

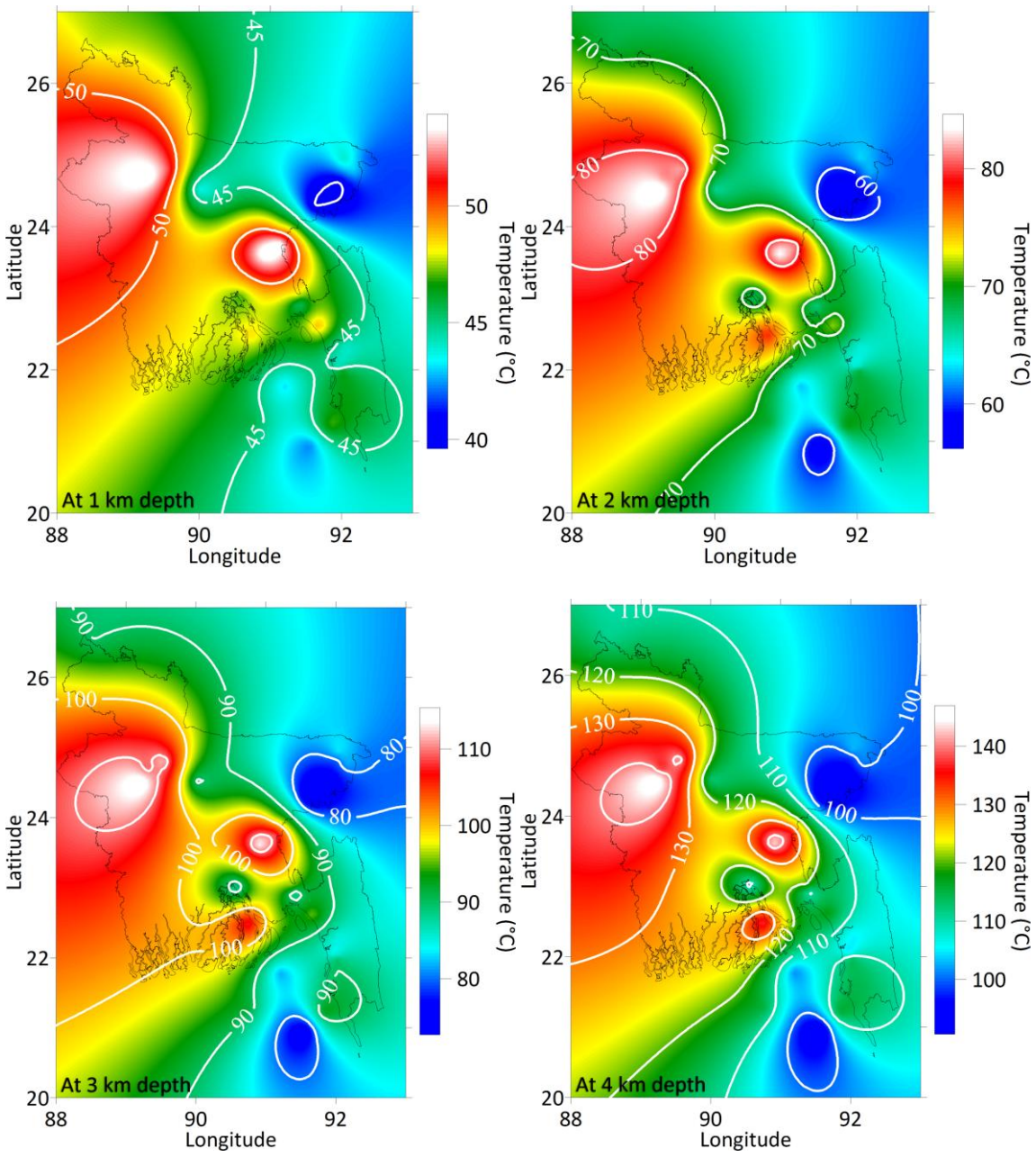

Figure 4.4 Subsurface temperature distributions at 1 km, 2 km, 3 km, and 4 km depth in the Bengal basin (data source: BAPEX).

Table 4.1 Temperature data collected from exploration wells located in the eastern Bengal basin (data source: BAPEX).

Name	Longitude	Latitude	Estimated temperature				Geothermal Gradient (°C/km)
			1 Km	2 Km	3 Km	4 Km	
ARCO-1	90.72861	21.25748	45.7	68.9	91.5	115.0	23.1
Atgram-1	92.32978	24.99588	41.8	61.0	80.5	100.2	19.5
Bakhrabad-2	90.88885	23.61639	54.0	84.0	114.0	144.0	30.0
Beani Bazar	92.13679	24.75859	43.0	62.5	81.8	101.0	19.3
BINA-1	91.43665	20.99455	42.2	56.4	73.0	89.5	15.8
BODC-1	91.88177	20.83720	44.0	64.0	84.0	104.0	20.0
Bogra-XI	89.40175	24.93491	52.0	82.0	112.0	142.0	30.0
Cox's Bazar	91.79688	21.15396	47.0	70.0	93.0	116.0	23.0
Fenchuganj-2	91.87305	24.59348	39.5	57.5	75.5	93.5	18.0
Feni-1	91.40912	22.97042	47.5	71.0	95.0	119.0	23.8
Feni-2	91.39715	22.95150	45.0	66.0	87.0	108.0	21.0
Habiganj	91.38514	24.20239	44.0	64.0	84.4	104.4	20.1
Hazipur	90.08885	24.58864	43.5	66.2	89.5	112.2	22.9
Jaldi-1	92.08836	22.09958	44.0	64.0	84.0	104.0	20.0
Jaldi-3	92.11399	22.07280	46.5	69.0	89.8	114.3	22.6
Kailashtila	91.93514	24.81257	43.0	61.0	79.5	98.0	18.3
Kuchma-XI	89.14137	24.78355	54.0	81.0	109.0	136.0	27.3
Kutubdia-1	91.16751	21.89365	43.0	62.5	81.5	101.0	19.3
Muladi-1	90.42365	23.13880	47.0	67.8	88.0	108.8	20.6
Muladi-2	90.44021	23.13604	47.0	67.8	88.0	108.8	20.6
Patharia-5	92.11238	24.52117	44.0	64.5	85.0	105.0	20.3
Rashidpur-1	91.61837	24.28692	39.9	56.0	72.2	90.4	16.8
Saldanadi-1	91.12409	23.66647	54.0	81.0	109.0	137.0	27.7
Shabajpur-1	90.73006	22.49287	48.5	78.5	108.5	138.5	30.0
Shalban Hat	88.40022	26.55273	47.8	68.5	90.0	111.0	21.1
Singra-1	89.03430	24.57387	53.0	85.0	116.0	147.8	31.6
Sitakund	91.64103	22.64745	49.0	72.0	95.5	118.0	23.0
Sylhet-7	90.97508	23.82465	44.0	63.0	83.5	103.0	19.7
Titas-11	91.18971	24.04294	48.5	72.5	97.0	122.0	24.5

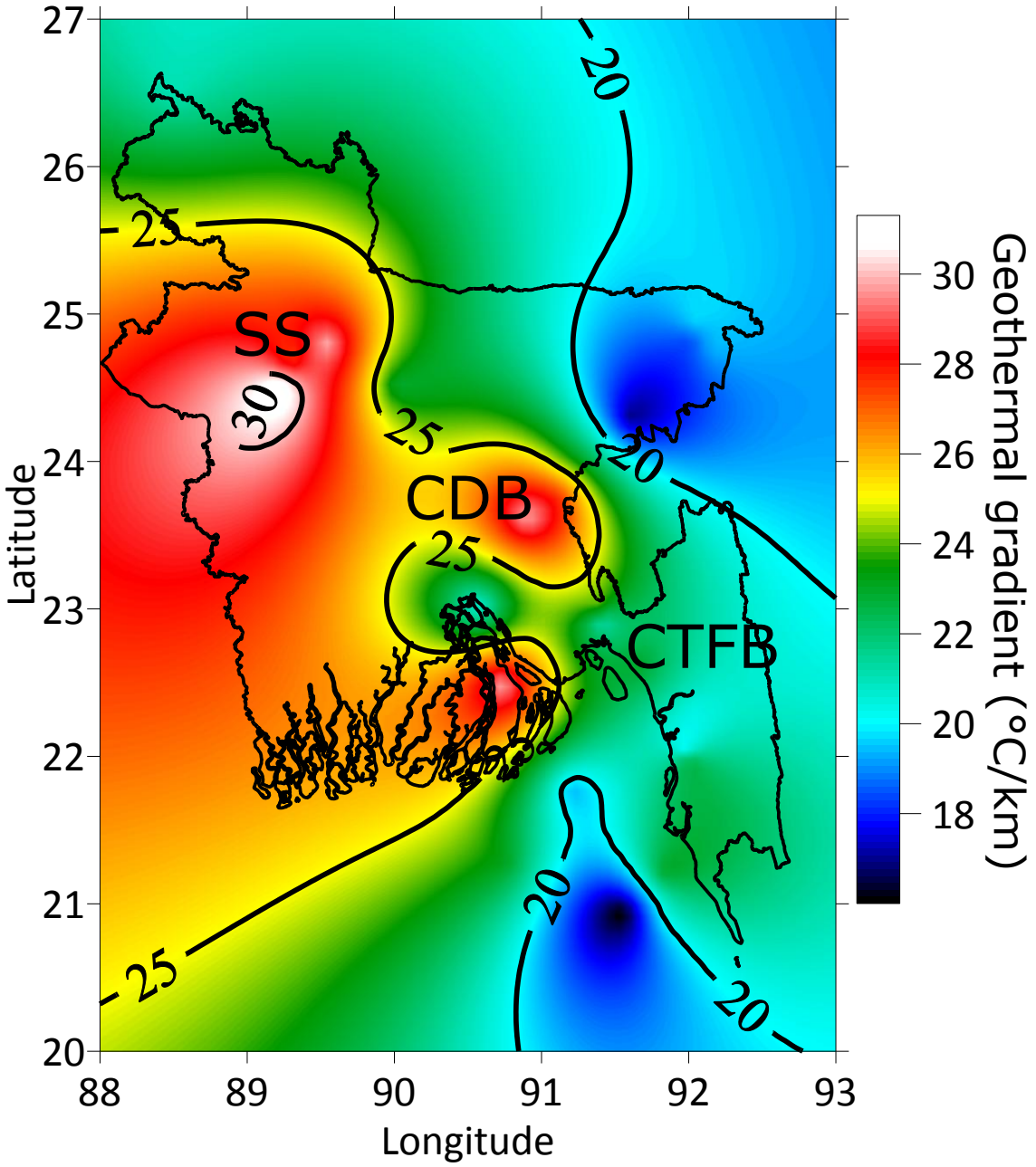

Figure 4.5 Geothermal gradient map of the Bengal basin (SS=Stable Shelf, CDB=Central Deeper Basin, CTFB=Chittagong–Tripura Fold Belt; data source: BAPEX).

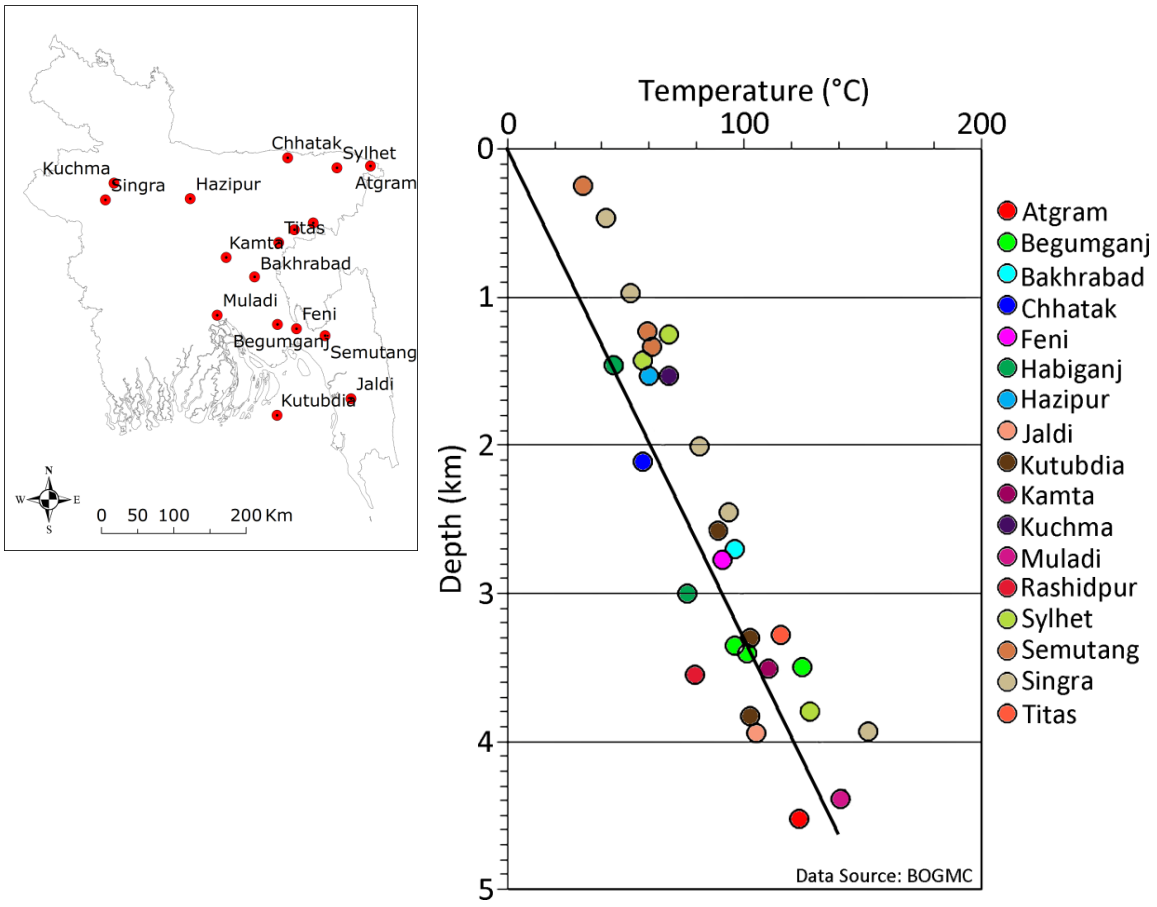

Figure 4.6 Change in formation temperature at depths in the Bengal Basin [data source: BAPEX, and Matin et al. (1982)].

In the Beani Bazar–1X well, the average sonic velocity in the Miocene Bhuban Formation (3640 m – 4109 m) is 4386 m/sec (Fig. 4.7). In this well, sonic velocity gradually increases at shallower depths due to increasing compaction. However, in the Miocene Bhuban Formation, the depth–velocity distributions show an initial decrease in sonic velocity. The velocity gradually increases with depth toward the lower part of the formation. In this area, overpressure zones have been reported at around ~4 km depth.

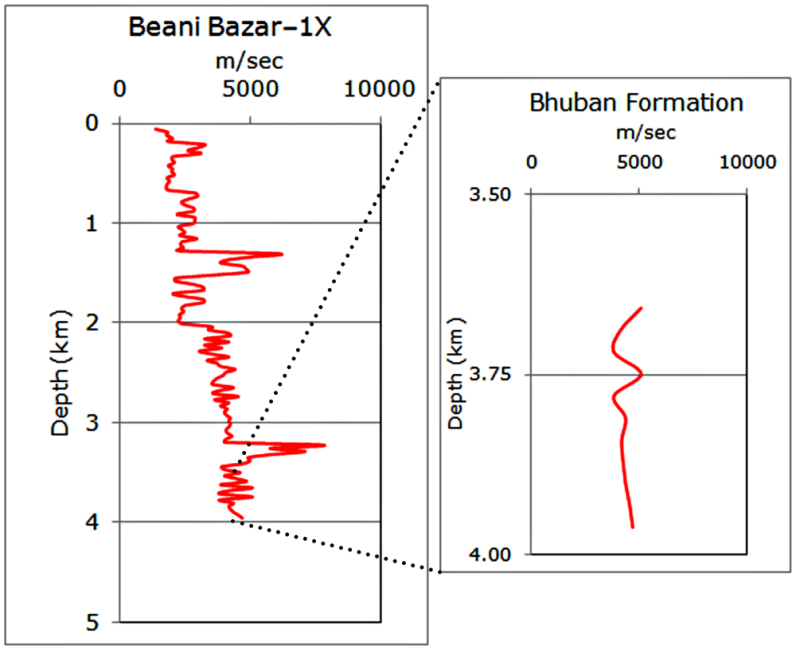

Figure 4.7 Sonic velocity logs for Beani Bazar –1X well shows an initial decrease and then a gradual increase in sonic velocity with depth in the Miocene Bhuban Formation (data source: BAPEX).

Fenchuganj–2 well shows decrease in sonic velocity and formation resistivity below 4.4 km depth (Fig. 4.8). In Fenchuganj structure, overpressure zones have been reported at depths below 3 km. The Habiganj–8 well show decrease in resistivity and sonic velocity from their usual trends at depth below 1.2 km (4.9).

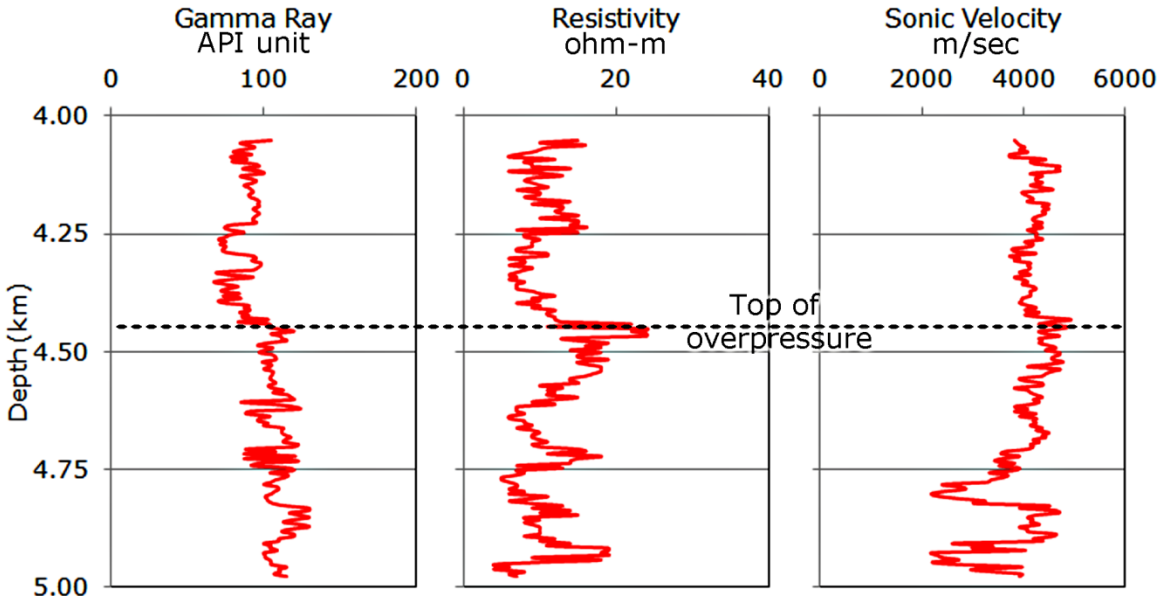

Figure 4.8 Composite geophysical logs for Fenchuganj–2 well show decrease in velocity and resistivity at depths below 4.4 km (data source: BAPEX).

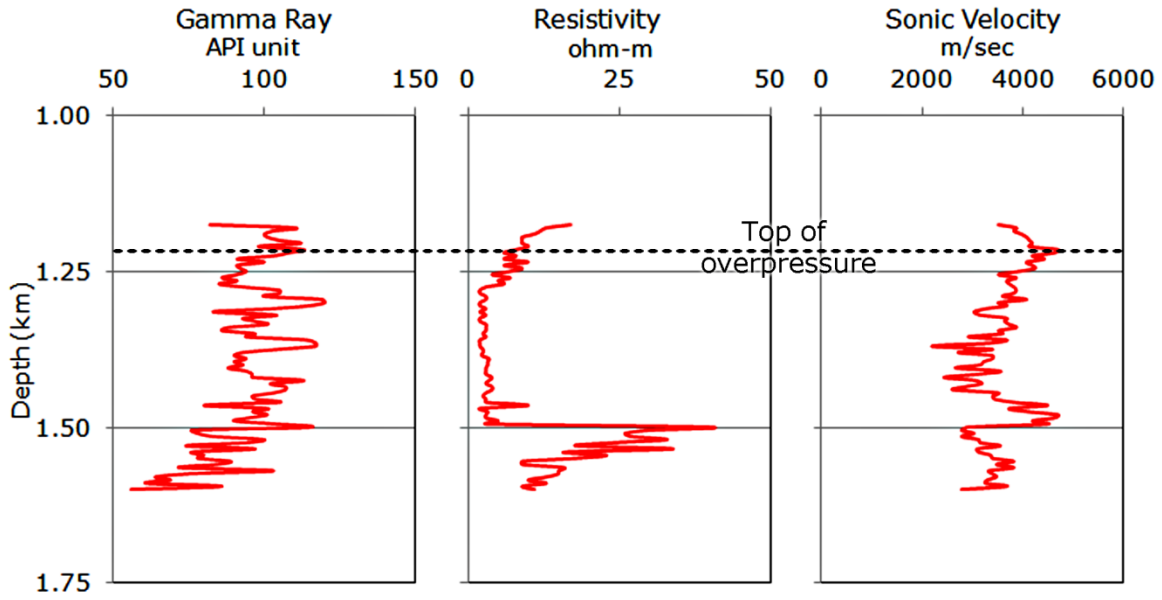

Figure 4.9 Composite geophysical logs for Habiganj–8 well show decrease in resistivity and sonic velocity at depths below 1.2 km (data source: BAPEX).

Zahid and Uddin (2005) studied sonic logs from Bakhrabad, Titas, Sitakund and Rashidpur structures (Fig. 4.10). Accroding to their interpretations, the variation in velocity is 32% from Miocene to Pliocene stratigraphic units in Titas and Bakhrabad structure, whereas 21% in Rashidpur structure (Zahid and Uddin, 2005). The Titas–11, Bakhrabad–9, and Rashidpur–4 wells show a gradual increase of velocity with depth, reflecting a normal trend of velocity increment due to increasing compaction, whereas in the Sitakund structure, the velocity–depth distributions show a short interval of initial increase followed by a decrease in velocity with increasing depth, indicating the probable presence of overpressure zones in the depth range of about 3000–4000 m (Zahid and Uddin, 2005).

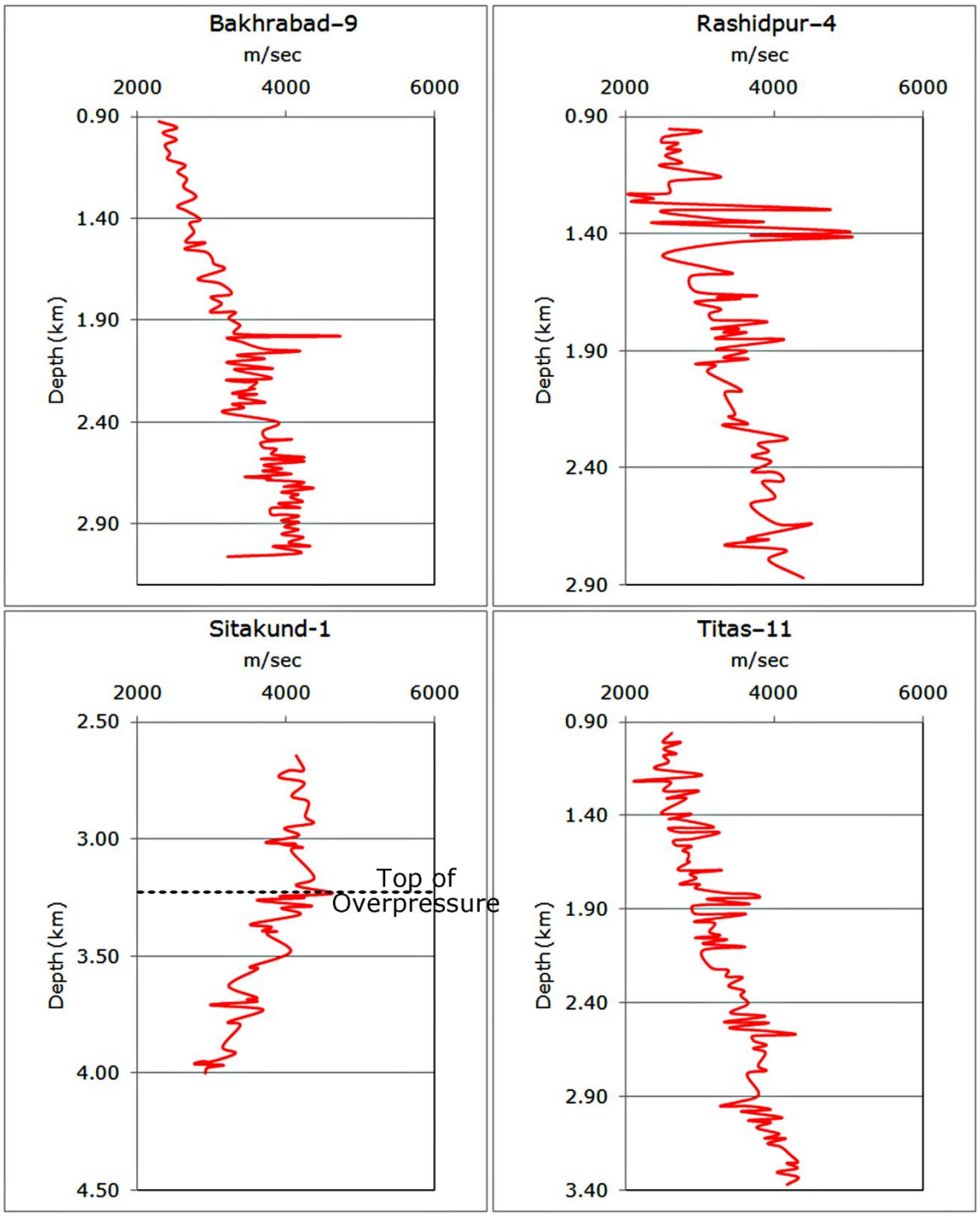

Figure 4.10 Sonic velocity logs studied by Zahid and Uddin (2005). Gradual decrease in sonic velocity with depth in Sitakund–1 well suggests the presence of overpressure zone.

Formation pressure distribution in different wells suggests that most of the exploratory wells drilled in the eastern Bengal basin reflect overpressure (Fig. 4.11). The wells located in the eastern fold belt mostly fall within the overpressure zone (0.0959 atm/m to 0.2232 atm/m). The uplifted Patharia structure located in the northeastern corner of Bangladesh shows a variable pressure gradient ranging from (0.12 atm/m to 0.18 atm/m) at shallower depths (1km–1.5km; Fig. 4.11). Figs. 4.12 and 4.13 show the depth to the top of the Miocene Bhuban Formation and the total thickness of the Bhuban Formation respectively.

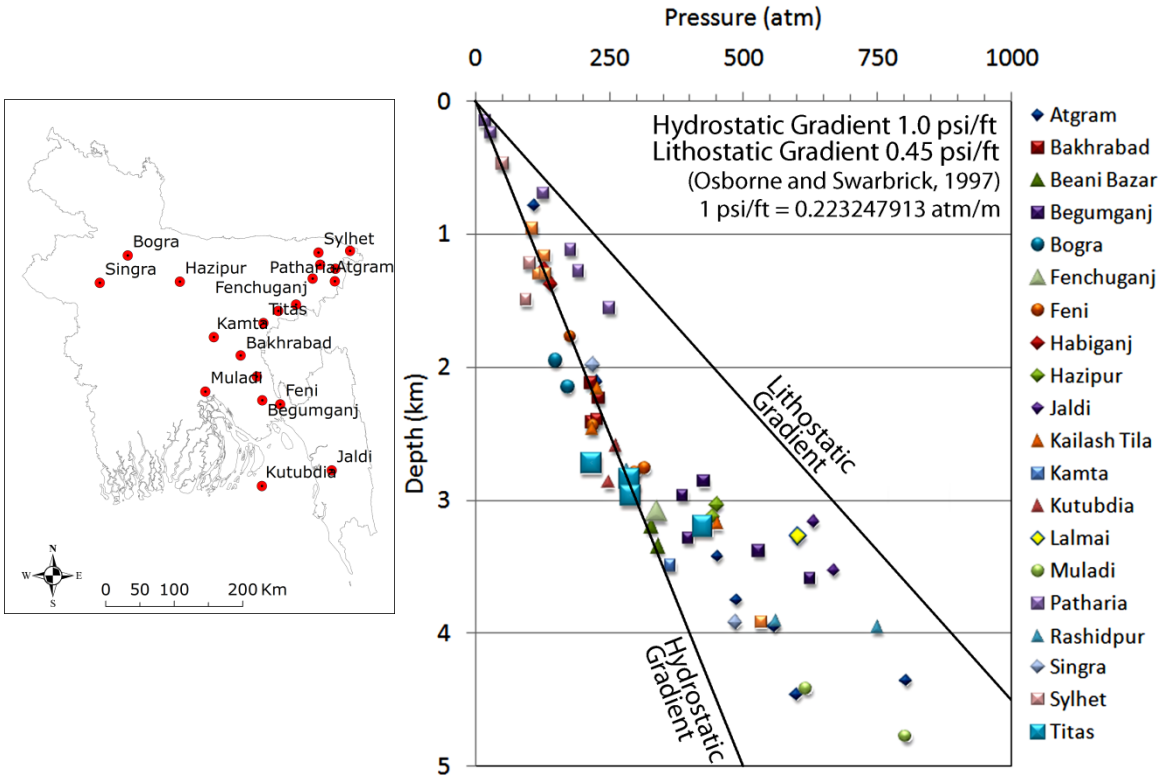

Figure 4.11 Depth–pressure plots indicate that most of the wells in the eastern Bengal basin reflect overpressure [data source: BAPEX, and Matin et al. (1982)].

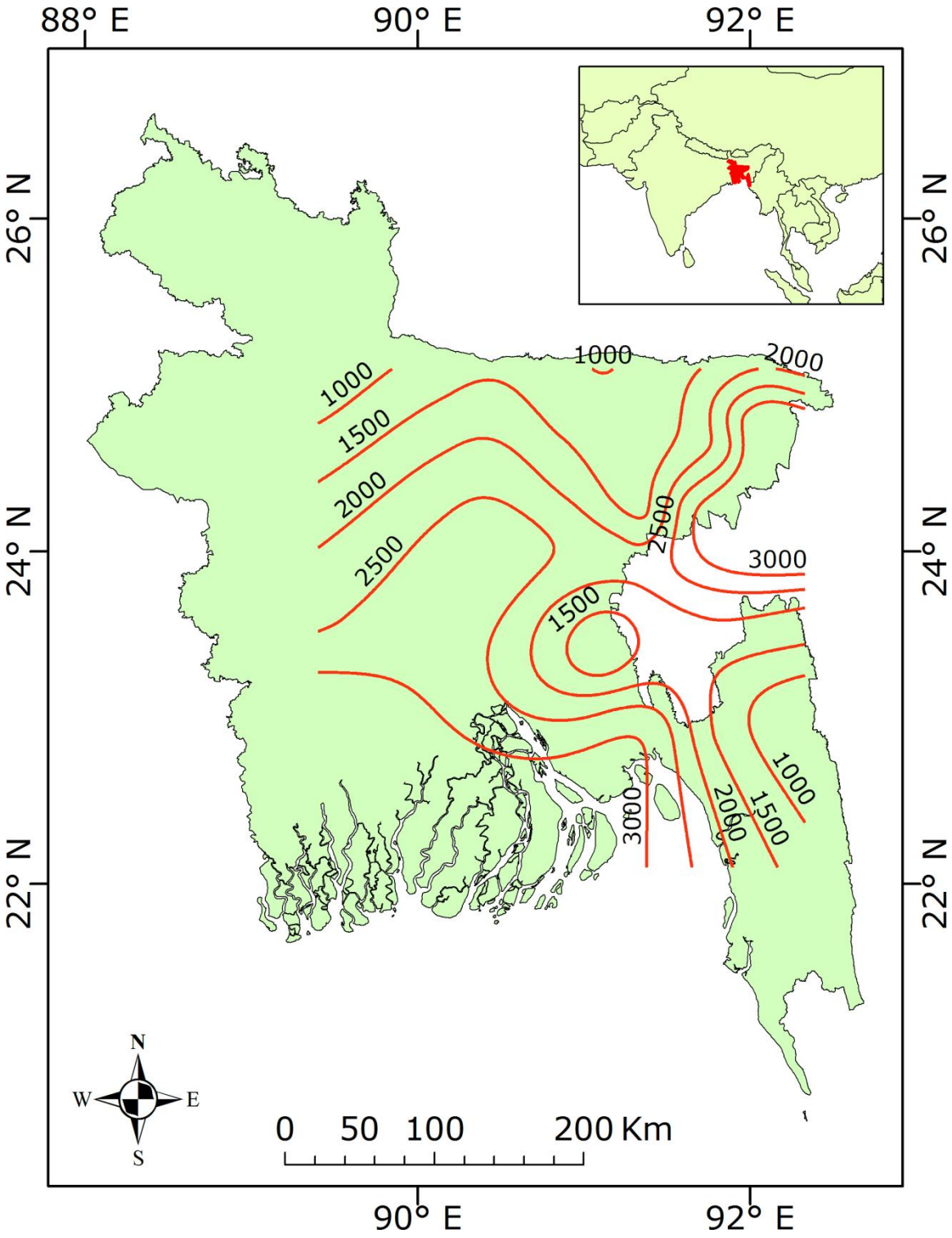

Figure 4.12 Depth to the top (m) of the Miocene Bhuban Formation in the Bengal basin [data source: Khan, (1991b)].

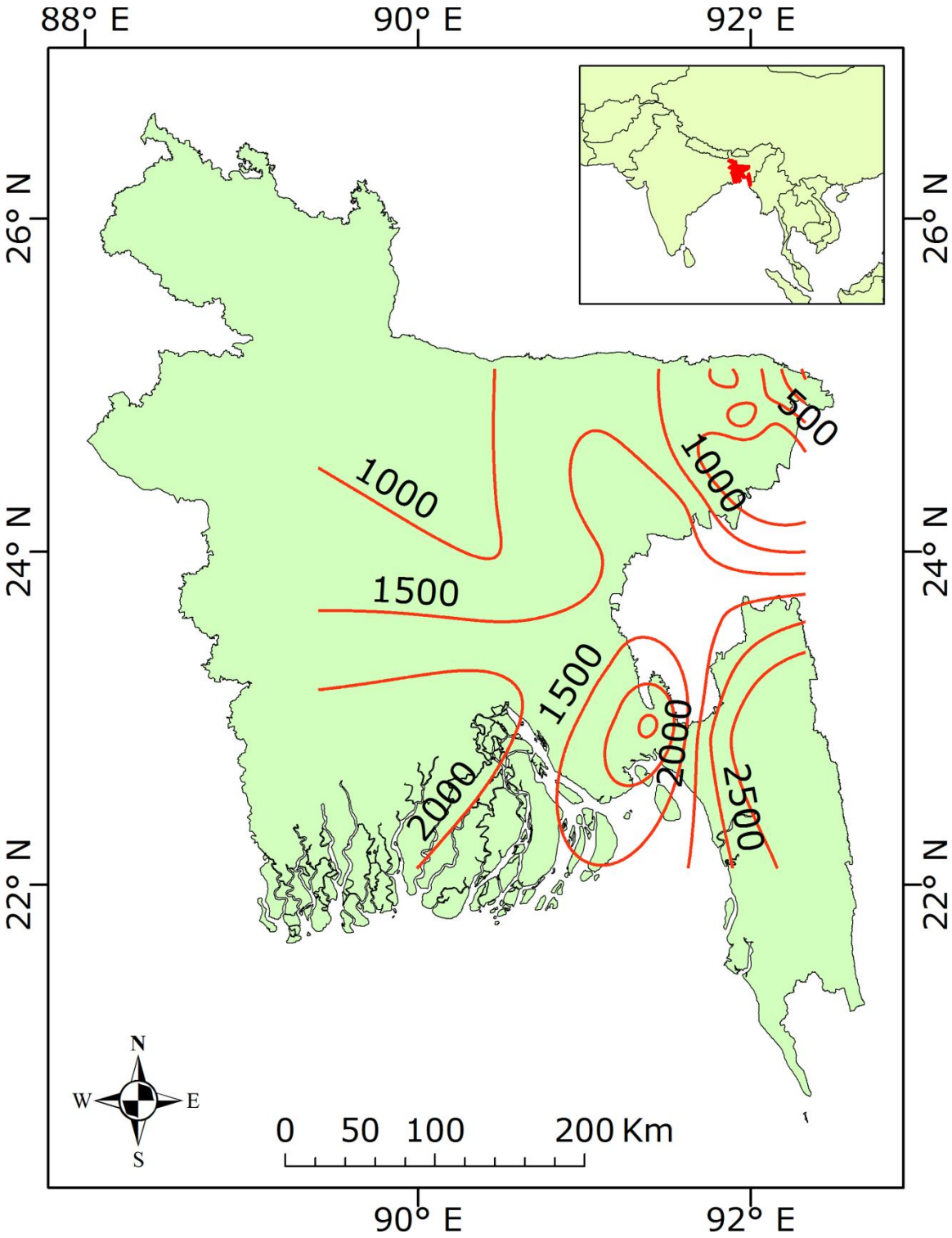

Figure 4.13 Total thicknesses (m) of the Miocene Bhuban Formation in the Bengal basin [data source: Khan (1991b)].

Formation pressure change at depth below 3 km suggests that the pressure gradient increases toward the east (Fig. 4.14). Abnormal formation pressure occurs at shallower depths (3 km) in the eastern and southeastern Bengal basin. The formation pressure gradient also increases from >0.12 atm/m to <0.15 atm/m toward the east and southeast (Fig. 4.14).

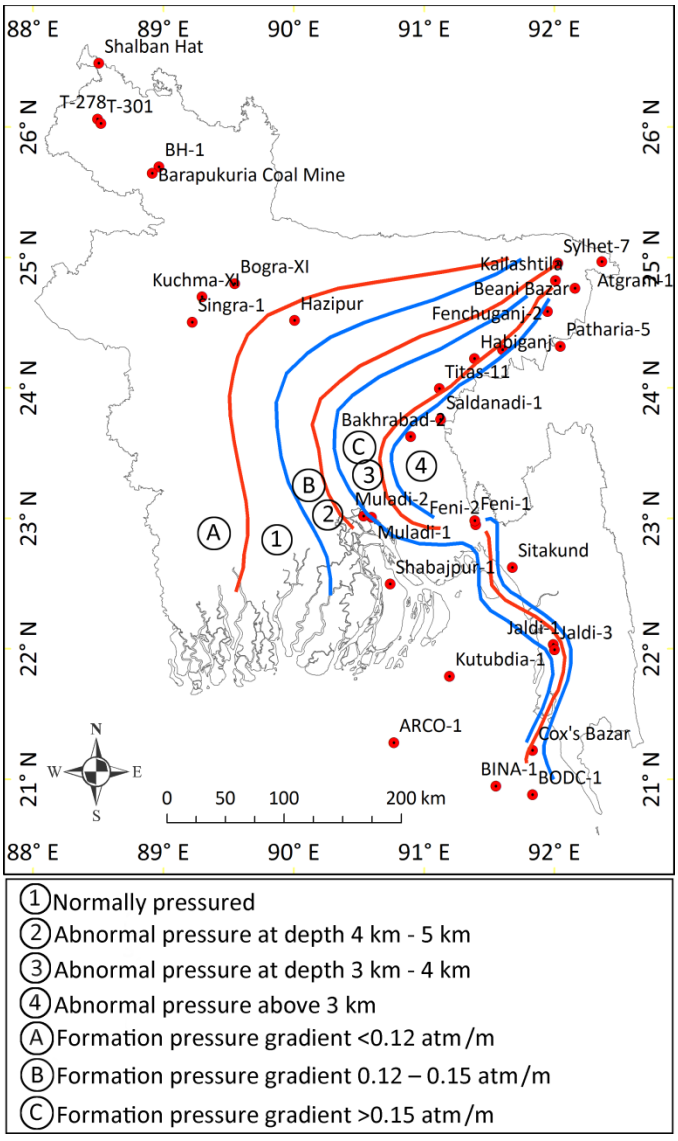

Figure 4.14 Formation pressure change at depth below 3km and presumed depth of abnormal pressure zones (modified after Matin et al., 1982). Red lines separate depth zones and blue lines separate pressure gradients.

Figure 4.15 shows the relationship between depth to the top of the Bhuban Formation and depth to the top of overpressure zones in deep exploratory wells in the eastern Bengal basin. Depth to the top of overpressure zone is shallower where depth to the top of Bhuban Formation is shallower.

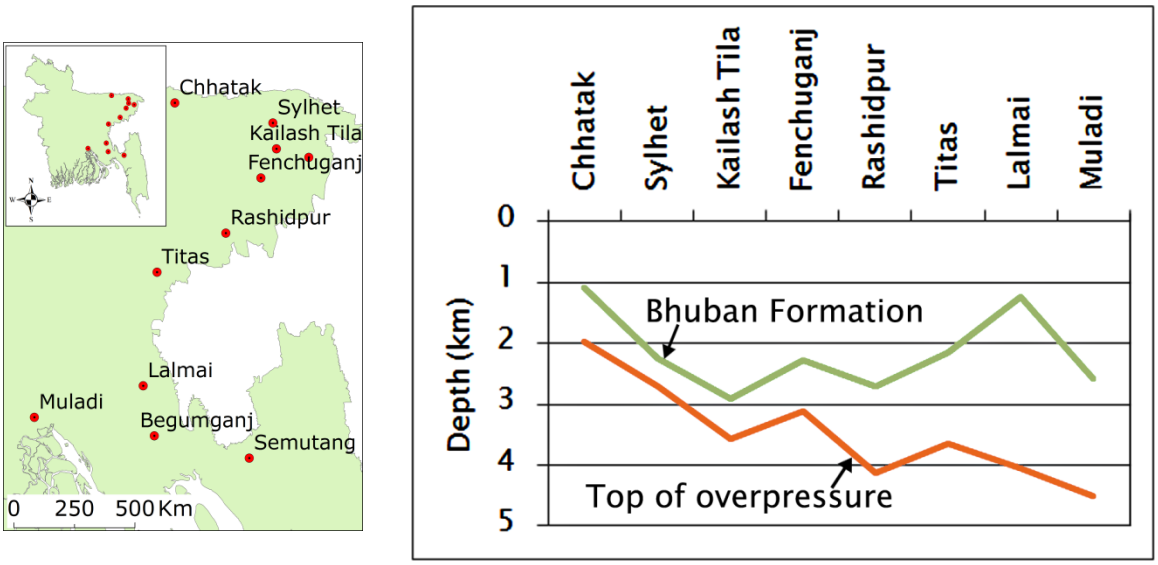

Figure 4.15 Relationship between the depth to the top of overpressure zone and the depth to the top of the Miocene Bhuban Formation [northeast–southwest direction; data source: (Khan, 1991b), and BAPEX].

Figure 4.16 shows that the distribution of pressure gradients at depths below 3 km increases toward the east. The depth to the top of overpressure occurs at shallower depths toward the east (Fig. 4.17).

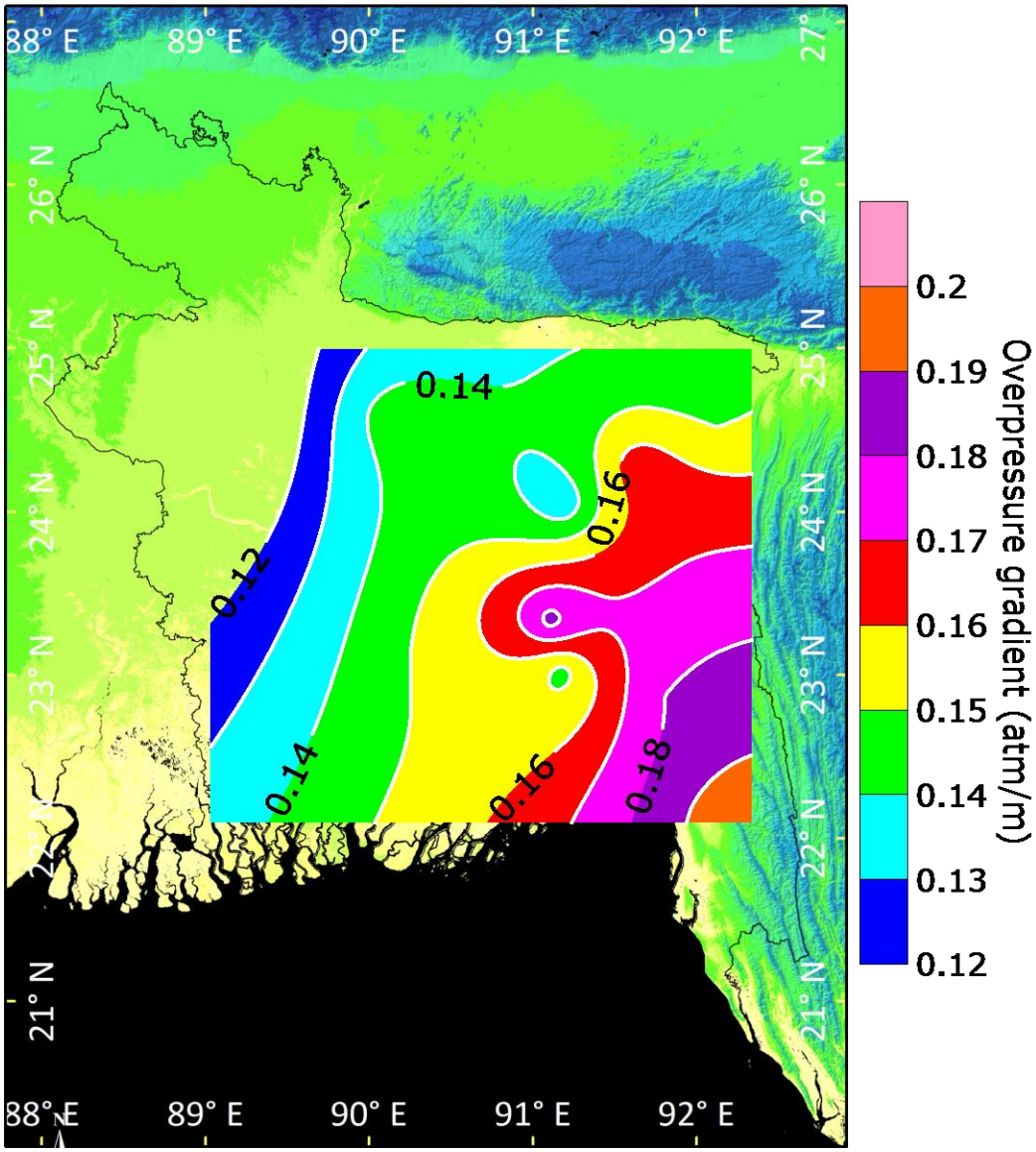

Figure 4.16 Pressure gradient increases toward the east at depths below 3 km [data source: BAPEX and Matin et al., 1982].

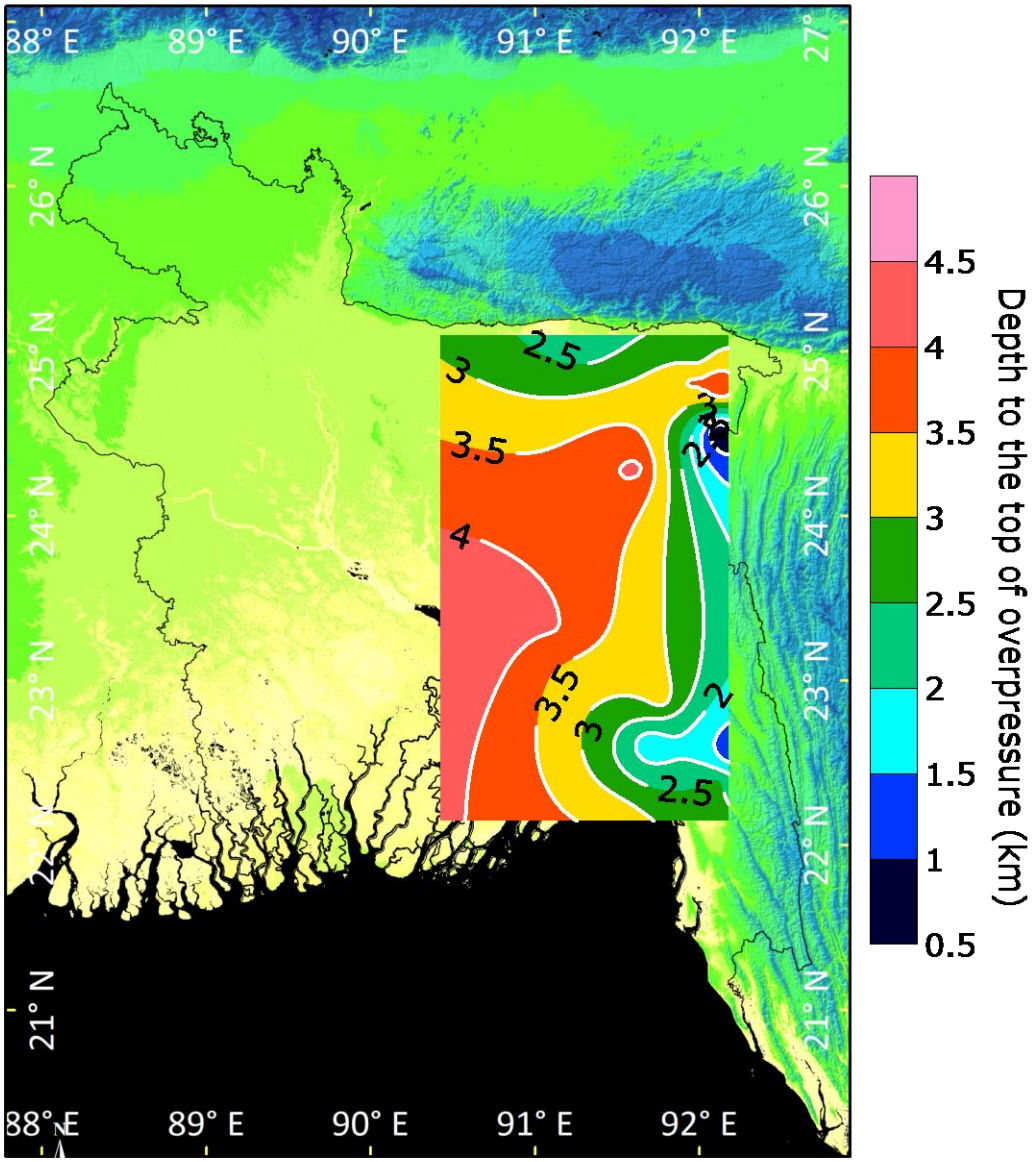

Figure 4.17 Depth to the top of overpressure increases toward west (data source: BAPEX).

CHAPTER 5: X–RAY DIFFRACTION ANALYSIS OF CLAY MINERALS

5.1 INTRODUCTION

An understanding of clay diagenesis can be acquired by examining their bulk mineralogy using X–ray diffraction (XRD) analysis. Burst (1959) carried out one of the first detailed investigations of clay mineral assemblages and reported that, with increasing depth of burial, swelling smectite clay minerals transform into non–swelling illite (Fig. 5.1). Since then, many investigations have reported that progressive lithification of clay with depth of burial coincides with progressive loss of swelling clay minerals in many geological sequences. Decrease and disappearance of kaolinite, appearance and increase in chlorite, and loss of K–feldspars are other diagenetic changes observed with increasing temperature and pressure with burial. Hower et al. (1976) performed a detailed mineralogical and chemical investigation on Oligocene–Miocene sediments of the Gulf Coast of the United States and found that the most abundant mineral, illite/smectite, undergoes a conversion from less than 20 percent to about 80 percent illite layers over an interval of 1250 m to 5500 m. Lanson et al. (1998) studied smectite–illite diagenetic transformations in five different sedimentary basins using X–ray diffraction techniques and documented that in all sedimentary basins that experienced a low steady geothermal gradient the physicochemical characteristics of intermediate mixed layered illite/smectite (I–S) are similar. However, both relative abundance and crystallinity of the end–member illite increases as a function of the age of the sediment.

In basins that have higher geothermal gradients, the I–S subpopulation is higher for a given illite content, indicating a slightly different reaction pathway. Yang and Hesse (1991) used XRD analysis of clay minerals as an indicator of diagenesis in an overthrust belt in the southern Canadian Appalachians.

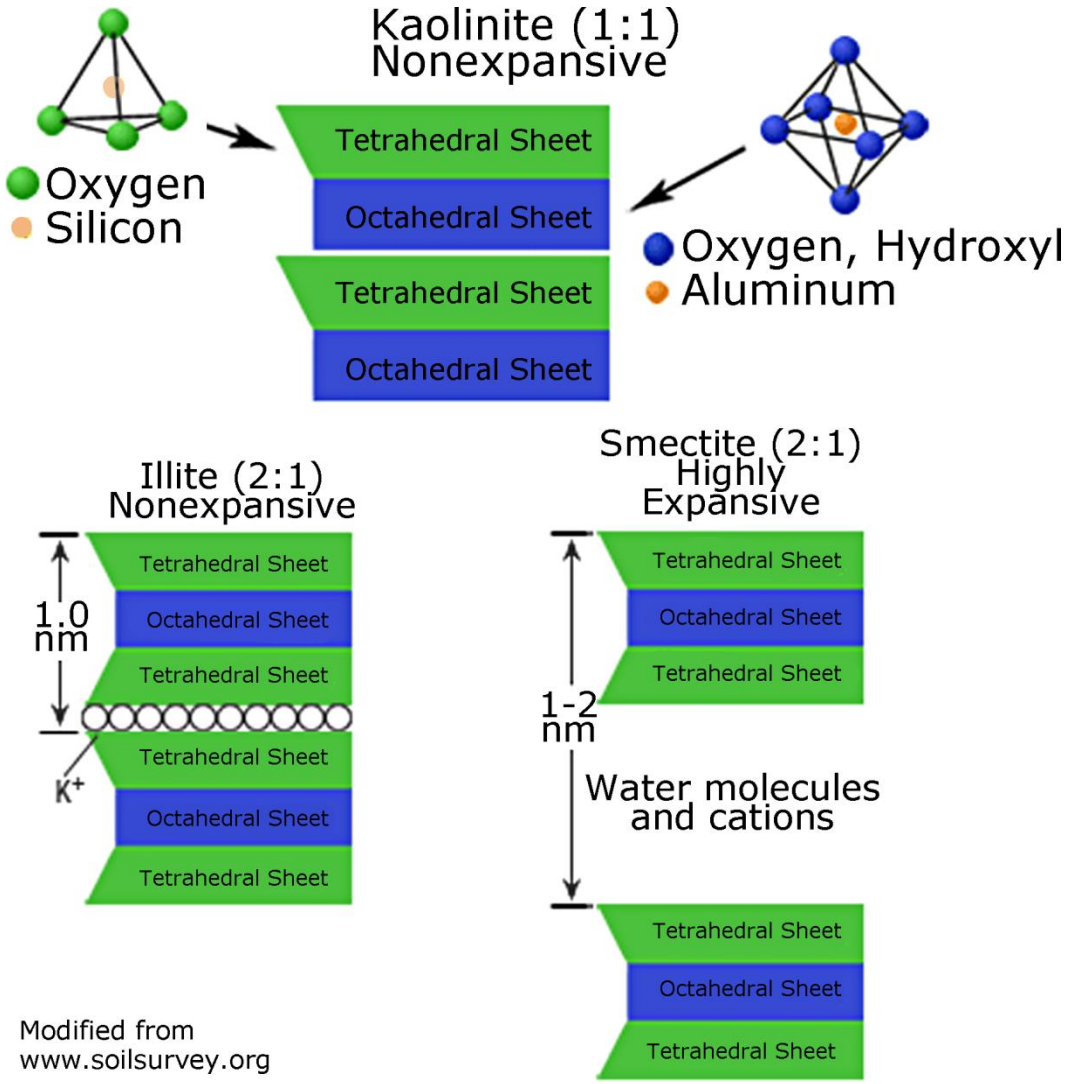

Figure 5.1 A schematic diagram shows the **s**tructures of Illite and Smectite clay.

For the purpose of the present study, a total of eleven clay samples were analyzed from Kamta-1X, Patharia–5, Sitakund–1, Kailash Tila–4, Fenchuganj–2, and Atgram–IX

wells covering a depth range of 1450.50 m to 4005.98 m. Results were used to assess the diagenetic changes in clay minerals with burial and to relate these changes to overpressure.

5.2 SAMPLE PREPARATION

For bulk mineralogical analysis ~5 g of sample were washed, dried, and crushed into small fragments using a pestle and mortar. Whole–rock powder was mounted on the sample holder of the Rigaku X–ray powder diffractometer located in Chemistry building at Auburn University and the surface was smoothed by pressing the powder with a glass slide. The whole rock powder samples were analyzed over an angular range of 5° to 60° (Fig. 5.2).

To analyze clay mineralogy, the glass slide method was utilized in this study to prepare oriented mounts because of its ease of application. About 1 g of dry sieved sample was placed in a 10–ml cylinder and about 5 ml of distilled water was added and mixed thoroughly using a glass rod. After 15–20 minutes, the upper solution was then pipetted (using an eyedropper) and placed slowly on a clean glass slide so that the liquid covers the entire surface of the slide. The slide was dried at room temperature.

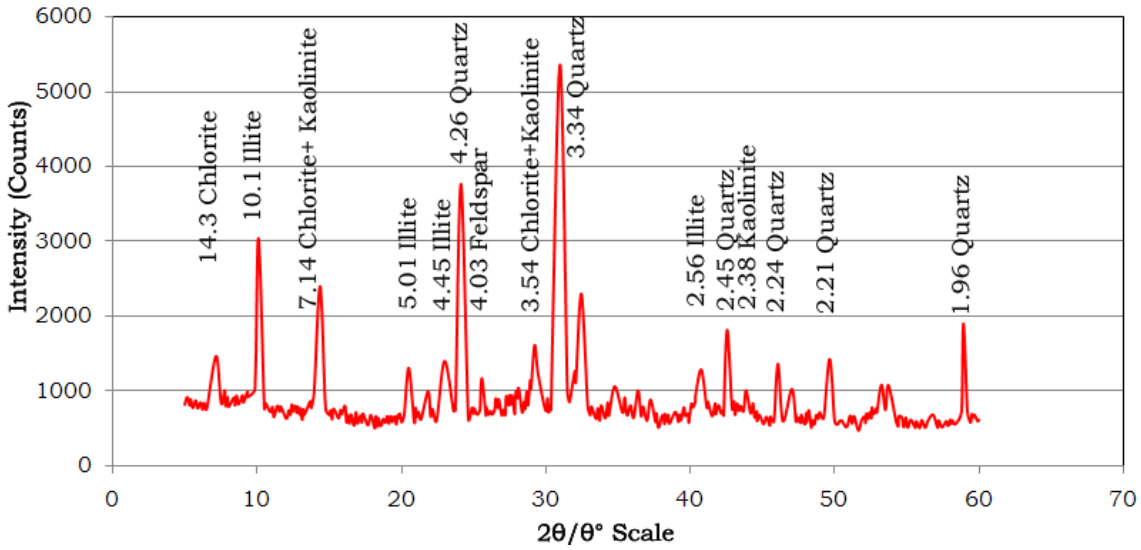

Figure 5.2 X-ray diffraction pattern showing bulk mineralogy of the clay fractions of the Miocene Bhuban Formation from Kamta–1Xwell (3540.17 m – 3545.63 m depth).

The clay samples were analyzed under three separate conditions.

i. Air dried

ii. After ethylene glycol treatment; and

iii. After heating at 550° C for an hour.

Study of transformation of smectite to illite via interstratified clay minerals (illite/smectite mixed layer clay) requires precise qualitative and quantitative determinations of the different layers in the mixed layer clay and is generally based on XRD patterns after specific treatments of clay samples (Mosser-Ruck et al., 2005). Ethylene glycol solvation is a classical method used to identify high–charged smectite and vermiculite. Different methods of glycolation (EG vapor or liquid EG) produce significant differences in the XRD patterns. In this study, liquid EG solvation method was used because when a material is saturated with liquid ethylene glycol, a higher

d–value is observed. For example, high charged smectite and vermiculite (d value ~14–15 Å) expanded to 17 Å when liquid ethylene glycol is used.

The samples were scanned from 3° to 30° at 0.2 deg/min scan speed. X–ray diffraction patterns of the separated clay fraction of selected representative samples are shown in Figs. 5.3–5.6. The relative abundances of clay and non–clay minerals in the clay fractions are shown in Table 5.1. Match! X–ray powder diffraction analysis software was used to analyze the diffractograms. The relative percentages of clay samples were determined automatically by matching the curve with the reference patterns database from American Mineralogists Crystal Structure Database (AMCSD).

5.3 MINERALOGY

5.3.1 Non–clay mineralogy

Quartz is one of the most abundant minerals in all the samples and is consistently present throughout the depth ranges studied. Feldspars are also common as indicated by reflections at 3.18 Å and 3.25–3.28 Å (K–feldspar). Plagioclase is also indicated by moderate reflections at 4.02 – 4.03 Å, 3.75– 3.767 Å and 3.66 Å. Carbonates including calcite, dolomite, and siderites occur in minor to tress amounts.

5.3.2 Clay mineralogy

Illite is the most abundant clay mineral present in all the samples. It is identified by a series of reflections at 9.97 –10.1 Å, 4.98 – 5.01 Å, and 1.89 –1.92 Å. No significant change in the intensity is observed on glycolated samples but a slight collapse is observed when samples were heated to 550° C.

Chlorite is readily identified by its basal reflections at 14.1–14.3 Å and 4.74–4.73 Å. The basal reflections at 7.0 Å and 3.56 Å could not be used directly for identification of chlorite due to interference with kaolinite reflections. No change in chlorite peak intensities is noted with burial.

Kaolinite is a major constituent in the studied samples. The presence of kaolinite and chlorite together in the samples made it difficult to recognize kaolinite on the basis of its major reflections at 7 Å and 3.58 Å.

None of the samples show discrete or pure smectite, but an illite/smectite mixed layer phase has been identified in the representative clay samples (14.2–14.5 Å; Figs. 5.3–5.6). The relative percentages of illite in clay fractions increase with depth in the Bengal basin (Table 5.1).

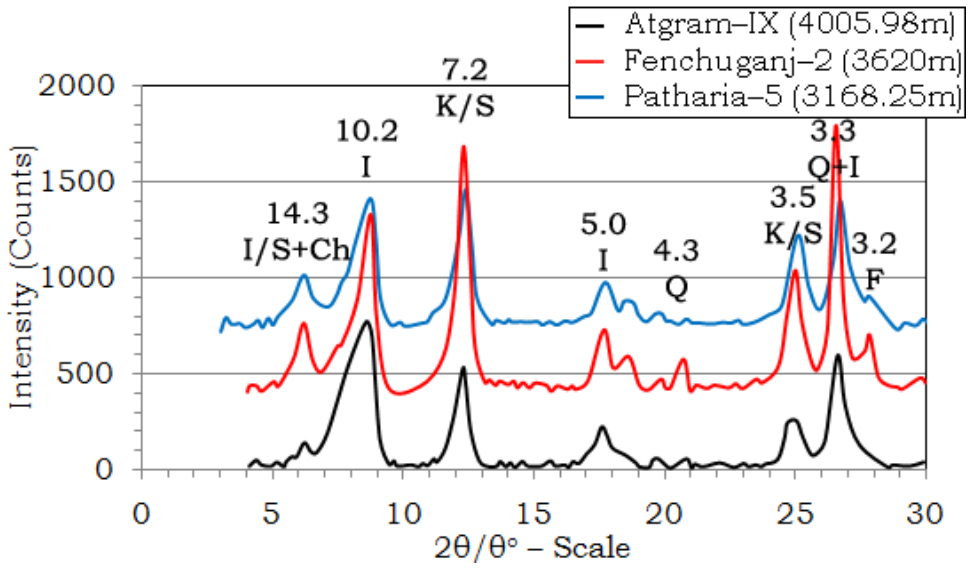

(a)

Figure 5.3 X–ray diffractograms for the oriented, non–heated clay fractions of three exploration wells [I/S+Ch= Illite–Smectite+Chlorite; I=Illite; K/S=Kaolinite–Smectite; Q=Quartz; Q+I=Quartz–Illite; F=Feldspar] .

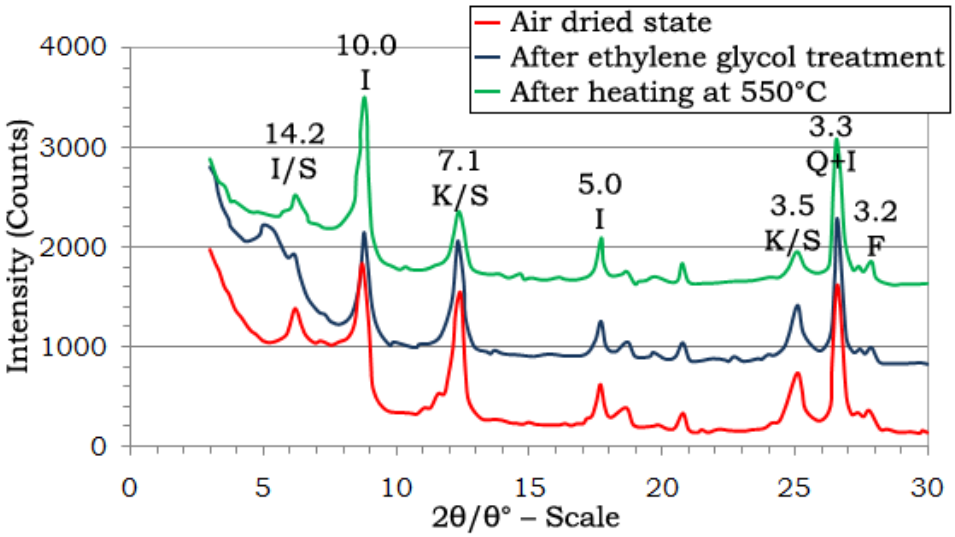

Figure 5.4 X–ray diffractograms for the oriented, air dried, ethylene glycol treated, and heated to 550°C clay fractions of the Kailash Tila–4 well.

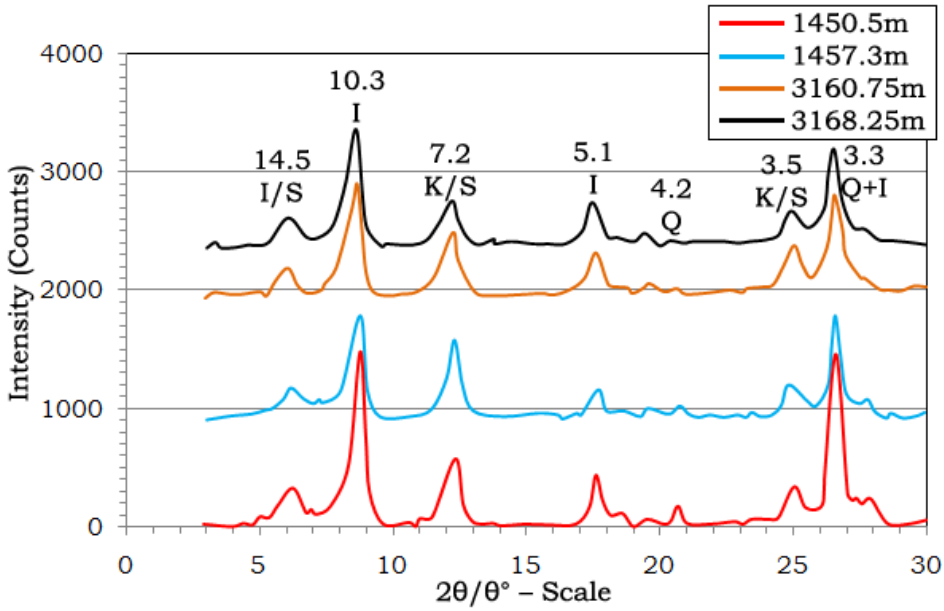

Figure 5.5 X–ray diffractograms for oriented, heated clay fractions from four different depths of the Patharia–5 well [I/S+Ch= Illite–Smectite+Chlorite; I=Illite; K/S=Kaolinite–Smectite; Q=Quartz; Q+I=Quartz–Illite; F=Feldspar].

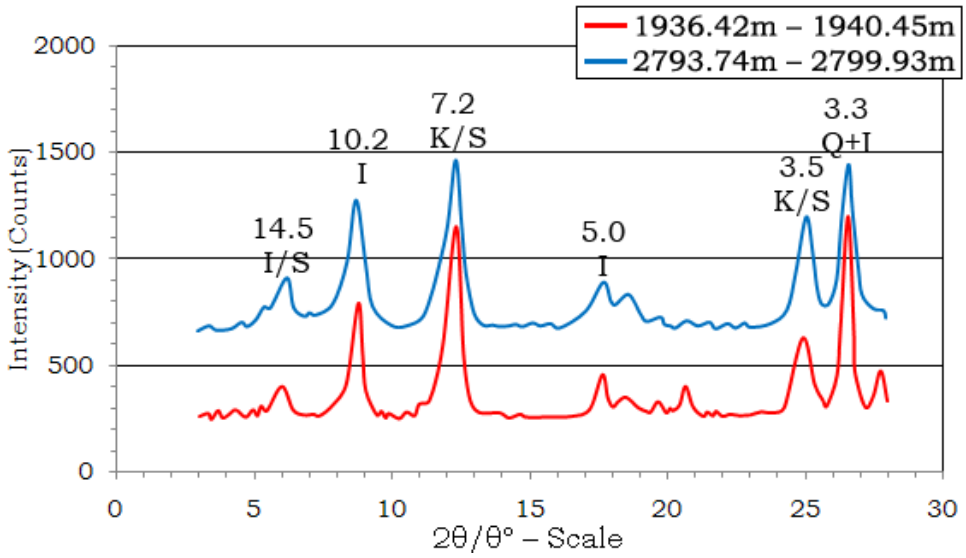

Figure 5.6 X–ray diffractograms for oriented, non–heated clay fractions from two different depths of the Sitakund–1 well [I/S+Ch= Illite–Smectite+Chlorite; I=Illite; K/S=Kaolinite–Smectite; Q=Quartz; Q+I=Quartz–Illite; F=Feldspar]

Table 5.1 Relative clay and non–clay mineral abundance in clay fraction samples of the Bengal basin [(G) = Glycolated, (H) = Heated at 550°C, I = Illite, I/S = Illite–Smectite, K= Kaolinite, K/S = Kaolinite–Smectite, Ch = Chlorite].

Sample	Core, Box	Depth to top (m)	Depth to Bottom (m)	I (%)	I/S (%)	K (%)	K/S (%)	Ch (%)
Atgram – IX	Core 3	3990.75	4005.98	61		16		
Fenchuganj – 2	Core 10, Box 6	3615.00	3624.00	35		24		
Kailash Tila – 4	Sample 7	3121.00	3122.00	22			38	27
Kailash Tila – 4 (G)	Sample 7	3121.00	3122.00	29	8		58	
Kailash Tila – 4 (H)	Sample 7	3121.00	3122.00	33	13		45	2
Patharia – 5	Core 6	3168.25		36	7		33	7
Patharia – 5 (H)	Core 2, Box 7	1450.50	1457.30	18	28		39	2
Patharia – 5 (H)	Core 2, Box 7	1450.52	1457.30	36	7		30	
Patharia – 5 (H)	Core 6	3160.75		49	10		41	
Patharia – 5 (H)	Core 6	3168.25		58	11		31	
Sitakund 1	Core 7, Box 3	1936.42	1940.45	27	6		56	
Sitakund 1	Core 10, Box 3	2793.74	2799.93	41	8		49	

In this study, the percentage of smectite could not be calculated due to the absence of 17Å reflections. This is possibly due to the transformation of illite/smectite to illite during burial diagenesis. Imam (1994) studied Neogene samples from the Bengal basin and noted the disappearance of the 17 Å peak in the samples collected from greater depths. He noted that the absence of the 17 Å peak is diagenetic and caused by the illite/smectite becoming orderly interlayered with illite. If an ethylene glycol solvate sample shows reflections between 5.3 Å and 8.7 Å, then the interstratifications are considered ordered to some extent (Srodon, 1980). The representative clay samples analyzed in this study show gradual decrease of the 17 Å peak with increasing depths.

The transformation of smectite to illite through intermediate mixed–layer illite/smectite (I /S) clay is a well established clay diagenetic reaction in mudrocks associated with progressive burial (Weaver, 1956; Dunoyer de Segonzac, 1970; Perry and Hower, 1972; Hower et al., 1976; Boles and Frank, 1979; Srodon et al., 1992; Sato et al., 1996; Srodon, 1999). Mixed layer illite/smectite (I/S) is dominant in the clay-size fraction of mudrocks from Tertiary basins. The transformation of smectite to illite flushes hydrocarbons from mudrocks (Burst, 1969; Bruce, 1984b), acts as a catalyst in hydrocarbon generation (Johns and Shimoyama, 1972), produces high pore–fluid pressure (Powers, 1967), and provides cementation agents to sandstones (Towe, 1962; Boles and Frank, 1979; Lahann, 1980).

5.4 CLAY DIAGENESIS

5.4.1 Illite/Smectite (I/S) mixed layer clay

The diagenetic transformation of illite/smectite involves the gradual loss of smectite layers due to conversion to illite with increasing temperature. This also results in a change in the nature of interstratifications of the illite and smectite layers from a random to an ordered state (Perry and Hower, 1970). The diagenetic transition of smectite to illite is accompanied by the expulsion of interlayer water from smectite to the pore water system, which is referred to smectite dehydration (Powers, 1967; Burst, 1969; Perry and Hower, 1970; Imam, 1994).

Illite/smectite mixed layers occur through loss of water and adsorption of Na^+, K^+, and Mg^+, and rearrangement of ions within the lattice (Millot, 1970). In the Bengal basin, the transformation of smectite to illite took place through intermediate illite/smectite mixed layer clay (Imam, 1983; Imam and Shaw, 1985, 1987; Imam, 1994; Mannan, 2002).The most important change with burial in the clay minerals of the Miocene Bhuban Formation of the Bengal basin is the gradual decrease in the 17 Å peak (18 Å for glycolated samples) of the illite/smectite mixed layer clays (Imam, 1983; Imam, 1994; Mannan, 2002). In this study the illite/smectite mixed layer clay is identified by 14.2–14.5 Å peaks (Figs. 5.3–5.6).

Imam (1983) proposed two possible causes for such a change in the 17Å peak: (i) The amount of illite/smectite gradually decreased with increasing depth (ii) a gradual diagenetic change of the illite/smectite mixed layer clay with burial.

There have been no significant changes in provenance during the Neogene time in the Bengal basin that could produce a change in clay mineral composition. However, climatic changes may have contributed to some extent. Variation in clay minerals deposited in various subenvironments could have been the possible reason for producing a change in clay mineral composition. A discontinuous sedimentation process could have caused a lateral change in clay mineral composition during sedimentation (Gibbs, 1977). In such cases, smaller clay particles should be deposited further away from the shore. The illite/smectite mixed layer clay would be in smallest clay fraction (Srodon, 1981). Therefore, in the Bengal basin, clay fractions from the deeper part of the basin should have more illite/smectite mixed layer clay. Therefore, the absence of 17 Å peak in clay samples collected from the deeper part of the Bengal basin cannot be explained as a result of absence of illite/smectite clay minerals.

There is substantial evidence for diagenetic modifications of expanding clay minerals (Burst, 1969; Dunoyer de Segonzac, 1970; Perry and Hower, 1972; Hower et al., 1976; Boles and Frank, 1979; Imam, 1994). Previous studies suggest that there will be a gradual decrease in smectite proportion in illite/smectite mixed layer clay due to transformation of smectite to illite layers with increasing depth of burial.

The gradual loss of the 14.2–14.5 Å peak in the diffractograms (Figs. 5.3–5.6) of the clay fractions of Miocene Bhuban Formation represents a gradual decrease in smectite percentage in illite/smectite mixed layer clay with increasing burial depth due to the diagenetic transformation of smectite to illite. Therefore, mineral transformation due to the increase in burial depth may have contributed in the development of overpressure.

CHAPTER 6: PETROFACIES ANALYSIS

6.1 INTRODUCTION

Diagenetic mineral reactions have been widely credited for the generation of overpressure in sedimentary basins. Growth of cement in the pore spaces of sediments generates overpressure if there is a net reduction in pore volume and the fluid cannot escape from the rock due to lateral and vertical seals. For this mechanism to be effective, cementation must not be inhibited by overpressure, the ions for cementation must be locally sourced, and the seals must have very low permeability (Osborne and Swarbrick, 1999). Bjorkum and Nadeau (1996) suggested that quartz cementation is a source of overpressure in deeply buried clastic reservoirs. Bruce (1984a) inferred that the transformation of smectite to illite is a major cause of overpressure in clays, and in reservoirs interbedded with clays. Overpressure could potentially inhibit pressure solution (chemical compaction) by decreasing effective stress at grain contacts (Porter and James, 1986). Petrographic study was conducted on sandstones from the Miocene Bhuban Formation to identify compaction–induced hydrofracturing, secondary porosity development through feldspar dissolution and dissolution of calcite cement.

6.2 THIN SECTION PREPARATION

Twelve resin–impregnated thin sections were made from eight exploration wells namely Bogra–2, Fenchuganj–2, Habiganj–7, Kailash Tila–4, Muladi–2, Patharia–5,

Saldanadi–1, and Singra–1. Blue epoxy was used to help identify porosity in the sandstones.

6.3 DIAGENESIS OF SANDSTONE

Petrographic study of sandstones from the Miocene Bhuban Formation from eastern Bengal basin indicates that the analyzed rocks are dominated by monocrystalline quartz, feldspars, sedimentary lithic fragments, polycrystalline quartz, and chert grains. Both plagioclase and potassium feldspars were observed. Heavy minerals and low–grade metamorphic fragments also were found. These Miocene sandstones are orogenic and plot in the "recycled orogenic" provenance field of Dickinson (1985) (Figs. 6.1-6.3; Table 6.1; Uddin and Lundberg, 1998b; Zahid, 2005; Rahman, 2008).

When sediments are first deposited, they are in a liquid–like state and are incapable of fracturing (Lambe and Whitman, 1969). Porosity gradually decreases as the solid particles settle down into an interlocked state. Laboratory studies show that when porosity is reduced to, or below, that for the Atterberg's plastic limit, sediments become semisolid and capable of fracturing when subjected to stresses above their load-bearing limit (Lambe and Whitman, 1969; Nolen-Hoeksema, 1993). Low permeability sedimentary rocks commonly are fractured (Wang and Xie, 1998). Wang and Xie (1998) carried out systematic numerical experiments to study compaction–induced hydrofracturing. Their study shows that compaction–induced hydrofractuing may be common in clay–rich basins and in sand–clay sequences. The frequency of such hydrofracturing depends on sediment permeability, sedimentation rate, and nature of sedimentary sequence. An important result is that compaction–induced hydrofracturing

may occur at shallow depths in clay–rich basins, but it may mobilize enhanced fluid flow throughout the sedimentary basin (Wang and Xie, 1998).

Table 6.1 Normalized modal compositions of sandstones of the Miocene Bhuban Formation (in QtFL, Qt=total quartz, F=feldspar, L=lithic fragments; in QmFLt, Qm=monocrystalline quartz, F=feldspar, Lt=total lithic fragments, in QmPK, Qm=monocrystalline quartz, P=plagioclase feldpsar, K=potassium feldspar).

Sample Name	Depth (m)	Qt	F	L		Qm	F	Lt		Qm	P	K
Fenchuganj-2	2420	50	23	27		44	23	33		66	22	12
Fenchuganj-2	3420	70	21	9		63	21	16		75	18	7
Fenchuganj-2	3620	62	25	13		55	25	20		69	17	14
Habiganj-7	3054	68	23	9		61	23	16		73	16	11
Kailash Tila-4	3116	49	15	36		45	15	40		75	11	14
Kailash Tila-4	3262	65	13	22		58	13	29		82	11	7
Patharia-5	2299	56	13	31		50	13	37		79	9	12
		Qt	F	L		Qm	F	Lt		Qm	P	K
	MEAN:	60	19	21	MEAN:	54	19	27	MEAN:	74	15	11
	STDEV	8	5	11	STDEV	8	5	10	STDEV	6	5	3

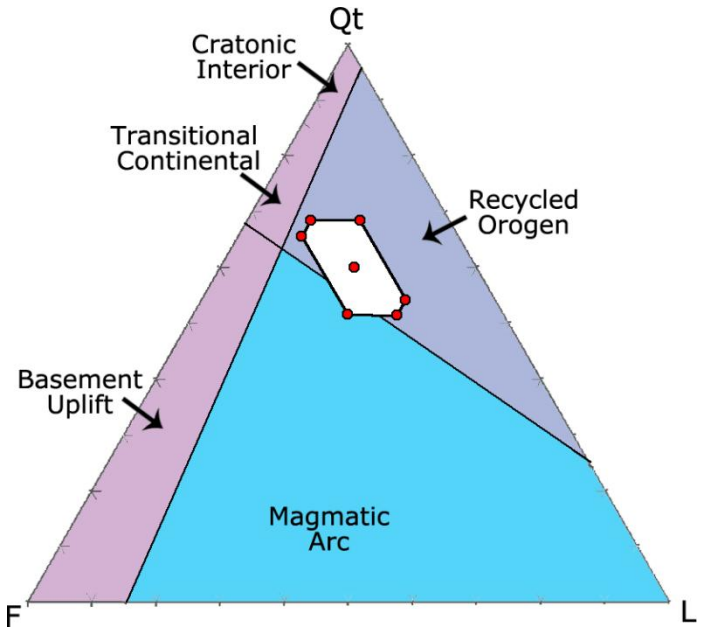

Figure 6.1 QtFL plot showing overall sandstone modes of the Miocene Bhuban Formation from the Bengal basin. Standard deviation polygon is drawn around the mean (shown as a red dot). Provenance fields are from Dickinson (1985). Qt=total quartz; F=feldspar; L=lithic grains.

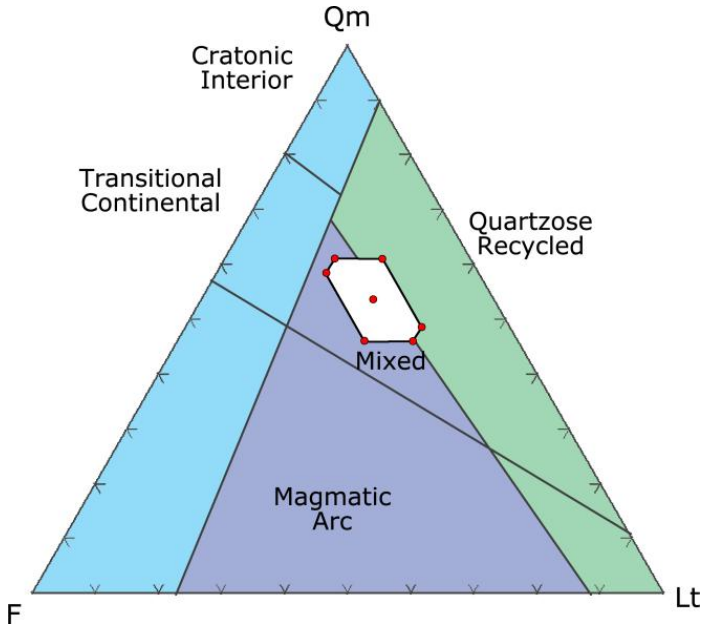

Figure 6.2 QmFLt plot of the Miocene Bhuban Formation from the Bengal Basin, showing mean (red dot) and standard deviation polygon, with appropriate provenance fields from Dickinson (1985). Chert and other polycrystalline quartz are included in the total lithic counts (see Table 6.1). Qm=monocrystalline quartz; F=feldspar; Lt=total lithic fragments.

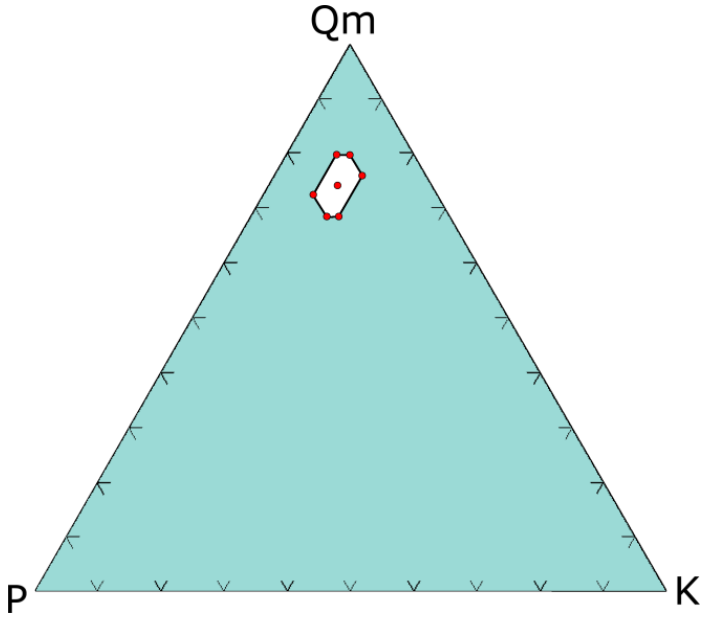

Figure 6.3 QmPK plot of the Miocene Bhuban Formation from the Bengal Basin, showing mean (red dot) and standard deviation polygon. Qm=monocrystalline quartz; P=plagioclase feldspar; K=potassium feldspar.

Hydrofracturing commonly is assumed to occur in deeply buried, low–permeability rocks. Tissot and Welte (1984) suggested that hydrofracturing is initiated at depths below 3 km to 4 km. However, high–resolution seismic imaging in the southern North Sea (Henriet et al., 1991) and direct examination of freshly exposed quarry faces on land (Henriet et al., 1991) show regional occurrence of fractures in Paleocene and Miocene clays at depths greater than a few hundred meters.

Hydrofracturing enhances permeability of a rock. Horath (1989) showed that the bulk permeability of a fractured turbidite sequence is up to three orders of magnitude greater than that of intact specimens. Capuano (1993) estimated the bulk permeability of hydrofractured clays to be several orders of magnitude greater than that of intact clays. Roberts and Nunn (1995) suggested that enhanced permeability in a fractured seal may be short–lived (<100 years). However, microscopic study of Gulf Coast clay samples (Capuano, 1993) revealed secondary minerals precipitated along hydrofractures, which suggests that hydrofractures may remain open for a significant amount of time for fluids to pass through and for chemical reactions to take place. Apparently the fractures retain the enhanced hydraulic conductivity even after the fractures are closed. This enhanced connectivity may be due to the microscopic roughness on the fracture surfaces that keeps some space open along the closed fractures and maintains an enhanced permeability (Wang and Xie, 1998).

The presence of corroded quartz grains, oversized pores, porosity channels between grains and cement, chlorite–rimmed ghost grains, and partially dissolved rock fragments satisfies the criteria for secondary porosity (Schmidt and MacDonald, 1976).

High porosity sandstones (≥10%) are overpressured in many deep siliciclastic reservoirs of the Gulf Coast, North Sea, Gulf of Thailand, and Scotia Shelf (Parker, 1974; Lindquist, 1977; Thomson, 1982; Loucks et al., 1984; Lonoy et al., 1986; Trevena and Clark, 1986; Jansa and Urrea, 1990; Weedman et al., 1996). Zones of secondary porosity have been reported above the top of overpressure zones (Brown et al., 1989), within the overpressured intervals (Lindquist, 1977; McBride, 1977; Taylor, 1990), and both above and below the top of overpressure zones (Loucks et al., 1984; Trevena and Clark, 1986; Jansa and Urrea, 1990; Weedman et al., 1996).

Jansa and Urrea (1990) and Weedman (1992) presented studies of diagenesis both above and below a zone of low permeability that maintained a pressure seal. Despite differences in study areas, both the investigations reported a similar diagenetic sequence. They also noted similar compaction trends. Weedman (1992) showed that the degree of repacking is greater above the pressure seal than below and used the term 'secondary compaction' to describe this phenomenon and to emphasize the role of secondary porosity in the acceleration of late–stage compaction.

6.4 DIAGENESIS OF SANDSTONE IN THE BENGAL BASIN

Thin–sections prepared from core samples collected from the exploratory wells in the eastern Bengal basin were carefully analyzed and numerous microfractures were revealed in sandstone within the overpressure zones from the Miocene Bhuban Formation. These microfractures are occupied by gray to black, argillaceous material (clay matrix) producing convoluted fracture paths. These microfractures were most likely formed due to the release of fluids through compaction of sediments.

In thin section prepared from the Fenchuganj–2 well (depth 3620 m) located in the northwestern Bengal basin, compaction–dependent hydrofracturing have been identified in sandstone of the Miocene Bhuban Formation (Fig. 6.4). Blue epoxy resin highlights pore spaces. In the Fenchuganj–2 well, overpressure zones have been reported at depths below 3124 m (Imam, 2005).

A sandstone core sample from Singra–1 well (depth 1800m –1804m) shows an example of channel development due to hydrofracturing (Fig. 6.5). Singra–1 is located in the stable shelf and no overpressure information has been reported in this area. The geothermal gradient calculated from temperature logs shows that this area has a higher geothermal gradient, which may have influenced fluid–volume expansion and thus led to the generation of fluid channels in the sandstones.

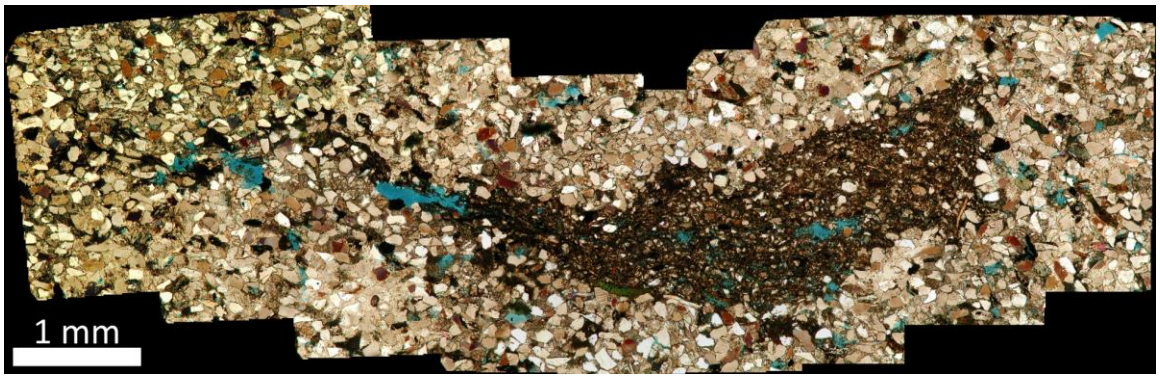

Figure 6.4 Compaction–induced hydrofracturing in a sand layer from Fenchuganj–2 well (depth 3620 m). Blue epoxy resin shows porosity in sandstone.

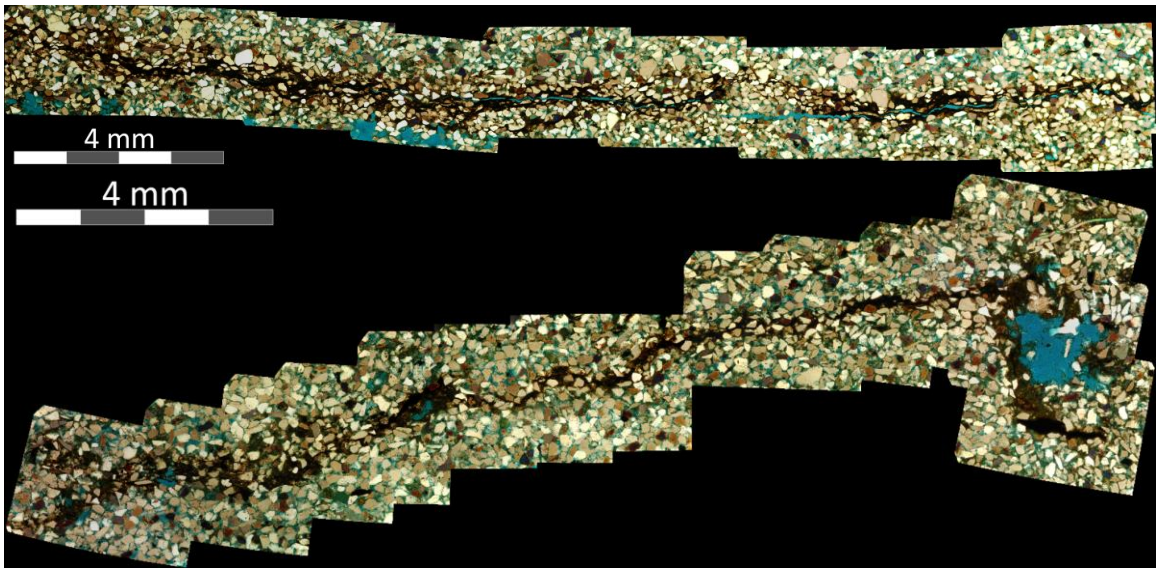

Figure 6.5 Development of fluid channels by hydrofracturing in a sand layer from Singra–1 well (depth 1800 m –1804 m). Blue epoxy was used to identify porosity in sandstone.

Photomicrographs of sandstone core samples collected from Fenchuganj–2 wells (depth 2420 m, 3420 m, and 3620 m) show decrease in porosity with increasing depth from 2420 m to 3420 m (Fig. 6.6). The porosity again increases from 3420 m to 3620 m. The sample at 2420 m depth shows well preserved primary interparticle porosity (blue stain). The sample from 3420 m shows complete loss of primary interparticle porosity by matrix infilling. The depth–pressure plots (Fig. 4.11) show that the pressure gradient for Fenchuganj–2 well at depths below 3 km is higher than the hydrostatic gradient. Moreover, the top of the overpressure zone in the Fenchuganj–2 well has been reported at 3124 m depth (Imam, 2005). Therefore, the porosity reduction in the 3420 m sample from the Fenchuganj–2 well may have taken place due to compaction and clay influx through the pores.

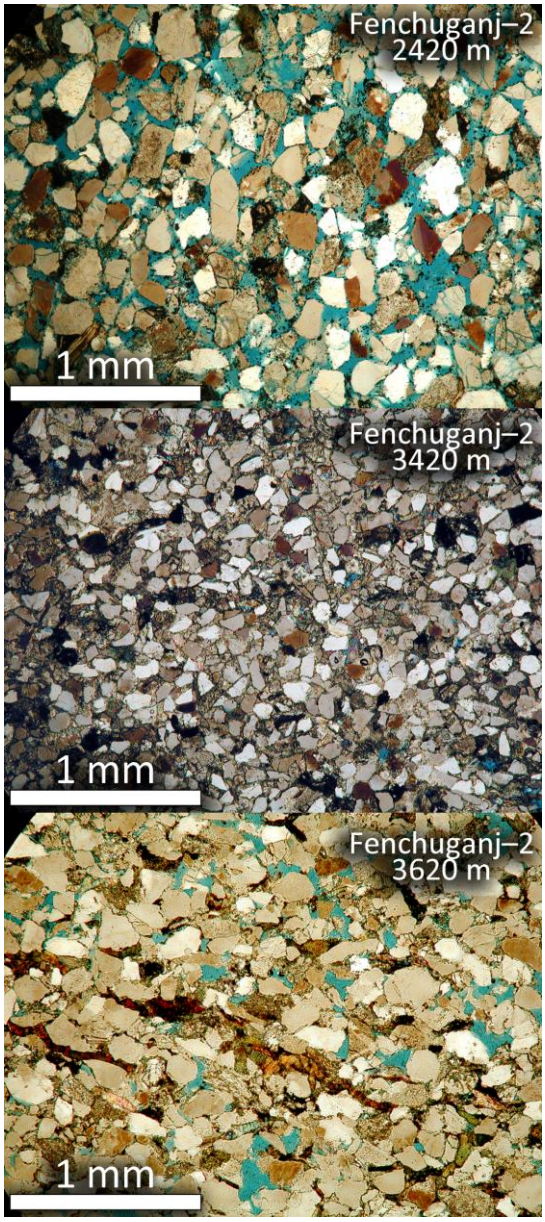

Figure 6.6 Photomicrographs of core samples collected from Fenchuganj–2 well. The photographs show that significant porosity reduction took place between 2420 m to 3420 m.

Secondary porosity in sandstone develops through feldspar dissolution during deep burial. Wilkinson et al. (1997) studied the sequence of diagenesis in sandstones of the Fulmer Formation, United Kingdom Central Graben, and found that sandstones have lost at least 30% feldspar after burial deeper than 3 km. They have inferred that the

secondary porosity is being created by a process of void support by high overpressure, combined with vertical leakage of overpressure pore fluid focused on a structurally high leak point.

Sandstone core samples from the Kailash Tila–4 well (depth 3116 m) shows secondary porosity development through dissolution (Fig. 6.7).

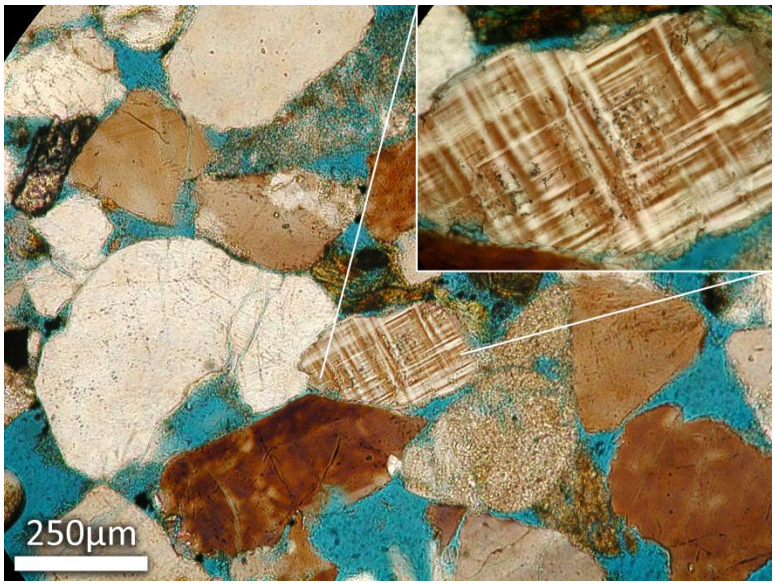

Figure 6.7 Photomicrograph of sandstone core sample collected from the Kailash Tila–4 well (depth 3116 m) showing example of feldspar dissolution.

The photomicrograph of the sandstone from the Kailash Tila–4 well (depth 3262 m) shows that secondary leaching of feldspar along weak planes develops porosity (Fig. 6.8). Parallel sets of fractures developed at high–angles to the twinning plane suggest that compaction played a major role in the development of secondary porosity (Fig. 6.8).

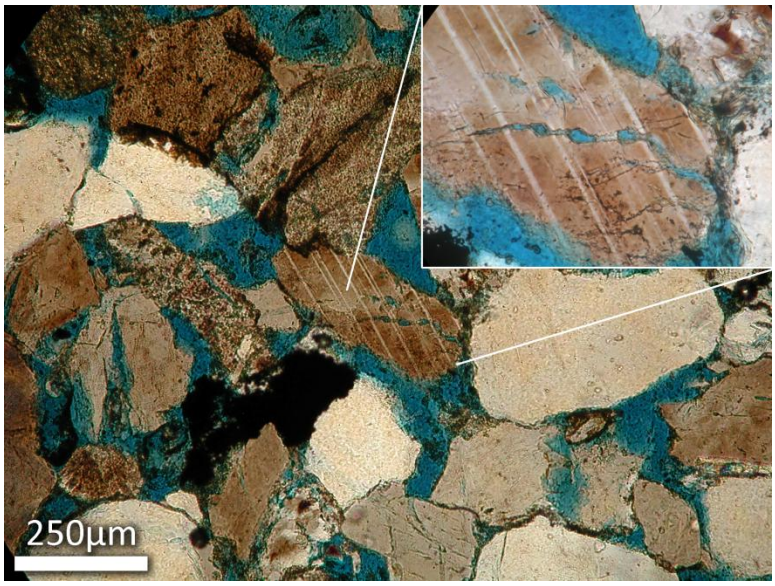

Figure 6.8 Photomicrograph of a sandstone core sample collected from the Kailash Tila–4 well (depth 3262 m).

Photomicrographs of a sandstone sample from the Patharia–5 well (Fig. 6.9) shows abundant secondary porosity coupled with partially preserved primary porosity. The leaching of grain is recognizable by the presence of molds of former particles.

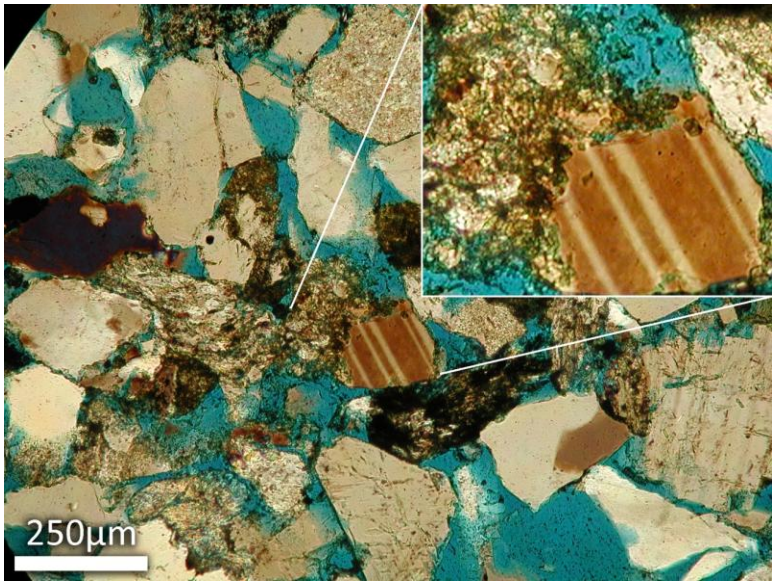

Figure 6.9 Photomicrograph of a sandstone core sample collected from the Patharia–5 well (depth 2299 m).

Photomicrographs of a sandstone sample from the Fenchuganj–2 well (2420 m; Fig. 6.10) shows partial dissolution of detrital grains. Numerous fractures developed in plagioclase feldspar through dissolution.

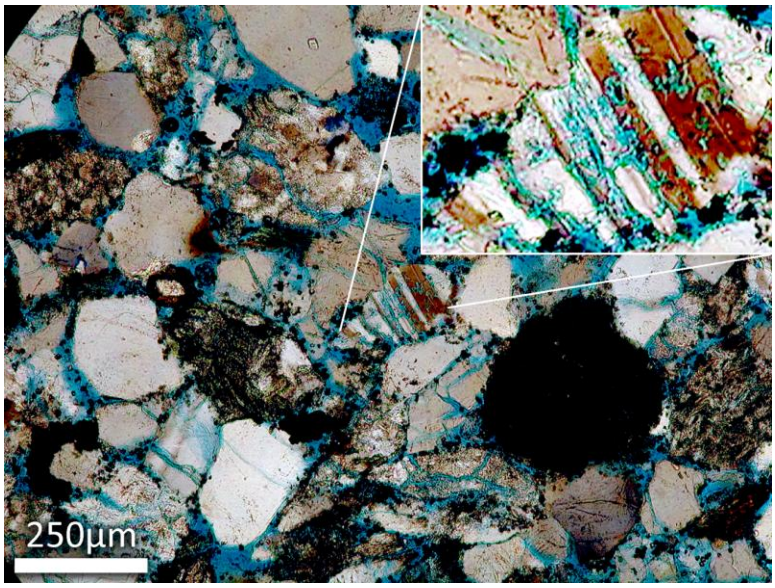

Figure 6.10 Photomicrograph shows development of fractures in plagioclase feldspar along weak planes (sandstone core sample from the Fenchuganj–2 well at 2420 m depth).

CHAPTER 7: $^{40}AR/^{39}AR$ DETRITAL MUSCOVITE AGES

7.1 INTRODUCTION

^{40}Ar is a naturally occurring isotope produced by radioactive decay of ^{40}K through electron–capture and positron–emission pathways (Faure, 1986). In the $^{40}Ar/^{39}Ar$ technique, the sample is irradiated in a nuclear reactor via bombardment by a fast, high–energy neutron beam to produce ^{39}Ar from ^{39}K (Merrihue and Turner, 1966; McDougall and Harrison, 1999). The amount of ^{39}Ar produced in any given sample will be dependent on the amount of ^{39}K present initially, length of irradiation process, and neutron flux density and neutron capture cross section for ^{39}K.

The decay of ^{40}K to ^{40}Ar is used to date geologic events such as the cooling of igneous rocks and minerals. $^{40}Ar/^{39}Ar$ ages of detrital muscovites should provide a time of cooling of the source rock through the closure temperature interval for muscovite (typically, 300°–400°C; Hames and Bowring, 1994). The concept is based on the assumption that no additional radiogenic ^{40}Ar is lost during transport or after deposition (Hodges et al., 2005). The time interval between muscovite cooling and sediment deposition is inferred to be the amount of time required to erode 10–12 km of sediments (depending upon the geothermal gradient and error of uncertainty in the closure temperature).

The age of a sample is given by the age equation:

$$t = \frac{1}{\lambda} \ln(J \times R + 1)$$

Where λ is the radioactive decay constant of ^{40}Ar production, J is the J–factor (parameter associated with the irradiation process), and R is the $^{40}Ar/^{39}Ar$ ratio (see Merrihue and Turner, 1966; McDougall and Harrison, 1999 for a complete discussion of the method). The J parameter is ascertained by irradiating the unknown sample along with a sample of known age to calculate the amount of ^{39}Ar produced from ^{39}K. Detrital mineral populations from a sedimentary sample show a range of $^{40}Ar/^{39}Ar$ mineral ages, reflecting mixed provenance with multiple age modes. In such a sample, the youngest mode has sedimentological significance: the difference between the depositional age and muscovite cooling age represents the maximum duration of transport from source to depocenter (Fig. 7.1). Ar–Ar ages for detrital muscovites in Miocene–Pliocene Bengal fan samples indicate that sediment residence times in fluvial systems on the southern flank of the Himalayas are remarkably brief (Copeland and Harrison, 1990).

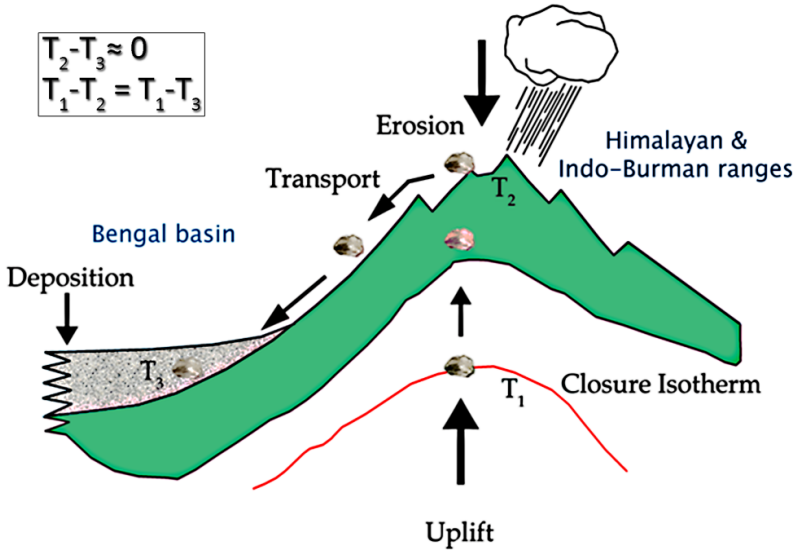

Figure 7.1 Schematic representation of the trajectory and life history of a muscovite grain in the Himalayan system (based on Cerveny, 1986).

Rapid transport is related to high relief in the source region. Comperatively young detrital muscovite cooling ages may indicate a well–developed Himalayan orogenic front existed; uplift and unroofing ages may come close to be the depositional ages of the clastic wedges (Hodges et al., 2005; Brewer et al., 2006).

For the current study, three Miocene Bhuban Formation samples from the Bengal basin were analyzed to calculate maximum stratigraphic age.

7.2 PREVIOUS WORK

Recent work in the eastern Himalayas by Hodges et al. (1994) and DeCelles et al. (2004) indicate that mountain building processes were operating well before the Miocene, prior to the deposition of Siwalik sequences in the western Himalayas and the distal portion of the Bengal fan. The Himalayan–Bengal delta and fan, in the eastern part of the Himalayas, represents the largest orogenic depositional system active today. The 16–km–thick proximal portion of this system acts as a repository of stratigraphic information of the Himalayan orogeny. Although much of this orogenic wedge remains buried, marginal uplifts expose stratigraphic sequences representing most of its Eocene to Pleistocene depositional history.

Rahman and Faupl (2003) studied sandstones of the Miocene Surma Group using a stepwise-heating $^{40}Ar/^{39}Ar$ method (McDougall and Harrison, 1999) for multigrain samples of white mica. They found that most samples yielded plateau ages of 25 to 35 Ma and concluded that sediments were derived from the eastern Himalayas. Uddin et al. (2005) studied muscovites from Bengal basin. They have found cooling ages between 12 Ma to 516 Ma with conspicuous modes at 17 Ma and 26 Ma, suggesting a combination of

sources. Copeland et al. (1995) focused on low temperature (100°–350°C) cooling history of the Gangdese batholiths and found ages generally from 70 to 40 Ma. Miocene muscovite grains from the Assam Basin (28 Ma to 81 Ma) may have been derived from several sources, including the Eohimalayan events (Hodges et al., 1994) of the eastern Himalayas, the Tibetan Plateau, and the Indo-Burman Ranges. Rahman (2008) analyzed single crystal muscovites from Oligocene and Miocene sequences of Bengal and Assam basins and concluded that there are two principle modes in detrital age (Cretaceous and Tertiary).

7.3 GOAL FOR CONSTRAINING AND UNDERSTANDING OVERPRESSURE

In eastern Bangladesh, overpressure zones have been encountered in the Miocene Bhuban Formation in exploratory wells. Incomplete dewatering of fine–grained sediments, clay diagenesis, and tectonic compression associated with the Indo–Burman ranges are possible causes for overpressure development in the Bengal basin (Zahid and Uddin, 2005). Equilibrium compaction (vertical loading stress) is easily maintained by fluid expulsion under normal conditions (Swarbrick and Osborne, 1998). However, in the case of rapid sedimentation, fluids cannot be expelled fast enough. As a result, increases in pore–fluid pressure lead to overpressure development.

For the current study, three samples were chosen from the upper, middle, and lower parts of the Miocene Bhuban Formation. $^{40}Ar/^{39}Ar$ analysis of muscovite grains were performed to provide maximum stratigraphic age and, hence, to evaluate the rate of sedimentation in the eastern Bengal basin.

7.4 METHODS

For this study, three subsurface core samples were chosen from the upper, middle, and lower part of the Miocene Bhuban Formation from the Kamta–1 well. Detrital muscovite samples were handpicked from three representative samples for $^{40}Ar/^{39}Ar$ study. Once prepared, muscovite samples were sent for irradiation at the McMaster nuclear reactor facility in Hamilton, Ontario, Canada. Samples were analyzed at Auburn University in the Auburn Noble Isotope Mass Analysis Laboratory (ANIMAL). ANIMAL is equipped with a low–volume, high–sensitivity 10–cm radius sector mass spectrometer and automated sample extraction system (based on a CO_2 laser) for analysis of single crystals. Uncertainties reported are the standard deviation, representing the precision of analysis, and do not include systematic errors arising from uncertainties in the decay constant or monitoring age. All analyses represent single crystal total fusion of muscovite grains with a CO_2 laser. Sample Kamta–15 contained relatively larger muscovite grains typically 2–3 mm in diameter (Fig. 7.2), whereas, samples from Kamta –19 and Kamta–23 contained much smaller grains (generally 0.5–1 mm in diameter; Fig. 7.2). Approximately 25 analyses per samples were performed using 1σ error.

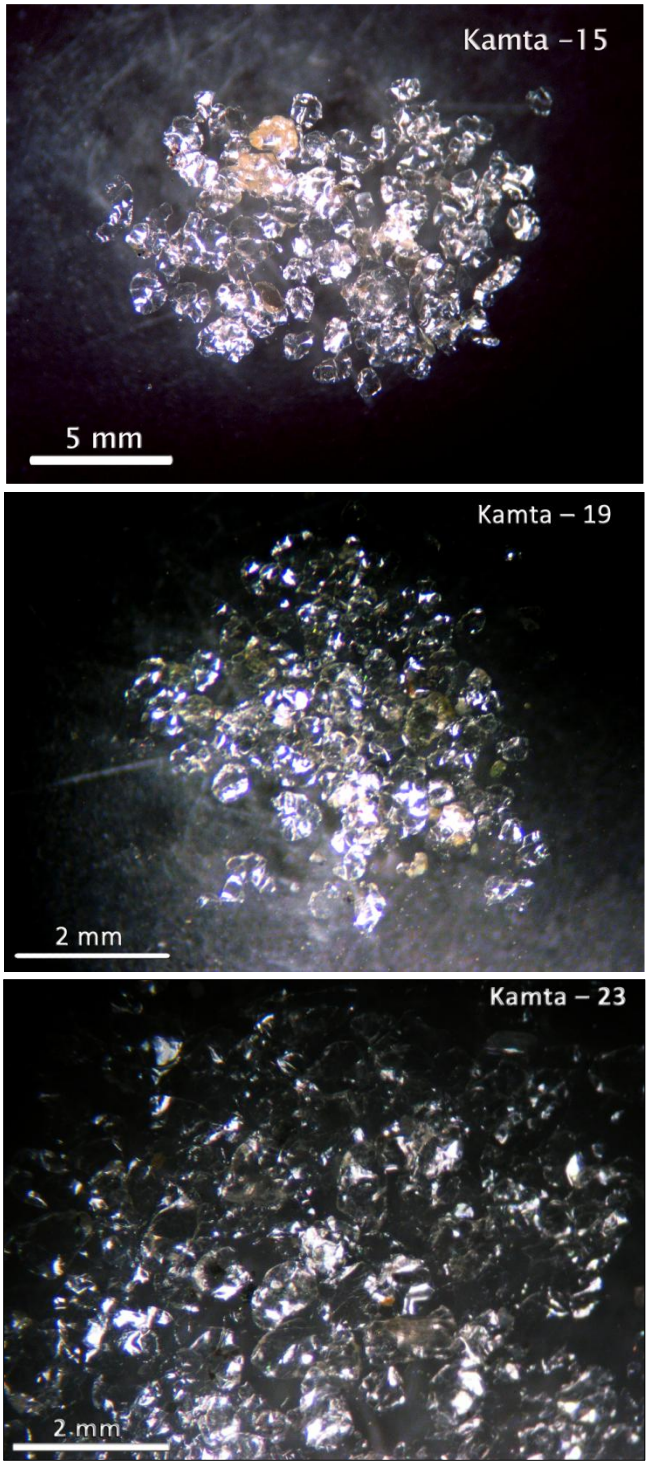

Figure 7.2 Photomicrograph of detrital muscovite grains handpicked from Kamta–15, Kamta–19, and Kamta–23 subsurface samples from the upper, middle, and lower Miocene Bhuban Formation.

7.5 RESULTS

The seven analyses from Kamta–15 detrital muscovite grains from the upper part of the Miocene Bhuban Formation indicate youngest age ranging from 15.25±0.09 Ma to 16.24±0.11 Ma. The weighted mean age of the seven youngest detrital muscovite grains is 15.75±0.35 Ma (=tσ√MSWD, where MSWD is Mean Square Weighted Deviation) with a MSWD of 9.9. The remaining 18 analyses show scatter beyond the expected analytical precision. The probability distribution plot shows a unimodal muscovite cooling age distribution with a major peak age of 16 Ma and a much smaller peak at 31.76 Ma (Fig. 7.3 A).

In total 25 detrital muscovite grains were analyzed from Kamta–19. Cooling ages distribution range from 15.58±0.34 Ma to 29.42±0.13 Ma (Fig. 7.3 B). The nine youngest analyses from Kamta–19 show muscovite cooling ages ranging from 15.58±0.34 Ma to 16.18±0.22 Ma. The weighted mean age of the nine youngest analyses is 15.92±0.14 Ma (=1.96σ) with a MSWD of 0.79. The remaining analyses scatter beyond the expected precision range. The probability distribution plot shows a unimodal distribution with a major peak at 16 Ma and a few more additional peaks at 18.23 Ma, 19.41 Ma, and 28.82 Ma.

The detrital muscovite cooling ages for the five youngest analyses from Kamta–23 range from 15.81±0.15 Ma to 16.11±0.31 Ma. The weighted average age of the five youngest analyses is 16.03±0.11 Ma (=1.96σ) with MSDW of 0.75. The remaining analyses scatter beyond the precision limit. The major peak on the probability distribution plot is located at 16.24 Ma. A few minor peaks of older ages are also present on the

probability distribution plot (Fig. 7.3 C).Figure 7.4 shows muscovite cooling ages distribution for the three samples collected from the Kamta–1 well and some previously published studied on the regional detrital age.

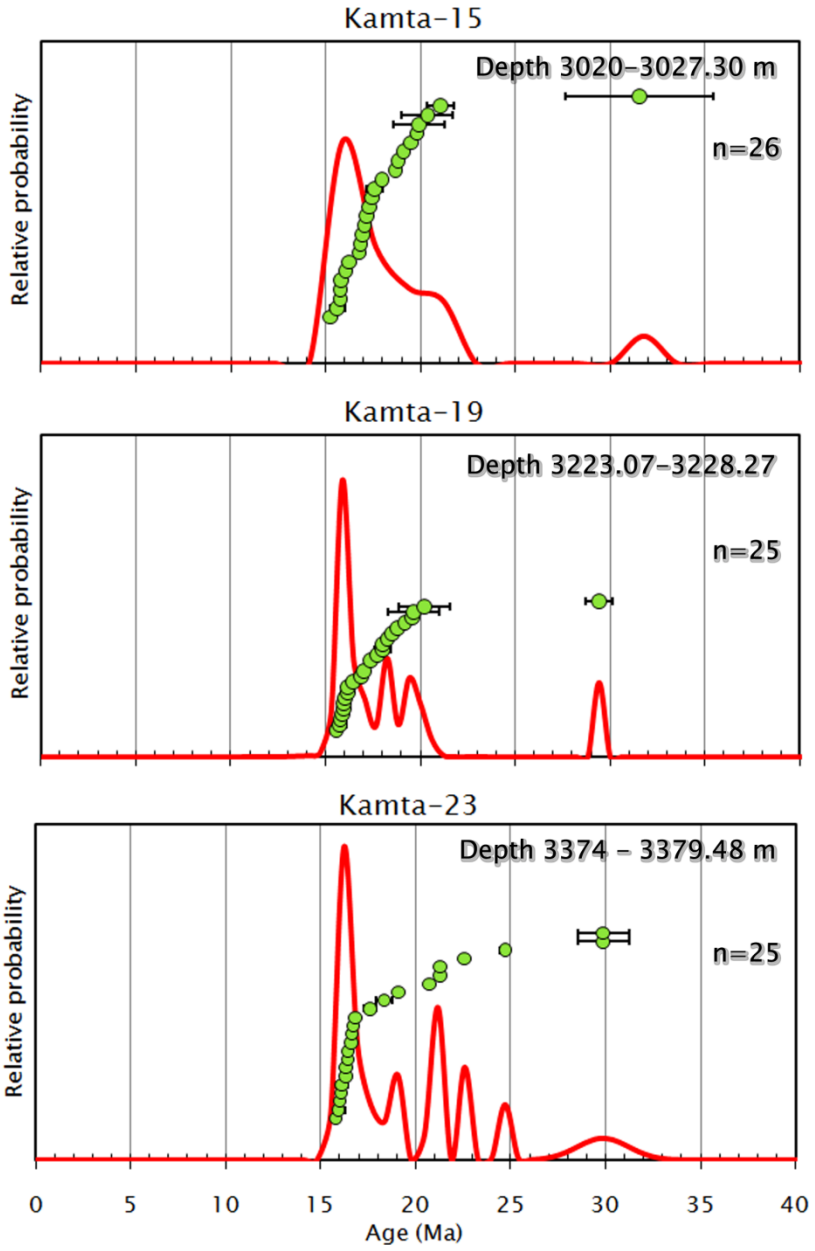

Figure 7.3 Probability density plots for $^{40}Ar/^{39}Ar$ ages of single muscovite crystals from Kamta–15, Kamta–19, and Kamta–23 samples from the Miocene Bhuban Formation of the Bengal basin (in stratigraphic order). Error bars represent 1σ (one standard deviation). Blue circles represent the cooling age of the detrital muscovite grains.

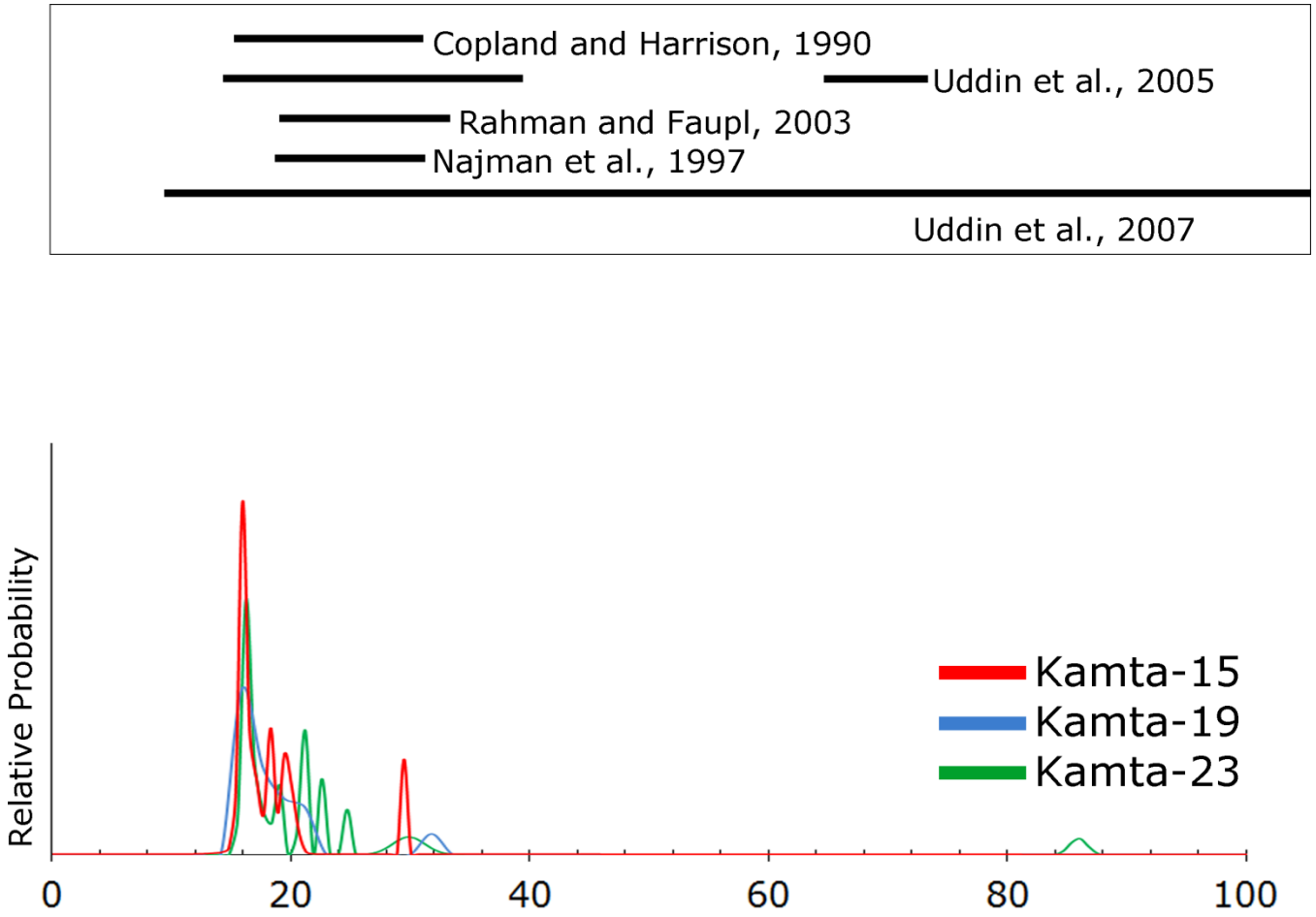

Figure 7.4 $^{40}Ar/^{39}Ar$ cooling ages of single crystal muscovite from the three samples collected from the Miocene Bhuban Formation. The data are compared with regional studies as cited.

CHAPTER 8: DISCUSSION

8.1 SYNTHESIS

The Bengal basin, a complex foreland basin south of the eastern Himalayas, holds more than 20 km of mostly orogenic sediments derived from the Himalayas and the Indo–Burman ranges (Uddin and Lundberg, 2004). The basin originally formed as a trailing margin of the Indian continental crust, complicated by the convergence with Asia and Burma. Seismic and isopach data show evidence of thickening of basin fill toward the south, opposite to the pattern typically found in foreland basins (Uddin and Lundberg, 2004). Geographic location and rapid orogenic sedimentation have resulted in the occurrence of overpressure in the Bengal basin. Geophysical log analysis, X–ray diffraction of clays, petrographic study of sandstone from the Miocene Bhuban Formation, and $^{40}Ar/^{39}Ar$ analyses of detrital muscovite provide insights on the distribution of overpressure in the Bengal basin.

8.2 GEOPHYSICAL LOG ANALYSIS

In total, twenty–nine borehole temperature logs have been analyzed from the Bengal basin up to a depth of 4 km. Subsurface temperatures at 1 km, 2 km, 3 km, and 4 km show that the deeper part of the basin in the northeast has lower temperatures relative to stable shelf area in the northwest. Areas close to the Indo–Burman ranges show relatively high temperatures compared to the surrounding areas. The deeper part of the Bengal basin covering central, eastern, and southern Bangladesh has an average

geothermal gradient of 20° C/km. In the eastern Bengal basin, the geothermal gradient ranges from 15.8° C/km to 30° C/km (Fig. 4.5). In the southeastern part of the basin, the Sitakund structure shows a relatively high geothermal gradient of 25° C/km. However, the presence of a hot spring and several prominent gas seeps has been confirmed in this area.

In the stable shelf area, geothermal gradients vary from 21.1° C/km to 31.6° C/km (Fig. 4.5). However, a shallow water well (T–278) in the Thakurgaon district shows an anomalously high geothermal gradient (140° C/km). Unfortunately, there has been no systematic investigation undertaken to address this problem.

Temperature–depth profile of the Bengal basin shows an average geothermal gradient of 30.35 °C/km (Fig. 4.6).

Composite geophysical logs (Gamma ray, resistivity, and sonic velocity) for the Fenchuganj–2 well show decrease in velocity and resistivity at depths below 4.4 km which indicates the presence of overpressure. Composite geophysical logs from the Habiganj–8 well show that the depth to the top of the overpressure zone is ~1.2 km. Zahid and Uddin (2005) showed that in the Sitakund–1 well, sonic velocity decreases at depth below 3 km, indicating the probable presence of overpressure zones.

Pressure–Depth profiles of the Bengal basin suggest that the pressure gradient increases toward the east at depths below 3 km (Fig. 4.14). Overpressure zones have a linear relationship with the depth to the top of the Miocene Bhuban Formation in the Bengal basin (Fig. 4.15).

Overpressure in the Bengal basin is constrained within the Miocene Bhuban Formation. Therefore, the depth to the top of the overpressure zone decreases towards the east as the top of the Miocene Bhuban Formation occurs at shallower depths toward the east (Figs. 4.12, 4.17).

The Sylhet trough is surrounded by uplands to the east and north. Overpressure generation in this area (Atgram–1, and Patharia–5) could have been due to hydraulic head difference between the discharge and recharge areas.

8.3 X–RAY DIFFRACTION ANALYSIS OF CLAY MINERALS

Illite, kaolinite, chlorite, mixed layer illite/smectite and kaolinite/smectite are the main clay minerals identified in the samples from the Bengal basin. The transformation of illite to smectite through intermediate illite/smectite mixed layer clay is a widely recognized clay diagenesis reaction with progressive burial. In this study, the percentage of smectite could not be calculated due to the absence of 17Å reflections. However, a large amount of mixed layer kaolinite/smectite was identified at 14.2 – 14.5 Å in most of the analyzed samples. The abundance of illite/smectite mixed layer clay in the Bengal basin suggests that diagenetic transformation of illite to smectite took place through gradual loss of smectite layer with increasing temperature resulting in an ordered interstratification of illite and smectite layers. The most important change with burial depth is the gradual loss of the 17Å peak intensity of the illite/smectite mixed layer clay. Imam (1983) proposed that the reduction of the 17Å peak is caused by gradual diagenetic changes in the illite/smectite mixed layer clay with increasing burial depth. The diagenetic transformation of smectite to illite decreased the smectite percentage in the

illite/smectite mixed layer clay. Smectite dehydration played an important role in overpressure development in many sedimentary basins. Therefore, overpressure development in the Bengal basin may have influenced by smectite dehydration.

8.4 PETROFACIES ANALYSIS

Secondary porosity is a common diagenetic feature in deeply buried (>2 km) Neogene sandstones and may account for 35–40% of the total porosity observed (Imam and Shaw, 1987). Secondary porosity arises mostly from feldspar dissolution and to a lesser extent from dissolution of calcite cements. The dissolution process generally requires acidic water. Hydrofracturing commonly occurs in deeply buried low permeability rocks. Tissot and Welte (1984) suggested that hydrofracturing is initiated at depths below 3 km to 4 km. Compaction–induced hydrofracturing have been observed in the Fenchuganj–2 well at depth of 3620 m (Fig. 6.1). In Fenchuganj–2 well, the top of overpressure zone was encountered at 3124 m depth (Imam, 2005). The presence of argillaceous matrix in hydrofractures suggests that clay injection influenced porosity reduction and hence, influenced overpressure generation in the Fenchuganj–2 well. However, in the Singra–1 well hydrofractures also have been identified at 1800 m depth. Since Singra–1 well is located in the stable shelf area, hydrofractures were not likely associated with tectonic compression. However, overburden stress may have played a role in hydrofracture generation.

Sandstone samples from Kailash Tila–4, Patharia–5, and Fenchuganj–2 shows development of secondary porosity caused by dissolution of feldspar.

8.5 ^{40}AR/^{39}AR ANALYSIS OF DETRITAL MUSCOVITE AGES

^{40}Ar/^{39}Ar analysis of detrital muscovites from the Kamta–1 well of the Miocene Bhuban Formation shows muscovite cooling ages between ca 15 Ma and 554 Ma. Previous laser ^{40}Ar/^{39}Ar analysis of individual detrital muscovites from Miocene sequences of the Bengal basin yielded cooling ages between ca 12 Ma and 516 Ma. However, the youngest ages (current and previous studies) suggest detrital muscovite cooling age ranging from 15 Ma to 16 Ma. The youngest analyses from Kamta–15 (depth 3020 –3027.30 m), Kamta–19 (depth 3223.07 – 3228.27 m), and Kamta–23 (depth 3374 –3379.48 m) have a weighted mean average cooling ages of 15.75±0.35 Ma, 15.92±0.14 Ma, and16.03±0.11 Ma respectively. Based on these cooling ages and the depth of the samples rates of sedimentation between stratigraphic levels for samples Kamta–15 and Kamta–19 and between samples Kamta–19 and between Kamta–19 and Kamta–23 are estimated to be 1.188 m/y (i.e., 1.188 km/my) and 1.28 mm/year (i.e., 1.28 km/my). Rapid sedimentation at rates >1 mm/year generate overpressure in many sedimentary basins in the world (Rubey and Hubbert, 1959; Fertl et al., 1976; Behrmann et al., 2006). Therefore, rapid sedimentation in the Bengal basin may have played an important role in overpressure development in the Bengal basin.

CHAPTER 9: CONCLUSIONS

The following conclusions can be drawn based on the studies of geophysical logs, thin–section petrography, x–ray diffraction of clay minerals, and geochronology:

1. There is no record of abnormal high pore–fluid pressure in the northwestern shelf area, in the Hinge Zone area, or in some small structures in the platform area of the Bengal basin.

2. The depth to the top of the overpressure zone is linearly related to the depth to the top of the Miocene Bhuban Formation. Overpressure depths decrease and the amount of abnormal pressure increases toward the east.

3. With increasing burial depth, smectite transforms into illite through and intermediate illite/smectite mixed layer clay. Diagenesis of clay minerals likely played an important role in the development of overpressure in the Bengal basin.

4. Secondary porosity developed through feldspar dissolution. Compaction–induced hydrofracturing and clay injection are common features in sandstones from the Miocene Bhuban Formation.

5. $^{40}Ar/^{39}Ar$ analysis of detrital muscovite from Kamta–1 well indicate rates of sedimentation were high (1.18 km/my–1.28 km/my) during the Miocene. High rates of sedimentation may have contributed to the development of overpressure in the Bengal basin.

REFERENCES

Ahmed, A., 1983, Oligocene stratigraphy and sedimentation in the Surma Basin, Bangladesh: University of Dhaka, Dhaka, 96 p.

Alam, M., 1989, Geology and depositional history of Cenozoic sediments of the Bengal Basin of Bangladesh: Palaeogeog Palaeoclim Palaeoecol, v. 69, p. 125-139.

Alam, M. M., 1991, Paleoenvironmental study of the Barail succession exposed in northeastern Sylhet, Bangladesh: Bangladesh Journal of Scientific Research, v. 9, p. 25– 32.

Ali, S. M. M., and Raghava, M. S. V., 1985, The Bouguer gravity map of Bangladesh and its tectono-geologic implications: Bangladesh Journal of Geology, v. 4, p. 43-56.

Ameen, S. M. M., Wilde, S. A., Kabir, M. Z., Akon, E., Chowdhury, K. R., and Khan, M. S. H., 2007, Paleoproterozoic granitoids in the basement of Bangladesh: A piece of the Indian shield or an exotic fragment of the Gondwana jigsaw?: Gondwana Research, v. 12, p. 380-387.

Bakhtine, M. I., 1966, Major tectonic feature of Pakistan. Part-II. Eastern Province: Science and Industry, v. 4, p. 89-100.

Banerji, R. K., 1981, Cretaceous-Eocene sedimentation, tectonism and biofacies in the Bengal basin, India: Palaeogeography Palaeoclimatology Palaeoecology, v. 34, p. 57-85.

Behrmann, J. H., Flemings, P. B., and John, C. M., 2006, Rapid Sedimentation, Overpressure, and Focused Fluid Flow, Gulf of Mexico Continental Margin: Scientific Drilling, v. 3, p. 12-17. doi:10.2204/iodp.sd.3.03.2006.

Berry, F. A. F., 1973, High fluid potentials in California Coast Ranges and their tectonic significance: American Association of Petroleum Geologists Bulletin, v. 57, p. 1219-1249.

Bethke, C. M., 1985, A numerical model of compaction-driven groundwater flow and heat transfer and its application to the paleohydrology of intracratonic sedimentary basins: Journal of Geophysical Research, v. 90, p. 6817-6828.

-, 1986, Inverse hydrologic analysis of the distribution and origin of Gulf Coast-type geopressured zones: Journal of Geophysical Research, v. 91, p. 6536–6545.

Bjorkum, P. A., and Nadeau, P. H., 1996, A kinetically controlled fluid pressure and migration model, Medium: X; Size: Pages: 15e p.

Boles, J. R., and Frank, S. G., 1979, Clay diagenesis in Wilcox sandstones of southwest Texas: Implications of smectite diageneis on sandstone cementation: Journal of sedimentary Petrology, v. 49, p. 55-70.

Bowers, G. L., 1995, Pore pressure estimation from velocity data: accounting for overpressure mechanisms besides undercompaction: SPE Drilling and Completion, June.

-, 2002, Detecting high overpressure, The Leading Edge, Society of Exploration Geophysicists, p. 174-177.

Bradley, J. S., 1975, Abnormal formation pressure: American Association of Petroleum Geologists Bulletin, v. 59, no. 6, p. 957-973.

Bredehoeft, J. D., Wesley, J. B., and Fouch, T. D., 1994, Simulations of the origin of fluid pressure, fracture generation, and the movement of fluids in the Uinta Basin, Utah: American Association of Petroleum Geologists Bulletin, v. 78, no. 1729-1747.

Brewer, I. D., Burbank, D. W., and Hodges, K. V., 2006, Downstream development of ta detrital cooling-age signal: Insights from $^{40}Ar/^{39}Ar$ muscovite thermochronology in the Nepalese Himalaya, in Willett, S.D., Hovious, N., Brandon, M.T., and Fisher, D., eds., Tectonics, climate, and landscape evolution: Geological Society of America Special Paper 398, Penrose Conference Series, p. 321-338.

Brown, D. M., McAlpine, K. D., and Yole, R. W., 1989, Sedimentology and sandstone diagenesis of Hibernia Formation oil field, Grand Banks of Newfoundland: American Association of Petroleum Geologists Bulletin, v. 73, p. 557-575.

Bruce, C. H., 1984a, Smectite dehydration-its relationship to structural dispostion and hydrocarbon migration in the Gulf of Mexico: American Association of Petroleum Geologists Bulletin, v. 80, p. 1654-1673.

-, 1984b, Smectite dehydration - its relations to structural development and hydrocarbon accumulation in northern Gulf of Mexico Basin: American Association of Petroleum Geologists Bulletin, v. 68, p. 673-683.

Brunschweiler, R. O., 1980, Lithostratigraphic monsters in modern oil exploration., In: Proc. Offshore Southeast Asia Conference: Singapore, p. 1-7.

Burst, J. F., 1959, Post diagenetic clay mineral-environmental relationships in the Gulf Coast Eocene: Clay and Clay Mineral, v. 6, p. 327-341.

-, 1969, Diagenesis of Gulf Coast clayey sediments and its possible relation to petroleum migration: American Association of Petroleum Geologists Bulletin, v. 53, p. 73-93.

Capuano, R. M., 1993, Evidence of fluid flow in microfractures in geopressured shales: American Association of Petroleum Geologists Bulletin, v. 77, p. 1303-1314.

Cerveny, P. F., 1986, Uplift and erosion of the Himalaya over the past 18 million years: evidence from fission track dating of detrital zircons and heavy mineral analysis [M.Sc. thesis]: Dartmouth College, Hanover, 198 p.

Chowdhury, K. R., Haque, M., Nasreen, N., and Hasan, R., 2003, Distribution of planktonic foraminifera in the northern Bay of Bengal: Sedimentary Geology, v. 155, p. 393-405.

Copeland, P., and Harrison, T. M., 1990, Episodic rapid uplift in the Himalaya revealed by $^{40}Ar/^{39}Ar$ analysis of detrital K-feldspar and muscovite, Bengal Fan: Geology, v. 18, p. 354-357.

Copeland, P., Harrison, T. M., Yun, P., Kidd, W. S. F., Roden, M., and Yuquan, Z., 1995, Thermal evolution of the Gangdese batholith, southern Tibet: A history of episodic unroofing: Tectonics, v. 14, no. 2, p. 223-236.

Curray, J. R., Emmel, F. J., Moore, D. G., and Raitt, R. W., 1982, Structure, tectonics and geological history of the northeastern Indian Ocean, in Nairn, A.E.M., and Stehli, F.G., eds.: The Ocean Basin and Margins, v. 6, The Indian Ocean: New York, Plenum, p. 399-450.

Curray, J. R., and Moore, D. G., 1971, The growth of the Bengal Deepsea Fan and denudation in the Himalayas: Geological Society of America Bulletin, v. 82, p. 563– 572.

DeCelles, P. G., Gehrels, G. E., Najman, Y., Martin, A. J., Carter, A., and Grarzanti, E., 2004, Detrital geochronology and geochemistry of Cretaceous - Early Miocene strata of Nepal: Implications for timing and diachroneity of initial Himalayan orogenesis: Earth and Planetary Science Letters, v. 227, p. 313-330.

Desikachar, O. S. V., 1974, A review of the tectonic and geological history of eastern India in terms of ‘plate tectonics’ theory: Journal of the Geological Society of India, v. 33, p. 137–149.

Dickinson, G., 1953 Geological aspects of abnormal reservoir pressures in Gulf Coast, Louisiana: American Association of Petroleum Geologists Bulletin, v. 37, p. 410-432.

Dickinson, W. D., 1985, Interpreting provenance relations from detrital modes of sandstone, in Zuffa G.G. editor, provenance of arenites: Dordrecht, Holland, Reidel, 333-361 p.

Dunoyer de Segonzac, G., 1970, The tranformation of clay minerals during diagenesis and low grade metamorphism: Sedimentology, v. 15, p. 181-346.

Faure, G., 1986, Principles of Isotope Geology: New York, John Wiley and Sons, 589 p.

Fertl, W. H., Chapman, R. E., and Hotz, R. F., 1994, Studies in abnormal pressures: Developments in Petroleum Science, v. 38.

Fertl, W. H., Chilingar, G. V., and Rieke, H. H., 1976, Abnormal Formation Pressures: Implications to Exploration, Drilling, and Production of Oil and Gas Resources, Developments in Petroleum Science: Amsterdam, Elsevier Scientific Publishing Company.

Fertl, W. H., and Chilingarian, G. V., 1987, Abnormation formation pressure and their detection by pulsed Neutron capture logs: Journal of Petroleum Science & Engineering, v. 1, p. 23-38.

Freed, R. L., and Peacor, D. R., 1989, Geopressured shale and sealing effect of smectite-to-illite transition: American Association of Petroleum Geologists Bulletin, v. 73, p. 1223-1232.

Gansser, A., 1964, Geology of the Himalayas: London, Interscience, 289 p.

Gibbs, R. J., 1977, Clay mineral segregation in the marine environment: Journal of Sedimentary Petrology, v. 47, p. 237-243.

Goulty, N. R., 1998, Relationships between porosity and effective stress in shales: First break, v. 16, p. 413-419.

Graham, S. A., Dickinson, W. R., and Ingersoll, R. V., 1975, Himalayan - Bengal Model for Flysh Dispersal in the Appalachian - Ouachita System: Geological Society of America Bulletin, v. 86, p. 273-286.

Hames, W. E., and Bowring, S. A., 1994, An empirical evaluation of the argon diffusion geometry in muscovite: Earth and Planetary Science Letters, v. 124, p. 161-167.

Hansom, J., and Lee, M.-K., 2005, Effects of hydrocarbon generation, basal heat flow, and sediment compaction on overpressure development: A numerical study: Petroleum Geoscience, v. 11, p. 353-360.

Henriet, J. P., Batist, M. d., and Verschuren, M., 1991, Early fracturing of Paleogene clays, southernmost North Sea: relevance to mechanisms of primary migration, in

A. M. Spencer, ed., Generation, accumulation and production of Europe's hydrocarbons: European Association of Petroleum Geologists Special Publication, v. 1, p. 212-227.

Hiller, K., and Elahi, M., 1984, Structural development and hydrocarbon entrapment in the Surma Basin, Bangladesh (northwest Indo–Burman Fold belt), Proceedings of 4th Offshore Southeast Asia Conference: Singapore, p. 6-50-6-63.

Hodges, K. V., Hames, W. E., Olszewski, W., Burchfiel, B. C., Royden, L. H., and Chen, Z., 1994, Thermobarometric and 40Ar/39Ar geochronologic constraints on Eohimalayan metamorphism in the Dinggye area, Southern Tibet: Contributions to Mineralogy and Petrology, v. 117, p. 151-163.

Hodges, K. V., Ruhl, K. W., Wobus, C. W., and Pringle, M. S., 2005, $^{40}Ar/^{39}Ar$ thermochronology of detrital minerals: Reviews in Mineralogy and Geochemistry, v. 58, p. 239-257.

Holtrop, J. F., and Keizer, J., 1970, Some aspects of the stratigraphy and correlation of the Surma Basin wells, East Pakistan: United Nations.

-, 1971, Some aspects of the stratigraphy and correlation of the Surma Basin wells, East Pakistan in Stratigraphic Correlation between Sedimentary Basins in the ECAFE Region (second volume), United Nations ECAFE Min. Resources Development Ser, v. 36, p. 143-154.

Hoque, M., 1982, Tectonic set-up of Bangladesh and its relation to hydrocarbon accumulation: Center for Policy Research, Dhaka, Bangladesh, 177 p.

Horath, F. L., 1989, Permeability evolution in the Cascadia accretionary prism: example from the Oregon prism and Olympic Peninsula melanges [M.Sc. thesis]: University of California, Santa Cruz, 150 p.

Hossain, I., and Tsunogae, T., 2008, Fluid inclusion study of pegmatite and aplite veins of Palaeoproterozoic basement rocks in Bangladesh: Implications for magmatic fluid compositions and crystallization depth: Journal of Mineralogical and Petrological Sciences, v. 103, p. 121-125.

Hossain, I., Tsunogae, T., and Rajesh, H. M., 2009, Geothermobarometry and fluid inclusions of dioritic rocks in Bangladesh: Implications for emplacement depth and exhumation rate: Journal of Asian Earth Sciences, v. 34, p. 731-739.

Hossain, I., Tsunogae, T., Rajesh, H. M., Chen, B., and Arakawa, Y., 2007, Palaeoproterozoic U–Pb SHRIMP zircon age from basement rocks in Bangladesh: A possible remnant of the Columbia supercontinent: Comptes Rendus Geoscience, v. 339, p. 979-986.

Hower, J., Eslinger, E. V., Hower, M., and Perry, E. A., 1976, Mechanisms of burial metamorphism of argillite sediment: Geological Society of America Bulletin, v. 87, p. 725-737.

Hunt, J. M., 1990, Generation and migration of petroleum from abnormally pressured fluid compartments: American Association of Petroleum Geologists Bulletin, v. 74, p. 1-12.

Imam, M. B., 1983, Diagenesis in the Neogene clastic sediments of the Bengal basin, Bangladesh [Ph.D. thesis]: Imperial College of Science & Technology, London, 221 p.

-, 1994, X-ray diffraction study on Neogene shales from the Patharia anticline, eastern Bangladesh, with emphasis on smectite clay dehydration and implication: Journal of the Geological Society of India, v. 44, p. 547-561.

-, 2005, Energy resources of Bangladesh: Dhaka, University Grants Commission of Bangladesh, 280 p.

Imam, M. B., and Hussain, M., 2002, A review of hydrocarbon habitats in Bangladesh: Journal of Petroleum Geology, v. 25 no. 1, p. 31–52.

Imam, M. B., and Shaw, H. F., 1985, The diagenesis of Neogene clastic sediments from the Bengal Basin, Bangladesh: Journal of sedimentary Petrology, v. 55, p. 665-671.

-, 1987, Diagenetic controls on the reservoir properties of gas bearing Nogene Surma Group sandstones in the Bengal basin, Bangladesh: Marine and Petroleum Geology, v. 4, p. 103-111.

Isaksen, G. H., 2004, Central North Sea hydrocarbon systems: generation, migration, entrapment, and thermal degradation of oil and gas: American Association of Petroleum Geologists Bulletin, v. 88, no. 11, p. 1542-1572.

Jansa, L. F., and Urrea, V. H. N., 1990, Geologic and diagenetic history of overpressured sandstone reservoirs, Venture gas field, offshore Nova Scotia, Canada: American Association of Petroleum Geologists Bulletin, v. 74, p. 1640–1658.

Johns, W. D., and Shimoyama, A., 1972, Clay minerals and petroleum-forming reaction during burial and diagenesis: American Association of Petroleum Geologists Bulletin, v. 56, p. 2160-2167.

Johnson, S. Y., and Nur Alam, A. M., 1991, Sedimentation and tectonics of the Sylhet trough, Bangladesh: Geological Society of America Bulletin, v. 103, p. 1513–1527.

Khan, A. A., 1991a, Tectonics of the Bengal basin: Journal of Himalayan Geology, v. 2, p. 91–101.

Khan, F. H., 1991b, Geology of Bangladesh: Dhaka, The University Press Limited, 207 p.

Khan, M. A. M., and Husain, M., 1980, A look at the geology of Bangladesh gas fields: Oil and Gas Journal, v. 78, no. 31, p. 92-95.

Khan, M. A. M., Ismail, M., and Ahmad, M., 1988, Geology of hydrocarbon prospects of the Surma basin, Bangladesh, Seventh Offshore southeast Asia conference: Singapore, p. 364-387.

Khan, M. R., and Muminullah, M., 1980, Stratigraphy of Bangladesh: Ministry of Petroleum and Mineral Resources, Government of Bangladesh, p. 35-40.

Khandoker, R. A., 1989, Development of major tectonic elements of the Bengal Basin: a plate tectonic appraisal: Bangladesh Journal of Scientific Research, v. 7, p. 221-232.

Kuehl, S. A., Harju, T. M., and Moore, W. S., 1989, Shelf sedimentation of the Ganges-Brahmaputra river system: Evidence for sediment bypassing to the Bengal fan: Geology v. 17, no. 1132-1135.

Lahann, R. W., 1980, Smectite diagenesis and sandstone cementation: the effect of reactions temperature: Journal of sedimentary Petrology, v. 50, p. 755-760.

Lambe, T. W., and Whitman, R. V., 1969, Soil mechanics: New York, Wiley, 553 p.

Lanson, B., Velde, B., and Meunier, A., 1998, Late-stage diagenesis of illitic clay minerals as seen by decomposition of x-ray diffraction patterns: Contrasted behaviors of sedimentary basins with different burial histories: Clay and Clay Minerals, v. 46, no. 1, p. 69-78.

Law, B. E., and Spencer, C. W., 1998, Abnormal pressure in hydrocarbon environments. In: Law, B.E., Ulmishek, G.F., and Slavin, V.I. (Eds.), Abnormal pressure in hydrocarbon environments: American Association of Petroleum Geologists Memoir, v. 70, p. 1-11.

Lee, M.-K., and Williams, D. D., 2000, Paleohydrology of the Delaware Basin, Western Texas: Overpressure Development, Hydrocarbon Migration, and Ore Genesis: American Association of Petroleum Geologists Bulletin, v. 84, no. 7, p. 961-974.

Lee, T., and Lawver, L. A., 1995, Cenozoic plate reconstruction of Southeast Asia: Tectonophysics, v. 251, p. 85-138.

Lindquist, S. J., 1977, Secondary porosity development and subsequent reduction, overpressured Frio Formation sandstone (Oligocene), south Texas: Gulf Coast Association of Geological Societies, Transactions, v. 27, p. 99–107.

Lindsay, J. F., Holliday, D. W., and Hulber, A. G., 1991, Sequence stratigraphy and evolution of the Ganges-Brahmaputra delta complex: American Association of Petroleum Geologists Bulletin, v. 75, p. 1233-1254.

Lonoy, A., Akselsen, J., and Ronning, K., 1986, Diagenesis of a deeply buried sandstone reservoir: Hild field, northern North Sea: Clay Minerals, v. 21, p. 497-511.

Loucks, R. G., Dodge, M. M., and Galloway, W. E., 1984, Regional controls on diagenesis and reservoir quality in lower Tertiary sandstones along the Texas Gulf Coast, in D. A. McDonald and R. C. Surdam, eds. Clastic diagenesis: American Association of Petroleum Geologists Bulletin Memoir, v. 37, p. 15-45.

Luo, M., Baker, M. R., and LeMone, D. V., 1994, Distribution and generation of the overpressure system, eastern Delaware Basin, Western Texas and southern New Mexico: American Association of Petroleum Geologists Bulletin, v. 78, no. 9, p. 1386-1405.

Mannan, A., 2002, Stratigraphic evolution and geochemistry of the Neogene Surma group, Surma basin, Sylhet, Bangladesh [Ph.D. thesis]: University of Oulu, Oulu, 162 p.

Matin, M. A., Denega, B. I., and Huq, M., 1982, Regional distribution of temperature and pressure gradient of Bangladesh (unpublished): Bangladesh Oil Gas and Minerals Corporation (BOGMC) data center.

McBride, E. F., 1977, Secondary porosity—importance in sandstone reservoirs in Texas (short note): Gulf Coast Association of Geological Societies, Transactions, v. 27, p. 121-122.

McDougall, I., and Harrison, M. T., 1999, Geochronology and thermochronology by the $^{40}Ar/^{39}Ar$ method: New York, Oxford University Press, 269 p.

McPherson, B. J. O. L., and Garven, G., 1999, Hydrodynamic and overpressure mechanisms in the Sacramento basin, California: American Journal of Science, v. 299, p. 429-466.

Merrihue, C., and Turner, G., 1966, Potassium-argon dating by activation with fast neutrons: Journal of Geophysical Research, v. 71, p. 2852-2856.

Millot, G., 1970, Geology of Clays, translated by W.R. Farrand and H. Paquet: Heidelberg, Springer-Verlag, 429 p.

Mitchell, A. H. G., 1993, Cretaceous-Cenozoic tectonic events in the western Myanmar (Burma)-Assam region: Journal of the Geological Society [London], v. 150, p. 1089–1102.

Molnar, P., 1984, Structure and tectonics of the Himalaya: Constraints and implications of geophysical data: Annual Review of Earth and Planetary Sciences, v. 12, p. 489-518.

Molnar, P., and Tapponnier, P., 1975, Cenozoic tectonics of Asia: Effects of continental collision: Science, v. 189, p. 419-426.

Mosser-Ruck, R., Devineau, K., Charpentier, D., and Cathelineau, M., 2005, Effects of ethylene glycol saturation protocols on XRD patterns: A critical review and discussion: Clays and Clay Minerals, v. 53, no. 6, p. 631-638.

Murphy, R. W., 1988, Bangladesh enters the oil era: Oil and Gas Journal, p. 76–82.

Murthy, M. V. N., Chakrabarti, C., and Talukdar, S. E., 1976, Stratigraphic revision of the Cretaceous-Tertiary sediments of the Shillong Plateau: Geological Survey of India Records, v. 107, p. 80-90.

Neuzil, C. E., 1995, Abnormal pressures as hydrodynamic phenomena: American Journal of Science, v. 295, p. 742-786.

Ni, J. F., Guzman-Speziale, M., Holt, W. E., Wallace, T. C., and Saeger, W. R., 1989, Accretionary tectonics of Burma and the three dimensional geometry of the Burma subduction zone: Geology, v. 17, p. 68– 71.

Nolen-Hoeksema, R. C., 1993, Porosity and consolidation limits of sediments and Gassmann's elastic-wave equation: Geophysical Research Letters, v. 20, p. 847-850.

Osborne, M. J., and Swarbrick, R. E., 1997, Mechanisms for generating overpressure in sedimentary basins: a reevaluation American Association of Petroleum Geologists Bulletin, v. 81, p. 1023-1041.

-, 1999, Diagenesis in the North Sea HPHT clastic reservoirs–consequences for porosity and overpressure prediction: Marine and Petroleum Geology, v. 16, p. 337-353.

Parker, C. A., 1974, Geopressures and secondary porosity in the deep Jurassic of Mississippi: Gulf Coast Association of Geological Societies, Transactions, v. 24, p. 69-80.

Perry, E., and Hower, J., 1970, Burial diagenesis in Gulf Coast pelitic sediments: Clay and Clay Mineral, v. 18, p. 165-177.

-, 1972, Late stage dehydration in deeply buried pelitic sediments: American Association of Petroleum Geologists Bulletin, v. 56, p. 2013-2021.

Porter, E. W., and James, W. C., 1986, Influecne of pressure, salinity, tempearture, and grain size on silica diagenesis in quartzose sanstones: Chemical Geology, v. 57, no. 359-369.

Powers, M. C., 1967, Fluid release mechanism in compacting marine mud rocks, their importance in oil exploration: American Association of Petroleum Geologists Bulletin, v. 51, p. 1240-1254.

Rahman, M. W., 2008, Sedimentation and Tectonic Evolution of Cenozoic Sequences From Bengal and Assam Foreland Basins, Eastern Himalayas: Auburn University, Auburn, 162 p.

Rahman, Q. M. A., and Sen Gupta, P. K., 1980, Geological log of GDH-31: Dhaka, Geological Survey of Bangladesh.

Reimann, K. U., 1993, Geology of Bangladesh: Berlin, Borntraeger.

Roberts, S. J., and Nunn, J. A., 1995, Episodic fluid expulsion from geopressured sediments: Marine and Petroleum Geology, v. 12, p. 195-204.

Rowley, D. B., 1996, Age of initiation of collision between India and Asia: A review of stratigraphic data: Earth and Planetary Science Letters, v. 145, no. 1-13.

Rubey, W. W., and Hubbert, M. K., 1959, Role of fluid presure in mechanics of overthrust faulting, Part 2. Overthrust belt in geosynclinal area of western Wyoming in light of fluid-pressure hypothesis: Geological Society of America Bulletin, v. 70, p. 167-205.

Ruth, P. V., Hillis, R., Tingate, P., and Swarbrick, R. E., 2003, The origin of overpressure in 'old' sedimentary basins: an example from the Cooper Basin, Australia: Geofluids, v. 3, p. 125-131.

Salt, C. A., Alam, M. M., and Hossain, M. M., 1986, Bengal Basin: Current exploration of the hinge zone of southwestern Bangladesh, In: Proc. 6th Offshore Southeast Asia Conference: Singapore p. 55-67.

Sato, T., Murakami, T., and Watanabi, T., 1996, Change in layer charge of smectites and smectite layers in illite/smectite during diagenetic alternation: Clay and Clay Mineral, v. 44, p. 460-469.

Schmidt, V., and MacDonald, D. A., 1976, Texture and recognition of secondary porosity in sandstones: Society of Economic Paleontologists and Mineralogists, v. 26 (special publication), p. 209-225.

Sclater, J. G., and Fisher, R. L., 1974, The evolution of the east central Indian Ocean, with emphasis on the tectonic setting of the Ninetyeast Ridge: Geological Society of America Bulletin, v. 85, p. 683–702.

Sengupta, S., 1966, Geological and geophysical studies in western part of Bengal basin, India: American Association of Petroleum Geologists Bulletin, v. 50, p. 1001–1017.

Shamsuddin, A. H. M., Brown, T. A., Lee, S., and Curiale, J., 2001, Petroleum systems of Bangladesh: Proceedings of the 13th SEAPEX Exploration Conference, April, 2001, Singapore.

Srodon, J., 1980, Synthesis of mixed-layer kaolinite/smectite: Clays and Clay Minerals, v. 28, p. 419-424.

-, 1981, X-ray identification of randomly interstratified illite/smectite in mixtures with discrete illite: Clay Minerals, v. 16, p. 278-304.

-, 1999, Nature of mixed-layer clays and mechanism of their formations and alternation: Annual Review of Earth and Planetary Sciences, v. 27, p. 19-53.

Srodon, J., Elsas, s., F., McHardy, W. J., and Morhgan, D. J., 1992, Chemistry of illite-smectite inferred from TEM measurements of fundamental particles: Clay Minerals, v. 27, p. 137-158.

Swarbrick, R. E., and Osborne, M. J., 1998, Mechanism that generate abnormal pressure: An overview In: Law, B.E., Ulmishek, G.F., and Slavin, V.I. (Eds.), Abnormal pressure in hydrocarbon environments: American Association of Petroleum Geologists Memoir, v. 70, p. 13-34.

Tanikawa, W., Shimamoto, T., Wey, S.-K., Lin, C.-W., and Lai, W.-C., 2008, Stratigraphic variation of transport properties and overpressure development in the Western Foothills, Taiwan: Journal of Geophysical Research, v. 113, p. B12403, doi:10.1029/2008JB005647.

Taylor, T. R., 1990, The influence of calcite dissolution on reservoir porosity in Miocene sandstones, Picaroon field, offshore Texas Gulf Coast: Journal of Sedimentary Petrology, v. 60, p. 322-334.

Thomson, A., 1982, Preservation of porosity in the deep Woodbine/Tuscaloosa trend, Louisiana: Gulf Coast Association of Geological Societies, Transactions, v. 30, p. 397–403.

Tissot, B. P., and Welte, D. H., 1984, Petroleum formation and occurrence: New York, Springer-Verlag, 699 p.

Towe, K. M., 1962, Clay mineral diagenesis as a possible source of silica cement in sedimentary rocks: Journal of sedimentary Petrology, v. 32, p. 26-28.

Trevena, A. S., and Clark, R. A., 1986, Diagenesis of sandstone reservoirs of Pattani Basin, Gulf of Thailand: American Association of Petroleum Geologists Bulletin, v. 70, p. 299-308.

Uddin, A., Hames, W., and Zahid, K. M., 2005, Detrital mineral chemistry and age constraints on Tertiary source terrain evolution for the Bengal basin: Abstract with Programs - Geological Society of America, v. 37, no. 7, p. 561.

Uddin, A., Hames, W. E., Rahman, M. W., and Zahid, K. M., 2007, Rapid middle Miocene denudation of the eastern Himalayas: Laser $^{40}Ar/^{39}Ar$ age constraints on Miocene sequences from the Bengal basin: Abstracts with Programs - Geological Society of America, v. 39, no. 6, p. 592.

Uddin, A., and Lundberg, N., 1998a, Cenozoic history of the Himalayan-Bengal system; sand composition in the Bengal Basin, Bangladesh: Geological Society of America Bulletin, v. 110, no. 4, p. 497-511.

-, 1998b, Unroofing history of the eastern Himalaya and the Indo-Burman ranges; heavy-mineral study of Cenozoic sediments from the Bengal Basin, Bangladesh: Journal of Sedimentary Research, v. 68, no. 3, p. 465-472.

-, 1999, A paleo-Brahmaputra? Subsurface lithofacies analysis of Miocene deltaic sediments in the Himalayan–Bengal system, Bangladesh: Sedimentary Geology, v. 123, p. 239-254.

-, 2004, Miocene sedimentation and subsidence during continent–continent collision, Bengal basin, Bangladesh: Sedimentary Geology, v. 164, p. 131-146.

Wang, C.-Y., and Xie, X., 1998, Hydrofracturing and Episodic Fluid Flow in Shale-Rich Basins—A Numerical Study: American Association of Petroleum Geologists Bulletin, v. 82, no. 10, p. 1857-1869.

Weaver, C. E., 1956, Distribution and identification of mixed-layer clays in sedimentary rocks: American Mineralogist, v. 41, p. 202-221.

Weedman, S. D., Brantley, S. L., Shiraki, R., and Poulson, S. R., 1996, Diagenesis, Compaction, and Fluid Chemistry Modeling of a Sandstone Near a Pressure Seal: Lower Tuscaloosa Formation, Gulf Coast: American Association of Petroleum Geologists Bulletin, v. 80, no. 7, p. 1045-1064.

Weedman, S. D., Guber, A. L., and Engelder, T., 1992, Pore pressure variation within the Tuscaloosa trend: Morganza and Moore-Sams fields, Louisiana Gulf Coast: Journal of Geophysical Research, v. 97, p. 7193-7202.

Wilkinson, M., Darby, D., Haszeldine, R. S., and Couples, G. D., 1997, Secondary Porosity Generation During Deep Burial Associated with Overpressure Leak-Off: Fulmar Formation, United Kingdom Central Graben: American Association of Petroleum Geologists Bulletin, v. 81, no. 5, p. 803-813.

Wolf, L. W., Lee, M.-K., Browning, S., and Tuttle, M. P., 2005, Numerical Analysis of Overpressure Development in the New Madrid Seismic Zone: Bulletin of the Seismological Society of America, v. 95, no. 1, p. 135-144.

Woodside, P. R., 1983, The petroleum geology of Bangladesh: Oil and Gas Journal, v. 81, no. 32, p. 149-155.

Xie, X., Bethke, C. M., Li, S., Liu, X., and Zheng, H., 2001, Overpressure and petroleum generation and accumulation in the Dongying depression of the Bohaiwan basin, China: Geofluids, v. 1, p. 257-271.

Yang, C., and Hesse, R., 1991, Clay minerals as indicators of diagenetic and anchimetamorphic grade in an overthrust belt, external domain of southern canadian appalachians: Clay Minerals, v. 26, p. 211-231.

Yardley, G. S., and Swarbrick, R. E., 2000, Lateral transfer; a source of additional overpressure?: Marine and Petroleum Geology, v. 17, no. 4, p. 523-537.

Yassir, N., and Addis, M. A., 2002, Relationships between pore pressure and stress in different tectonic settings: American Association of Petroleum Geologists Memoir, v. 76, p. 79-88.

Yassir, N. A., and Bell, J. S., 1996, Abnormally high fluid pressure and associated porosities and stress regimes in sedimentary Basins: SPE Formation Evaluation, v. 48, p. 5-10.

Zaher, M. A., 1970, Limestone deposits of the western part of the Takerghat area, district Sylhet, Pakistan, Rec. Geological Survey of Pakistan 20 (2), p. 57-75.

Zaher, M. A., and Rahman, A., 1980, Prospects and investigations for minerals in the northern part of Bangladesh. In: Petroleum and Mineral Resources of Bangladesh, Seminar and Exhibition Government of the People's Republic of Bangladesh, Dhaka, p. 9-18.

Zahid, K. M., 2005, Provenance and basin tectonics of Oligocene-Miocene sequences of the Bengal basin, Bangladesh [M.Sc. thesis]: Auburn University, Auburn, 162 p.

Zahid, K. M., and Uddin, A., 2005, Influence of overpressure on formation velocity evaluation of Neogene strata from the eastern Bengal Basin, Bangladesh: Journal of Asian Earth Sciences, v. 25, p. 419-429.

Zeng, L., and Xiao, S., 2003, The Formation of Overpressure and It's Influence on Oil and Gas in Kuche Foreland Thrust Structural Zone, Tarim Basin, Northwest China, American Association of Petroleum Geologists International Conference: Barcelona, Spain.

APPENDICES

Appendix–A

Kamta–23 (Miocene Bhuban Formation) detrital muscovite cooling age data.

Sample Name:	
Date Run:	4/27/09
Irradiation Package:	AU-13
Date of Irradiation:	2/5/2009
Elapsed Days:	82
Monitor Age (FC-2):	2.802E+07
Air 40Ar/36Ar:	293.0 + 2
J-Value	0.002856±0.000011
Sensitivity (volts/mol):	4.4646E-15

	40Ar(*+atm)	39rK	38Ar(atm+Cl)	37ArCa	36Ar(atm)	%Rad	R	Age (Ma)	%-sd
				au13.1d.mus; Kamta-23					
56	8.7602E-15 + 1.5E-17	1.89E-15 + 9.9E-18	4.8E-18 + 8.6E-20	1.4E-17 + 1.1E-18	3.916E-18 + 1.1E-19	87%	4.0332	20.73 + 0.16	0.78%
57	1.6198E-14 + 1.3E-17	4.61E-15 + 1.5E-17	1.1E-17 + 1.0E-19	3.7E-18 + 6.3E-19	4.996E-18 + 1.2E-19	91%	3.1906	16.42 + 0.07	0.44%
58	1.6536E-14 + 1.5E-17	3.81E-15 + 1.9E-17	8.6E-18 + 1.5E-19	1.1E-17 + 9.6E-19	2.553E-18 + 1.1E-19	95%	4.1408	21.28 + 0.12	0.58%
59	1.0764E-14 + 2.1E-17	3.24E-15 + 5.6E-18	7.1E-18 + 1.7E-19	3.2E-17 + 9.4E-19	2.198E-18 + 1.0E-19	94%	3.1251	16.08 + 0.07	0.41%
60	1.2124E-14 + 1.3E-17	3.61E-15 + 9.0E-18	8.9E-18 + 6.3E-20	9.3E-19 + 6.5E-19	1.979E-18 + 9.3E-20	95%	3.1940	16.43 + 0.06	0.37%
61	1.8566E-14 + 6.2E-17	1.06E-15 + 8.0E-18	4.3E-18 + 1.6E-19	4.4E-19 + 3.2E-19	1.620E-18 + 4.9E-20	97%	17.0358	85.97 + 0.73	0.85%
62	8.2568E-16 + 2.7E-18	2.21E-16 + 1.6E-18	6.6E-19 + 1.9E-20	3.8E-18 + 3.3E-19	2.397E-19 + 4.0E-20	91%	3.4206	17.59 + 0.32	1.79%
63	1.6908E-15 + 2.8E-18	5.13E-16 + 1.8E-18	1.3E-18 + 5.2E-20	3.8E-19 + 3.1E-19	3.862E-19 + 4.4E-20	93%	3.0724	15.81 + 0.15	0.92%
64	3.0997E-15 + 6.1E-18	6.40E-16 + 2.7E-18	1.6E-18 + 3.3E-20	4.9E-19 + 2.8E-19	9.811E-19 + 4.4E-20	91%	4.3932	22.57 + 0.16	0.69%
65	1.5027E-15 + 7.1E-18	4.50E-16 + 1.2E-18	1.3E-18 + 2.7E-20	1.5E-18 + 4.0E-19	3.381E-19 + 3.4E-20	93%	3.1153	16.03 + 0.15	0.93%
66	3.5499E-15 + 7.7E-18	9.98E-16 + 2.9E-18	3.0E-18 + 2.7E-20	2.7E-18 + 6.0E-19	9.742E-19 + 4.6E-20	92%	3.2693	16.82 + 0.10	0.57%
67	3.0796E-15 + 6.3E-18	8.64E-16 + 3.1E-18	2.0E-18 + 3.9E-20	1.6E-18 + 4.7E-19	9.924E-19 + 4.8E-20	90%	3.2267	16.60 + 0.11	0.68%
68	2.5497E-16 + 3.3E-18	4.45E-17 + 3.0E-19	1.0E-19 + 1.2E-20	-3.6E-19 + 3.4E-19	-1.423E-20 + -3.8E-20	102%	5.8258	29.86 + 1.35	4.51%
69	2.5497E-16 + 3.3E-18	4.45E-17 + 3.0E-19	1.0E-19 + 1.2E-20	-3.6E-19 + 3.4E-19	-1.423E-20 + -3.8E-20	102%	5.8258	29.86 + 1.35	4.51%
70	2.4371E-15 + 4.5E-18	6.12E-16 + 1.2E-17	1.6E-18 + 4.5E-20	3.7E-18 + 5.8E-19	8.616E-19 + 5.1E-20	90%	3.5649	18.33 + 0.41	2.25%
71	1.7079E-14 + 3.0E-17	3.87E-16 + 7.0E-18	7.9E-19 + 4.0E-20	4.0E-18 + 4.2E-19	4.343E-19 + 5.7E-20	99%	43.8336	213.42 + 3.89	1.82%
72	1.3669E-15 + 5.1E-18	3.83E-16 + 1.7E-18	1.1E-18 + 3.8E-20	4.4E-18 + 3.3E-19	5.097E-19 + 3.6E-20	89%	3.1727	16.32 + 0.18	1.10%
73	2.1301E-15 + 4.0E-18	5.03E-16 + 1.9E-18	1.7E-18 + 2.4E-20	9.2E-18 + 6.3E-19	1.704E-18 + 5.6E-20	76%	3.2353	16.65 + 0.19	1.17%
74	1.4524E-15 + 2.9E-18	2.86E-16 + 2.1E-18	5.8E-19 + 2.0E-20	1.0E-18 + 5.0E-19	2.532E-19 + 3.3E-20	95%	4.8115	24.70 + 0.26	1.07%
75	3.1114E-15 + 5.3E-18	8.56E-16 + 2.4E-18	1.9E-18 + 3.5E-20	1.7E-18 + 2.7E-19	1.115E-18 + 4.6E-20	89%	3.2494	16.72 + 0.10	0.61%
76	4.2052E-15 + 1.4E-17	1.28E-15 + 2.2E-17	4.3E-18 + 1.5E-19	2.7E-17 + 4.8E-19	6.388E-19 + 5.5E-20	96%	3.1313	16.11 + 0.31	1.90%
77	3.1401E-15 + 9.6E-18	6.88E-16 + 3.6E-18	2.0E-18 + 5.6E-20	8.4E-19 + 3.8E-19	9.713E-19 + 5.1E-20	91%	4.1444	21.29 + 0.18	0.85%
78	1.6432E-15 + 2.9E-18	4.00E-16 + 1.5E-18	8.3E-19 + 2.5E-20	1.5E-18 + 3.9E-19	5.434E-19 + 4.3E-20	90%	3.7113	19.08 + 0.19	0.98%
79	2.5854E-15 + 3.2E-18	7.72E-16 + 2.5E-18	1.3E-18 + 3.0E-20	1.7E-18 + 3.2E-19	4.566E-19 + 3.0E-20	95%	3.1734	16.33 + 0.08	0.52%
80	2.9261E-15 + 3.6E-17	7.74E-16 + 4.8E-18	2.5E-18 + 4.9E-20	2.9E-18 + 5.1E-19	1.789E-18 + 1.3E-19	82%	3.0975	15.94 + 0.38	2.37%

Kamta–15 (Miocene Bhuban Formation) detrital muscovite cooling age data.

au13.1e.mus; Kamta-15																				
	81	1.2727E-15	+	2.5E-18	3.15E-16	+	1.6E-18	1.1E-18	+	5.8E-20	1.8E-18	+	2.8E-19	4.416E-19	+	8.3E-20	90%	3.6310	18.7	+	0.4	2.23%
	82	1.5309E-15	+	2.0E-18	3.75E-16	+	1.2E-18	1.1E-18	+	3.2E-20	3.0E-18	+	4.3E-19	4.680E-19	+	7.3E-20	91%	3.7160	19.1	+	0.3	1.60%
	83	2.7393E-15	+	5.6E-18	7.85E-16	+	3.1E-18	2.4E-18	+	4.6E-20	2.0E-18	+	3.3E-19	5.761E-19	+	4.7E-20	94%	3.2728	16.8	+	0.1	0.71%
	84	3.6298E-15	+	6.8E-18	1.11E-15	+	3.5E-18	2.6E-18	+	2.8E-20	1.6E-18	+	2.5E-19	1.169E-18	+	5.0E-20	90%	2.9627	15.2	+	0.1	0.61%
	85	2.7168E-15	+	4.2E-18	8.20E-16	+	3.0E-18	1.5E-18	+	3.6E-20	2.3E-18	+	2.2E-19	4.352E-19	+	5.0E-20	95%	3.1561	16.2	+	0.1	0.71%
	86	3.9066E-15	+	4.8E-18	9.12E-16	+	3.5E-18	2.2E-18	+	4.4E-20	5.1E-18	+	6.4E-19	1.270E-18	+	6.4E-20	90%	3.8735	19.9	+	0.1	0.70%
	87	2.2515E-15	+	6.7E-18	6.59E-16	+	2.0E-18	1.4E-18	+	3.7E-20	-4.9E-19	+	5.0E-19	7.837E-19	+	5.1E-20	90%	3.0657	15.8	+	0.1	0.88%
	88	1.5434E-15	+	2.2E-18	3.83E-16	+	1.1E-18	1.3E-18	+	5.2E-20	1.2E-20	+	5.1E-19	6.936E-19	+	4.6E-20	87%	3.4953	18.0	+	0.2	1.08%
	89	9.9471E-16	+	8.1E-18	2.52E-16	+	8.4E-19	5.2E-19	+	2.5E-20	-6.8E-20	+	4.7E-19	1.310E-19	+	4.4E-20	96%	3.7883	19.5	+	0.3	1.65%
	90	1.4468E-15	+	2.9E-18	4.16E-16	+	9.8E-19	1.1E-18	+	3.1E-20	5.1E-19	+	4.8E-19	2.298E-19	+	5.2E-20	95%	3.3134	17.0	+	0.2	1.17%
	91	2.3831E-15	+	3.7E-18	7.43E-16	+	1.7E-18	1.8E-18	+	3.0E-20	5.8E-19	+	4.2E-19	2.179E-19	+	4.1E-20	97%	3.1191	16.1	+	0.1	0.60%
	92	2.4904E-15	+	5.5E-18	6.75E-16	+	3.4E-18	1.6E-18	+	3.0E-20	3.0E-19	+	4.3E-19	9.080E-19	+	4.6E-20	89%	3.2939	16.9	+	0.1	0.87%
	93	1.3444E-15	+	3.7E-18	4.03E-16	+	2.5E-18	1.1E-18	+	4.2E-20	1.2E-18	+	3.8E-19	3.720E-19	+	3.9E-20	92%	3.0627	15.8	+	0.2	1.20%
	94	4.0284E-15	+	6.6E-18	1.11E-15	+	3.7E-18	2.9E-18	+	5.3E-20	1.7E-18	+	4.0E-19	2.217E-18	+	6.2E-20	84%	3.0323	15.6	+	0.1	0.71%
	95	3.0075E-15	+	5.1E-18	8.29E-16	+	4.4E-18	2.3E-18	+	3.9E-20	1.9E-19	+	3.5E-19	8.325E-19	+	3.6E-20	92%	3.3305	17.1	+	0.1	0.72%
	96	3.2616E-15	+	1.2E-17	7.33E-16	+	1.8E-18	1.7E-18	+	4.8E-20	4.4E-18	+	5.0E-19	1.204E-18	+	1.2E-19	89%	3.9642	20.4	+	0.3	1.28%
	97	5.5447E-15	+	9.4E-18	1.38E-15	+	2.8E-18	2.8E-18	+	5.9E-20	3.6E-18	+	2.8E-19	7.414E-19	+	4.3E-20	96%	3.8542	19.8	+	0.1	0.37%
	98	2.9795E-15	+	5.3E-18	6.95E-16	+	1.7E-18	1.7E-18	+	2.5E-20	1.6E-18	+	3.6E-19	4.517E-19	+	3.9E-20	96%	4.0969	21.1	+	0.1	0.52%
	99	6.4506E-15	+	6.1E-18	1.03E-15	+	5.0E-18	2.6E-18	+	4.4E-20	2.6E-18	+	3.9E-19	4.931E-19	+	4.9E-20	98%	6.1509	31.5	+	0.2	0.56%
	100	5.7665E-14	+	2.3E-17	4.58E-16	+	1.8E-18	2.1E-18	+	4.6E-20	4.0E-18	+	7.0E-19	6.385E-19	+	5.1E-20	100%	125.5744	554.4	+	2.3	0.41%
	103a	1.1949E-15	+	3.7E-18	3.15E-16	+	9.8E-19	7.6E-19	+	2.9E-20	2.7E-19	+	4.3E-19	4.316E-19	+	3.7E-20	89%	3.3849	17.4	+	0.2	1.13%
	104	1.255E-15	+	3.0E-18	2.99E-16	+	1.4E-18	6.2E-19	+	2.3E-20	9.3E-19	+	2.7E-19	8.446E-19	+	4.0E-20	80%	3.3652	17.3	+	0.2	1.36%
	105	9.4846E-16	+	3.4E-18	2.31E-16	+	1.7E-18	4.6E-19	+	1.7E-20	1.6E-19	+	2.6E-19	5.391E-19	+	3.3E-20	83%	3.4209	17.6	+	0.3	1.60%
	106	1.3446E-15	+	3.5E-18	3.26E-16	+	2.0E-18	4.6E-19	+	1.1E-20	5.4E-19	+	2.3E-19	5.112E-19	+	4.0E-20	89%	3.6600	18.8	+	0.2	1.26%
	107	1.2015E-15	+	2.9E-18	3.57E-16	+	1.5E-18	7.8E-19	+	2.2E-20	-6.7E-20	+	3.8E-19	3.542E-19	+	4.3E-20	91%	3.0721	15.8	+	0.2	1.28%
	108	3.0281E-15	+	5.7E-18	8.67E-16	+	2.9E-18	2.0E-18	+	4.8E-20	3.4E-18	+	3.4E-19	6.809E-19	+	4.3E-20	93%	3.2599	16.8	+	0.1	0.61%

Kamta–19 (Miocene Bhuban Formation) detrital muscovite cooling age data.

au13.1f.mus; Kamta-19																			
	26	3.6014E-15	+	5.6E-18	1.12E-15	+	6.5E-18	4.3E-18	+	1.1E-19	1.3E-18	+	4.9E-19	6.181E-19	+	6.1E-20	95%	3.0660	15.8	+	0.1	0.83%
	27	1.1042E-15	+	9.8E-18	2.95E-16	+	2.5E-18	1.5E-18	+	6.0E-20	-6.0E-19	+	3.7E-19	6.375E-19	+	6.0E-20	83%	3.1024	16.0	+	0.4	2.43%
	28	5.2514E-15	+	1.2E-17	1.46E-15	+	2.7E-18	3.5E-18	+	3.2E-20	1.6E-18	+	5.0E-19	4.674E-19	+	4.7E-20	97%	3.5048	18.0	+	0.1	0.41%
	29	1.4124E-15	+	2.3E-18	4.18E-16	+	2.0E-18	1.0E-18	+	1.7E-20	1.2E-20	+	4.7E-19	3.752E-19	+	4.3E-20	92%	3.1149	16.0	+	0.2	1.11%
	30	3.808E-15	+	7.7E-18	6.52E-16	+	1.1E-18	1.2E-18	+	1.3E-20	5.9E-19	+	5.6E-19	2.335E-19	+	4.4E-20	98%	5.7389	29.4	+	0.1	0.44%
	31	1.7814E-15	+	2.8E-18	5.23E-16	+	5.6E-19	9.4E-19	+	2.5E-20	1.1E-21	+	5.1E-19	4.786E-20	+	4.3E-20	99%	3.3791	17.4	+	0.1	0.75%
	32	1.7893E-15	+	2.2E-18	4.87E-16	+	2.5E-18	8.8E-19	+	1.9E-20	7.9E-19	+	4.7E-19	2.037E-19	+	4.2E-20	97%	3.5486	18.2	+	0.2	0.90%
	33	2.5611E-16	+	2.5E-18	3.89E-17	+	1.8E-19	1.8E-19	+	3.0E-20	3.4E-19	+	3.1E-19	4.313E-19	+	4.4E-20	50%	3.3086	17.0	+	1.8	10.35%
	34	9.5899E-16	+	3.8E-18	2.33E-16	+	2.2E-18	5.9E-19	+	2.4E-20	6.1E-19	+	4.3E-19	2.248E-19	+	4.5E-20	93%	3.8231	19.7	+	0.4	1.87%
	35	1.4757E-15	+	1.6E-18	3.82E-16	+	3.0E-18	1.2E-18	+	2.1E-20	-7.0E-20	+	4.2E-19	9.850E-19	+	4.8E-20	80%	3.1038	16.0	+	0.2	1.56%
	36	4.5294E-15	+	1.0E-17	1.19E-15	+	5.1E-18	2.9E-18	+	5.5E-20	6.6E-19	+	3.8E-19	8.132E-19	+	4.9E-20	95%	3.5995	18.5	+	0.1	0.61%
	37	2.2426E-15	+	1.8E-18	5.94E-16	+	1.7E-18	1.6E-18	+	3.2E-20	6.4E-19	+	3.3E-19	8.092E-20	+	4.5E-20	99%	3.7329	19.2	+	0.1	0.67%
	38	8.5306E-16	+	3.8E-18	1.72E-16	+	1.1E-18	4.2E-19	+	3.5E-20	1.8E-19	+	5.7E-19	7.580E-19	+	6.3E-20	74%	3.6521	18.8	+	0.6	3.17%
	39	1.4398E-15	+	4.4E-18	4.35E-16	+	1.5E-18	1.2E-18	+	2.9E-20	9.8E-19	+	3.5E-19	2.491E-19	+	5.9E-20	95%	3.1439	16.2	+	0.2	1.36%
	40	3.9012E-15	+	6.1E-18	9.08E-16	+	3.0E-18	2.8E-18	+	4.5E-20	3.7E-18	+	4.2E-19	3.116E-18	+	7.5E-20	76%	3.2819	16.9	+	0.2	0.90%
	41	3.4009E-16	+	2.1E-18	9.98E-17	+	5.8E-19	3.0E-19	+	3.0E-20	2.2E-19	+	3.3E-19	-1.339E-20	+	-4.5E-20	101%	3.4473	17.7	+	0.7	3.96%
	42	1.6132E-15	+	2.9E-18	4.22E-16	+	1.7E-18	9.5E-19	+	2.3E-20	6.6E-19	+	5.5E-19	9.753E-19	+	5.0E-20	82%	3.1434	16.2	+	0.2	1.24%
	43	1.2409E-15	+	3.6E-18	2.67E-16	+	1.6E-18	1.3E-18	+	3.9E-20	2.6E-19	+	4.7E-19	1.467E-18	+	5.3E-20	65%	3.0267	15.6	+	0.3	2.21%
	44	7.2724E-16	+	3.4E-18	1.81E-16	+	1.3E-18	4.6E-19	+	2.4E-20	2.6E-19	+	4.3E-19	5.426E-20	+	4.5E-20	98%	3.9329	20.2	+	0.4	2.04%
	45	1.1448E-15	+	2.9E-18	3.57E-16	+	1.5E-18	7.3E-19	+	1.6E-20	5.1E-19	+	5.0E-19	1.816E-19	+	4.8E-20	95%	3.0574	15.7	+	0.2	1.39%
	46	7.1535E-16	+	4.0E-18	1.95E-16	+	1.8E-18	7.0E-19	+	2.2E-20	-4.0E-20	+	4.2E-19	3.901E-19	+	4.8E-20	84%	3.0845	15.9	+	0.4	2.70%
	47	7.0365E-16	+	3.7E-18	1.96E-16	+	1.3E-18	5.1E-19	+	2.2E-20	2.5E-18	+	4.6E-19	2.636E-19	+	4.4E-20	89%	3.1961	16.4	+	0.4	2.28%
	48	3.0642E-15	+	3.9E-18	8.20E-16	+	1.2E-18	1.9E-18	+	1.9E-20	2.2E-18	+	4.1E-19	6.459E-19	+	4.6E-20	94%	3.5052	18.0	+	0.1	0.52%
	49	8.1169E-16	+	4.9E-18	2.10E-16	+	8.5E-19	6.9E-19	+	2.5E-20	1.6E-18	+	6.4E-19	4.816E-20	+	4.5E-20	98%	3.8031	19.6	+	0.4	1.85%
	50	1.1668E-16	+	1.3E-18	2.83E-18	+	2.0E-19	5.6E-20	+	5.0E-20	3.0E-19	+	5.8E-19	3.631E-19	+	4.5E-20	8%	3.3259	17.1	+	31.7	185.13%